Development of a cell-based drug screening platform: extracellular recording and electrochemical impedance spectroscopy on microelectrode array chips

Sorensen, Per

Award date:
2007

Awarding institution:
University of Bath

Development of a Cell-Based Drug Screening Platform

-

Extracellular Recording and Electrochemical Impedance Spectroscopy on Microelectrode Array Chips

Volume 1 of 4

Sören Per Sörensen

A thesis submitted for the degree of Doctor of Philosophy

University of Bath

Department of Chemistry

October 2007

A Table of Contents

B List of Figures

C List of Tables

D Acknowledgements

Many individuals contributed to parts of the project and I would like to thank everybody who was involved. Particularly, this is addressed to the persons listed below: Thank you very much for your help!!!

Prof. Dr. Wolfgang Knoll, director of the materials science section at the Max-Planck Institute for Polymer Research (MPIP), offered me the chance to work on an interesting topic in a stimulating scientific community.

Prof. Dr.-Ing. Christiane Thielemann, supervisor in Mainz, introduced me into the fantastic world of biosensing. I am grateful for her inspiring ideas, constructive discussions, and an outstanding support.

Dr. A. Toby A. Jenkins, supervisor in Bath, is an expert in Electrochemical Impedance Spectroscopy and contributed substantial ideas to this project. I thank him for his great scientific advice, support and for his effort in supervising my work.

Dr. Mark Pottek, co-worker in Mainz, developed and optimised the preparation protocol of the cardiomyocytes. He also prepared the cardiomyocytes cell suspensions until January 2005. I appreciate his positive seriousness, his very substantial contributions, and that he was always willing to help if necessary. Thank you very much for proofreading this thesis so carefully.

Dr. Steffen Howitz, director of the Gesellschaft für Mikro-Silizumssyteme mbH (GeSiM), Grosserkmannsdorf, Germany, was responsible for the manufacture of several parts of the screening systems. In detail, this included glass sensor technology except the platinum black deposition, fabrication of silicon specimen, and other components of the biosensor platform. The competence and reliability of GeSiM as industrial partner was always an exceptional helpful support.

PD Dr. Ute Reuning, project leader at the Technical University in Munich (Frauenklinik rechts der Isar), offered substantial support in cell biology of OV-MZ-6 cells and competitively binding integrin ligands. She and her workgroup supplied cells, peptides and always offered advice.

Dr. Sven Ingebrandt, co-worker of the interface section (ISG2) at the research institute in Jülich, introduced me into the Flip-Chip Technology. This technology was used for the fabrication of sensor hybrids, composed of microelectrode array chip and printed circuit board.

Achim Gerstenberg, head of the MPIP Mechanical Workshop, and co-workers always provided rapid and accurate services.

Dirk Richter, head of the MPIP Electronic Workshop, and co-workers contributed their ideas and competency to this project. Exciting ideas evolved from countless discussions and were an important source to me.

Jochen Steininger, diploma student in Mainz, programmed an early version of the application software used in this thesis. His concepts regarding the high volume data processing were an immense advantage to me.

Margarida Vareiro, **Hayley Dash**, and **Jonathan Olds**, co-workers of Dr. A.T.A. Jenkins in Bath, welcomed me warmly during my stay in spring 2004.

Melanie Jungblut, **Hwei-Ling Khor**, **Carmen Schwind**, **Inga Vockenroth, and Anye Ngu Chifen**, co-workers in Mainz, thank you for your friendship and much more! And also **Charlotte Mears** for proof reading the manuscript.

E Summary

Two established methods, Electrochemical Impedance Spectroscopy (EIS) and extracellular recording, were implemented into a technology platform for non-invasive whole-cell biosensing. Electrical activity of cardiomyocytes and cell-substrate interaction of human ovarian cancer cells was monitored on electrode array chips. The performance of cells inside a microfluidic or closed low volume environment was investigated. Prior to the development of the entire microfluidic platform the two transducing methods were evaluated in single experiments.

Processes as cellular attachment and detachment were monitored using EIS and single frequency impedance sensing. Electrodes of different size and structure were employed and compared for their impedance response. It was shown that small electrodes ($A = 9 \cdot 10^{-6}$ cm²) are more sensitive to cell-substrate interaction than larger ones ($A = 9 \cdot 10^{-5}$ cm²) and that the frequency used for analysis has a profound influence on the sensitivity. Data were modelled using a common equivalent circuit that represents a cell layer on an electrode resulting in an increase of the impedance magnitude by <170 % due to cell attachment. In order to demonstrate the potential of this method for biomedical applications, experiments related to anti-cancer strategies were performed. Cell detachment was induced by addition of synthetic integrin ligands and by hypericin mediated photodynamic therapy and monitored with impedance-based biosensing.

Electrical activity of cardiomyocytes cultured on microelectrode arrays was monitored inside a microfluidic system. The chronotropic drug isoproterenol was applied using a robotic dispensing machine, and the resulting changes in spike rate and duration were compared with results gained by experiments with a large scale MEA chip.

The experimental findings inspired the development of a technology platform that was finally evaluated by monitoring extracellular signals from myocytes in response to Isoproterenol. Another topic was the comparison of cell-substrate interaction monitored on various electrode structures.

F List of Abbreviations

µTAS	Micro-total analysis system
AT	Amitriptyline
BioMEMS	Biological Micro-Electro-Mechanical System
CCD	Charge Coupled Device
COX	Cyclooxygenase
CPE	Constant phase element
DIV	Days *in vitro*
DMEM	Dulbeccos's modified eagle medium
DMSO	Dimethyl sulfoxide
ECIS	Electric Cell-substrate Impedance Sensing
ECM	Extracellular matrix
EDTA	Ethylenediaminetetraacetic acid
EIS	Electrochemical Impedance Spectroscopy
FBS	Foetal bovine serum
FLIC	Fluorescence interference contrast
GND	Ground potential (electrical)
HUVEC	Human umbilical vein endothelial cells
LFP	Local field potentials
MAPK	Mitogen-activated protein kinase
MDCK	Madin-Darby canine kidney
MEA	Microelectrode array
MTT	3-(4,5-dimethylthiazol-2-yl)-2,5-diphenyltetrazolium
PA	Photoactivation
PBPK	Physiologically based pharmacokinetic (model)
PBS	Phosphate buffered saline
PCB	Printed circuit board
PCMCIA	Personal Computer Memory Card International Association
PCR	Polymerase chain reaction
PDMS	Polydimethylsiloxane
PDT	Photodynamic Therapy (or Treatment)

PECVD	Plasma Enhanced Chemical Vapour Deposition
PMMA	Polymethyl methacrylate
PS	Polystyrene
QCM	Quartz crystal microbalance
REACH	Registration, Evaluation and Authorisation of Chemicals
ROS	Reactive oxygen species
SEM	Scanning Electron Microscopy
TER	Transepithelial or transendothelial resistance

1 Introduction

Sensors are important tools to understand, to monitor, and to control processes that are beyond the scope of our natural sensing "equipment", the sensitive organs of our body. The palette of technical sensors was extended by employing biological material as a sensitive element. A popular example of an early biosensor are the canary birds that accompanied British coal miners until the late 1980s in order to signal toxic gases, for instance the colourless, odourless, and tasteless carbon monoxide.

Biosensors are devices with biological material coupled to common sensor elements that transduce the response of the biologic element into measurable data. Particularly, cells have a high organisational complexity compared to anything encountered in the non-living world, as is exemplified by the presence of numerous internal compartments and specialised membranes. These specialisations serve to generate gradients of diffusible substances, enable transport of specific molecules, and coordinate enzymatic reactions [Goldsmith 2001].

Parallel to this structural complexity, cells are also specialised for different functions and are, for instance, able to detect analytes with higher specificity and sensitivity than human-made sensors can do. Hence, the transfer of these properties from *in vivo* to *in vitro* systems is a rational methodology for constructing 'new generation' biosensors with high sensitivity and selectivity. Whereas molecular assays are quite common in pharmaceutical research, using whole cells is comparably rare. *Whole cell biosensing* is mostly performed using optical detection methods involving specific labelling by fluorescent protein species or by nanobeads. These methods may interfere with cellular pathways. Therefore, research on methods that non-invasively investigate responses of a complete cell is of great interest, in particular as cells can be manipulated by genetic engineering to sense for a defined target [Aravanis 2001]. But, research has to aim at the presentation of reliable and reproducible assay formats as required by pharmaceutical industry.

A long-term perspective is the application of whole cell biosensing as a validated alternative for animal trials. The need of such alternative methods to at least reduce animal testing becomes clear after implementing the new European chemicals law – REACH; Registration, Evaluation and Authorisation of Chemicals. About 30,000 of the 103,000 notified chemical substances [ECVAM 2004] have to be analysed involving the usage of about 12.8×10^6 vertebrates and the amount of 6.51×10^9 € according to cautious estimations [IEH 2001]. The application of alternative *in vitro* testing methods for various kinds of toxicity are therefore of growing interest, although this will only help to reduce animal trials but will never substitute them.

Aiming at the commercial goal of reproducibility and reliability, this thesis focused on automation of cell-based sensing. The prototypic biosensing system developed consisted of a

computer controlled test substance dispenser, a user friendly sensor design, and a microchannel supplying cells with culture medium and test substances. The microchannel incorporated into a microfluidic unit and allowed continuous nutrient supply to cells and access of test substances at low dead volumes offering short sample/rinse cycles. This approach involved the culture and isolation of electrogenic cells, heart muscle cells from rat embryos, on planar electrode array biosensors. Their electrical activity was non-invasively sensed by extracellular recording revealing the cellular sensitivity to pharmacologically or toxicologically active agents.

In a second approach non-electrically active cells, i.e. human tumour cells were investigated using a different electrical transducing method, i.e. Electrochemical Impedance Spectroscopy. Tumour cells are characterised by robust cell infiltration mechanisms allowing to invade other tissues. Microscopic methods are applied to reveal whether a certain substance affects the cell-substrate interaction or not. Assays that transduce this interaction into physical parameters and allow to monitor tumour cell adhesion in real-time are useful for the to optimisation of cancer therapies, as shown for photodynamic therapy.

The results of these studies and the operation of the prototype microfluidic system led to the development of a second microfluidic technology platform that combined optical microscopy, impedance analysis, and extracellular recording.

2 Fundamentals

2.1 Cell Biology

2.1.1 Cell Adhesion

Cell-substrate interaction is of interest in biophysical and biomedical research. Cell adhesion provides important signals in cellular development and is responsible for several processes in tissue structure, tissue remodelling, and wound healing. Abnormalities in adhesion often indicate pathological conditions as cancer metastases or intravenous blood coagulation.

Adhesion of cells to extracellular structures requires a mixture of various multiadhesive or adhesion promoting proteins adsorbed to the substrate – the so-called *extracellular matrix* (ECM). This cell-protein adhesion is central to the design of compatible biomaterials and in tissue engineering [Gallant 2002].

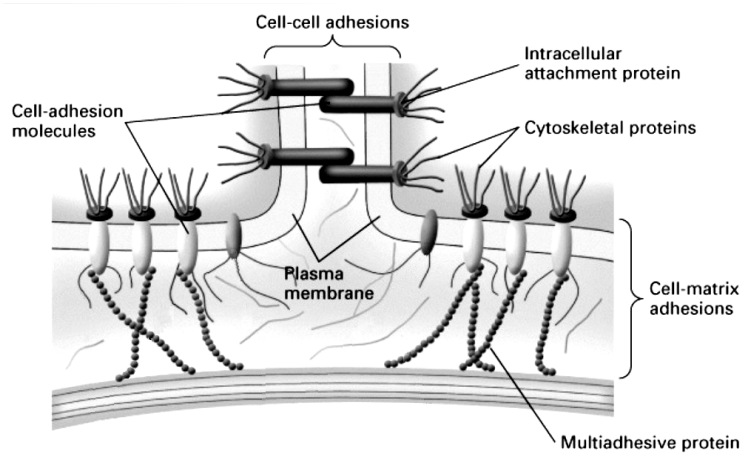

Figure 2-1: Cells adhering to a substrate. Cell-matrix adhesions are formed by cell-adhesion molecules that bind to multiadhesive proteins adsorbed onto the surface [Lodish 1996]. A cell-substrate gap of ~150 nm thickness is formed [Zeck 2003].

A generalised scheme of cells attached to a solid support is given in Figure 2-1. *Cell-adhesion molecules* recognise specific *multiadhesive proteins* (or adhesion promoting proteins) and form *cell-matrix adhesions*. For instance, *integrins* as membrane spanning cell adhesion molecules bind to extracellular proteins like *fibronectin* or *laminin*. *Cadherins* are responsible for cell-cell adhesions. Adhesion triggers an intracellular signal originating from the cell adhesion molecules. Bound receptors rapidly associate with *intracellular attachment proteins* that promote fast assembly of the *cytoskeleton*. This was found to be a highly regulated, two-stage process involving initial receptor-ligand interaction and subsequent adhesion strengthening and cell spreading. After the cytoskeleton assembly has been terminated, cells have transformed from spherical to stiff, irregularly shaped objects.

Later, *lamellipodia* develop focal adhesions that can further support robust cell adhesion [Gallant 2002, Small 2005]. They are composed of cytoskeleton proteins that prominently

appear as pioneering structures on the leading edge of the cell, and prevent withdrawal of the newly attached membrane during cellular motion. Therefore, focal adhesions are key elements in the adhesion process, because they are structural links between the cytoskeleton and the ECM and trigger signal pathways that control cell proliferation and differentiation. Furthermore, they play a central role in cell migration.

However, this layer-by-layer arrangement of extracellular protein and cell membrane leads to a measurable gap between the basal membrane and the support. This cell-substrate or basal gap can be characterised by Fluorescence Interference Contrast Microscopy and was found to be in the range of 150 nm [Zeck 2003].

Multiadhesive Proteins

The affinity of a protein to a biomaterials surface can be characterised by an adsorption constant, which is an indirect measure of the non-covalent bond at the surface. Two models have been used to quantify equilibrium protein adsorption data, the *Langmuir* and *Freundlich* adsorption isotherms [Young 1988]. Adsorption is dependent on surface charge and hydrophobicity of the substrate, on ion strength and pH value of the electrolyte, and on properties of the proteins.

Cell-matrix adhesions require specific interaction of proteins with membrane receptors. The tertiary structure of the protein is responsible for correct recognition. A slight change in conformation can cause steric repulsion leading to prevention of cellular adhesion. Protein conformation is also influenced by surface charge of the material the protein is adsorbed to as immunostaining revealed [Keselowsky 2003].

The binding sites that are responsible for cell-protein interaction usually contain the amino acid sequence Arginine-Glycine-Aspartate (RGD). This sequence binds to integrins and therefore forms an important cell adhesive motif present in some ECM proteins as collagen, fibronectin, laminin, and vitronectin [Ruoslahti 1987]. The identification of this major binding site offered new perspectives in biological surface science. For instance, a number of integrin ligands were synthesised on the basis of the RGD sequence partly resulting in higher affinities than naturally occurring ligands [Thumbshirn 2003] useful in tumour diagnostics and therapy (see Chapter 2.1.3).

2.1.2 Electrogenic Activity of Cardiomyocytes

Normally, the cell membrane of any cell is polarised because of an unequal distribution of ion species between the cell's interior and the extracellular environment. Cells that are able to de- and repolarise the membrane are characterised by *electrogenic activity*. For instance, these cells can generate an action potential by ion transfer across the membrane. Cells of the nerve system and muscle cells belong to this type. In the case of rhythmic contraction of e.g. heart muscle cells, the action potential is triggered by pacemaker cells that provide a specific set of ion channels allowing for rhythmic changes of the membrane potential.

The cardiac action potential has a duration of approximately 300-400 ms [Walker 1998] and remains depolarised for longer time periods, compared to other electrogenic cells. During the course of an action potential, the resting potential of a cell is altered by opening of ion channels that permit the flux of ions across the membrane. A typical action potential is given in Figure 2-2. It displays different phases that result from a sequence of ion currents.

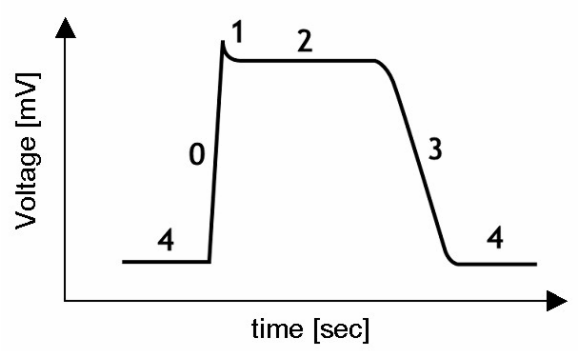

Figure 2-2: Cardiac action potential. The course is characterised by several phases (details see text). Its total amplitude is in the range of 30 to 100 mV at a duration of 300 to 400 ms.

Phase 0 corresponds to a fast membrane depolarisation. The onset of the action potential is due to an instantaneous increase in membrane permeability to Na^+ ions and a concomitant decrease in K^+ permeability. Once the enhanced flux of Na^+ ions across the membrane is lowered, a slight repolarisation occurs (phase 1). The membrane depolarisation causes an opening of voltage-gated Ca^{2+} channels that mediate an intense influx of Ca^{2+}, which antagonises the loss of K^+ ions. This results in a steady potential of about zero millivolts (so-called *plateau*; phase 2) and is the basis for the prolonged duration of the cardiac action potential. Moreover, the Ca^{2+} influx provides the high intracellular Ca^{2+} concentration essential to the contractile performance of myocytes. After closure of Ca^{2+} channels and increased K^+ permeability, the membrane potential repolarises (phase 3) to a negative resting level of about -60 mV (phase 4) until the next action potential is generated.

The Hodgkin-Huxley theory [Hodgkin 1952] allows one to simulate the course of an action potential. The ion conductance g_i of a single ion species is determined by the ion flow density i_M, the membrane potential V_M, and the Nernst potential E according to

$$g_i = \frac{i_M}{V_M - E_i}. \tag{2-1}$$

The Nernst potential E is the equilibrium potential of a model membrane that is only permeable for a single ion species and is described as

$$E_i = E_{in} - E_{out} = \frac{RT}{zF} \ln \frac{c^{in}}{c^{out}} \tag{2-2}$$

where R is the gas constant, T the temperature, z the valence of the specific ion, F the Faraday constant, and c the concentration of the specific ion inside (*in*) and outside (*out*) the cell.

The Hodgkin-Huxley model for the cell membrane is displayed in Figure 2-3. Ion species specific conductances g_i and Nernst potentials E_i are considered in parallel to the specific membrane capacitance c_M. Leak currents are summed up in the voltage-dependent leakage conductance g_L, and ion concentrations are given by an equilibrium potential E_L. The ion concentration is affected by the activity of the Na^+/K^+ pump and the Na^+/Ca^{2+} exchanger (active transporters).

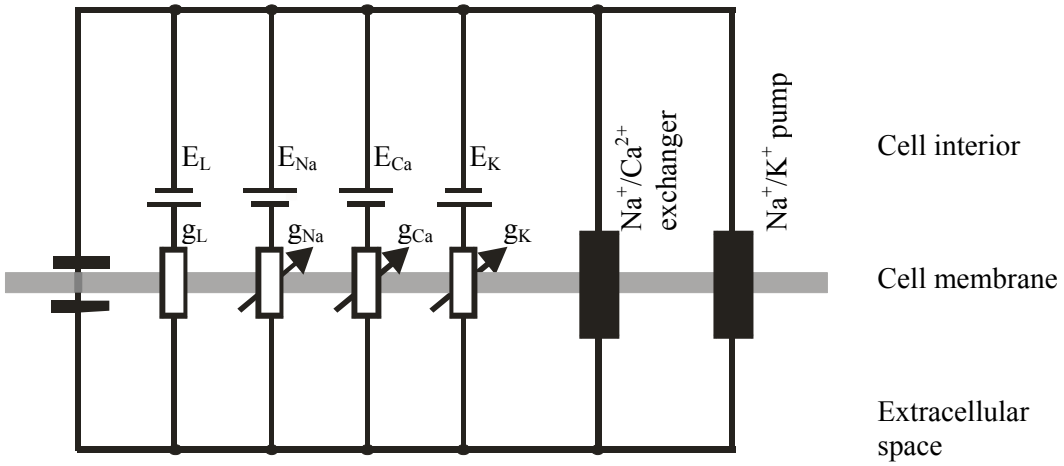

Figure 2-3: Hodgkin-Huxley model. The equivalent circuit describes the electrical properties of a cardiac cell according to [Hodgkin 1952]. Ion species involved contribute to the membrane potential by their Nernst potentials E_i and the specific ion conductances g_i. Index L refers to an overall leakage current. Moreover, membrane capacitance and active transporters contribute to the membrane potential.

As shown in Figure 2-3, not only a single ion species contributes to the membrane potential. To consider K^+, Ca^{2+}, and Na^+ fluxes, a *permeability coefficient P* was defined leading to the definition of the *Goldman equation*. The coefficient *P* is a measure for the permeability of a 1 cm² large membrane patch for a certain ion species with a concentration gradient of 1 mol across the membrane. Permeability is proportional to the number of open ion channels and to the number of ions that can pass a single channel in 1 s. The membrane potential across a plasma membrane can be calculated by an "extended" Nernst equation that weighs the ion concentrations according to the specific permeability coefficients. Ion concentrations are indexed "*i* " for intracellular values and "*o*" for values outside the cell.

$$E_m = \frac{RT}{F} \ln \frac{P_{K^+}\left[K^+\right]_o + P_{Na^+}\left[Na^+\right]_o + P_{Ca^{2+}}\left[Ca^{2+}\right]_i}{P_{K^+}\left[K^+\right]_i + P_{Na^+}\left[Na^+\right]_i + P_{Ca^{2+}}\left[Ca^{2+}\right]_o} \tag{2-3}$$

The Goldman equation can be used to calculate the membrane potential for known ion concentrations and ion permeabilities.

2.1.3 Tumour Cells

In tumour biology, cell adhesion is of interest because tumour invasion into the surrounding tissue and metastasis require fine tuning of adhesive contacts. Expression of ECM components and integrins is frequently modulated in response to changes within the tumour cell vicinity during tumour cell progression [Hapke 2001]. Tumour growth, for example, stimulates surrounding endothelial cells by release of growth factors to build up blood vessels in a process that is called angioneogenesis. Because cancer cells have a high oxygen demand, additional blood vessels are necessary for tumours that exceed a certain size (~3 mm^3). The activated endothelial cells often over-express the integrin receptor $\alpha_v\beta_3$, which serves as an indicator for the invasive phase of tumour cells [Thumbshirn 2003].

Integrin-Ligand Induced Tumour Cell Detachment

Following this idea, passivation of the $\alpha_v\beta_3$ integrin by binding to a tailor-made ligand is a promising approach in tumour therapy [Thumbshirn 2003]. Because the peptide sequence RGD was identified as the minimal fragment for stimulation of cell adhesion, it was the basis for further synthesis of peptide and non-peptide ligands. For example, the insertion of D-amino acids resulted in the synthetic $\alpha_v\beta_3$ selective ligand cyclo(-Arg-Gly-Asp-D-Phe-Val-) or c(-RGDfV-) [Thumbshirn 2003], which exhibits a higher affinity to the integrin receptors than adhesion promoting proteins. Using water soluble peptides the *tumour induced angioneogenesis* can be suppressed, because ECM molecules are less attractive to the receptors, and the cell on binding to the artificial ligand, loses contact to the surface. Consequently, reorganisation of the cytoskeleton takes place causing detachment of the cell from the substrate and induction of programmed cell death (apoptosis). By following this approach, proliferation (metastasis) was at least successfully hindered for cells that over-express $\alpha_v\beta_3$ integrins [Thumbshirn 2003].

However, before this strategy can be clinically investigated, promising substances need to be screened for their functionality. This is mainly done by culturing cells in culture flasks and visual observation of the cellular detachment in response to administered substances [Hapke 2003]. In contrast, biosensors capable of directly monitoring detachment have a great potential to perform this and other screening tasks more efficiently. Cell adhesion and cell spreading, for example, was investigated on quartz crystal microbalances [Li 2005]. In this study, a human ovarian cancer cell line (OV-MZ-6) was used as a model system for cell-substrate interaction. The same cell line was also subject to research on cellular adhesion [Hapke 2001] and is used as a model in this thesis, too.

Photodynamic Therapy

Photodynamic therapy (PDT) is a cancer therapy, that is – in contrast to the previously presented drug targeted approach - already approved by several countries although strong side-effects are apparent. In the late 19th century modern light therapy began, as the Danish Niels Finsen used UV light to treat cutanous tuberculosis and was awarded the Nobel Prize for his discoveries in 1903. But, ancient Egyptian, Indian, and Chinese civilizations used light to treat various diseases (as psoriasis, rickets, vitiligo and skin cancer). Nowadays, research aiming at optimising the technique and agents used is still highly promising. Photodynamic therapy has been used to treat cancers of the brain, lung, pancreas, intraperitoneal cavity, breast, prostate and skin [Dolmans 2003].

The therapy involves the administration of a photosensitiser into tumour tissue by local injection. Photosensitisers are able to absorb light because they are aromatic compounds carrying a large number of conjugated π-electrons. The therapy is continued by local irradiation leading to photoactivation of the sensitiser. Lasers, fluorescent lamps, or other light sources are applied at a wavelength matching its absorption spectrum. The activated substance produces reactive oxygen species (ROS) from tissue oxygen. Reactive oxygen species, in turn, kill tumours or destroy tumour-associated vasculature. Reactive oxygen species are characterised by a short half-life and damage only cells that are proximal to the area of the ROS production. For instance, the action radius of the highly reactive singlet oxygen is below 0.02 µm [Dolmans 2003]. Photodynamic therapy also evokes a tumour cell specific immune response to some extent. Cytotoxicity caused by PDT is limited to the area of photosensitiser localisation. If the tissue is not directly accessible to irradiation, a cylindrical fiberoptic is used to guide the light into the tumour.

The extent of photodamage and cytotoxicity is multifactorial. It depends on the type of sensitiser used (localisation, dose administered), the parameters of irradiation (light exposure dose, light fluence rate), the type of tissue (oxygen availability), and the interval between drug administration and light exposure [Dolmans 2003].

Haematoporphyrin derivatives are widely used as photosensitisers. The standard clinical sensitiser, Photofrin®, includes several of these compounds. Although Photofrin® was proven efficient, a number of drawbacks underpin the need of further research for an alternative substance: Its ingredients are poorly defined, its persistence in the body results in long-term skin photosensitisation, and the molar absorption coefficient is low.

The Photosensitiser Hypericin

A promising alternative is *hypericin*. This polycyclic dione is found in Hypericum plants (St. John's wort) and is most sensitive to light of 595 nm wavelength. It preferentially accumulates in the membranes of the endoplasmic reticulum and Golgi apparatus and mediates apoptosis by a number of biochemical pathways upon photoactivation. It is barely cytotoxic in the dark.

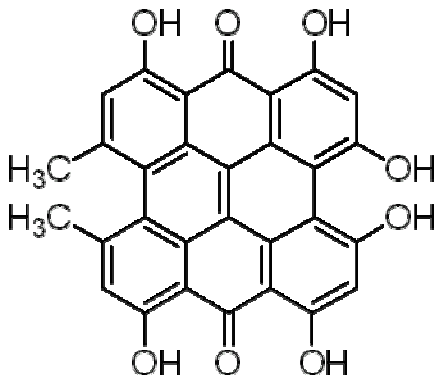

Figure 2-4: Structure of hypericin

Molecular biological research on biochemical pathways that lead to hypericin induced apoptosis was performed by Hendrickx and co-workers [Hendrickx 2003]. They suggested a possible improvement of the therapeutic efficacy by combination of photodynamic therapy with pyridinyl imidazole inhibitors of p38 mitogen-activated protein kinase (MAPK). The kinase may also be activated by photodynamic therapy**,** which in turn triggers angiogenesis and cell growth due to up-regulation of the gene that codes for cyclooxogenase-2 (COX-2). *In vivo* data on photodynamic therapy with Photofrin® revealed that COX-2 inhibition contributes to increased anticancer activity mainly by reducing the release of growth promoting factors, which otherwise may support tumour re-growth and neo-vascularisation after photodynamic therapy [Ferrario 2002, Hendrickx 2003, Makowski 2003].

A standard method to determine the effect of PDT is a common cell viability assay. The dye 3-(4,5-dimethylthiazol-2-yl)-2,5-diphenyltetrazolium bromide (MTT) is supplied to the cell culture and subsequently reduced by mitochondrial dehydrogenases of viable cells. The resulting product formazan is of blue colour and can be quantified photometrically. Hence, poor conversion of the yellowish MTT solution into blue formazan indicates cell impairment.

Several *in vitro* approaches were reported for PDT using hypericin [Paba 2001, Hendrickx 2003, Martinez-Poveda 2005]. Various excitation systems with and without filter systems were applied, as fluorescent lamps, argon lasers, and halogen lamps. Fluence rates ranged from 0.002 to 12 W/cm², exposure doses from 4 to 16 J/cm² or 120 J/cm² for an *in vivo* approach [Du 2003]. Hypericin was administered at concentrations from 1 to 1000 nM at incubation periods of 16 to

48 hours. As these parameters need to be individually adapted to the respective cell culture, the importance of a real-time monitoring system becomes obvious.

2.2 Cell-Based Biosensing

A biosensor is a solid-state sensor that carries biologically derived molecules on its sensor surface [Kovacs 1998, Ziegler 2000]. The biological material is the sensitive element of the device and acts as a primary transducer, corresponding to a secondary transducer that generates signals that can be monitored and processed. In the case of cell-based biosensors, whole cells are cultured on the sensor surface as primary transducer. Cell features as metabolic activity, selectivity of interactions, and electrogenic activity offer new perspectives in cell-based biosensing [Bousse 1996]. Because living cells require finely tuned physiological conditions, such sensing systems are not always robust and also require sample conditioning.

2.2.1 Impedance Analysis

Interpretation of cellular signals in cell-based biosensing is performed by a secondary transducing method, for instance electrochemical impedance spectroscopy (EIS).

Impedance Spectroscopy

Impedance Spectroscopy is a powerful method for characterising electrical properties of materials and their interfaces with electrically conducting electrodes. Generally, an electrical voltage (stimulus signal) is applied to the electrodes, and the resulting current passing through the solid or liquid sample is measured as response. The overall response is composed of many processes that are mainly the transport of electrons or charged ions through the bulk sample and its interfaces. Hence, the flow profile (or current response) reflects structural properties of the sample.

Different kinds of stimuli are applicable [Barsoukov 2005]. For instance, a *step function* is easily accomplished, but associated with the integral transformation of the time-varying current. *Random white noise* records the whole response over a wide spectrum instantly, but requires true white noise [Wiegand 2003]. In the most common method, a *small-amplitude AC signal* is applied that sweeps over a wide range from milli- to megahertz frequencies.

There are many fields of application, as quality control of paints and emulsions, electroplating, thin-film technology, corrosion, but also investigation of biological issues as biological membranes.

Impedance Theory

The response to a sinusoidal small-signal voltage *v(t)* with the frequency ω and the amplitude V_m

$$v(t) = V_m \sin(\omega t) \tag{2-4}$$

is the current

$$i(t) = I_m \sin(\omega t + \theta)\,. \tag{2-5}$$

The phase difference θ between the voltage and the current of the investigated system is zero for purely resistive systems, + 90° for an inductance *L*, and – 90° for a capacitance *C*. The response of a capacitor *C* and an inductance *L* is given by the equations

$$i_C(t) = C\frac{dv(t)}{dt} \tag{2-6}$$

and

$$v_L(t) = L\frac{di(t)}{dt} \tag{2-7}$$

In order to introduce the complex impedance, the two differential equations can be transformed into the complex domain

$$I(j\omega) = C\omega j\, V(j\omega) \tag{2-8}$$

and

$$I(j\omega) = \frac{V(j\omega)}{L\omega j} \tag{2-9}$$

with

$$j \equiv \sqrt{-1}\,. \tag{2-10}$$

The relation between the frequency domain voltage and current is now given by the complex impedance (analogous to Ohm's law for DC voltages)

$$Z(j\omega) = \frac{V(j\omega)}{I(j\omega)}\,. \tag{2-11}$$

This complex impedance function $Z(j\omega)$, or simply $Z(\omega)$, can be interpreted as a vector in the right-hand orthogonal system, as illustrated in Figure 2-5:

$$Z(\omega) = Z' + jZ'' \tag{2-12}$$

with the real part

$$\mathrm{Re}\{Z\} \equiv Z' = |Z|\cos(\theta) \tag{2-13}$$

and the imaginary part

$$\mathrm{Im}\{Z\} \equiv Z'' = |Z|\sin(\theta). \tag{2-14}$$

In the complex plane the vector is characterised by the phase angle

$$\theta = \tan^{-1}\left(\frac{Z''}{Z'}\right) \tag{2-15}$$

and the modulus

$$|Z| = \sqrt{(Z')^2 + (Z'')^2}. \tag{2-16}$$

The arrow tip moves along a curve for varying frequencies, because impedance is frequency dependent (except for ideal resistors).

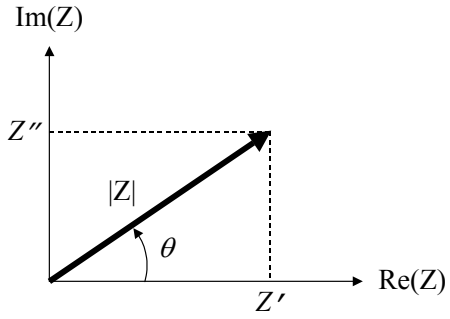

Figure 2-5: Impedance displayed in the complex plane. After [Barsoukov 2005].

Impedance Data Acquisition and Analysis

To determine impedances technically, the sample is connected to at least two probing electrodes and the impedance value is computed from the stimulation signal and the response. Real and imaginary parts are acquired and stored. Impedance magnitude and phase are derived by equations (2-15) and (2-16) for each frequency point.

Electrical properties of the investigated system are finally modelled from experimental data. Therefore, a so-called *equivalent circuit* is developed for the specific situation that describes the investigated system as a network of impedances. Structures that hinder current flow are represented by resistors, those that accumulate charge by capacitors, those that induce current as inductors. The circuit is then improved by a repeated modelling process.

In Figure 2-6 an example equivalent circuit is shown that was simulated in the frequency domain (A) and in the complex domain (B to D). Impedance magnitude and impedance phase are displayed in *Bode diagrams* which is advantageous for an initial survey covering a wide frequency range (Figure 2-6 B+C). Impedance imaginary part over real part is displayed in the *Nyquist plot* that focuses on low frequency data (Figure 2-6 D).

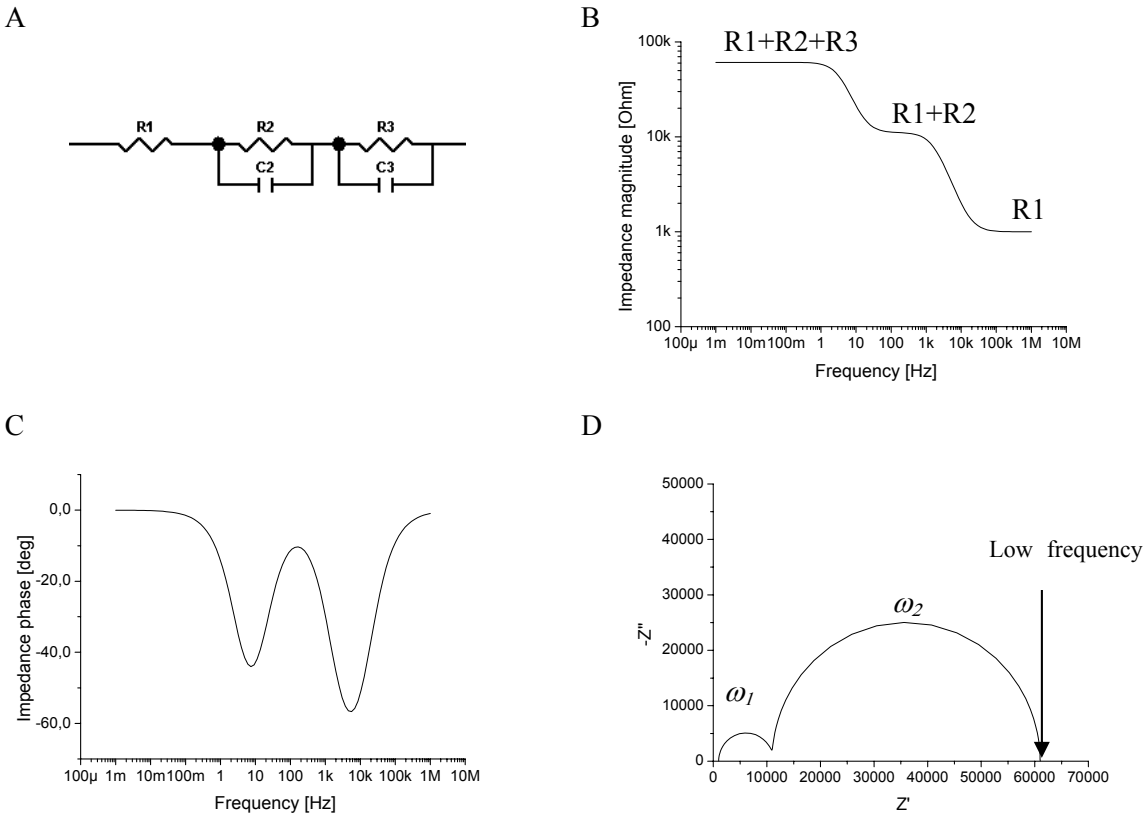

Figure 2-6: Impedance simulation of a sample circuit. (A) Equivalent circuit with R1 = 1 kΩ, R2 = 10 kΩ, C2 = 10 nF, R3 = 50 kΩ, and C3 = 1 µF. (B, C) Bode diagrams with impedance magnitude and impedance phase over frequency. (D) Nyquist plot with negative imaginary part of real part over impedance Z. Apex frequencies ω_1 and ω_2 allow an estimation of the capacitance C of the RC element, according to equation (2-17).

Information on the components contributing to the system response can be derived from both kinds of representations. The slope m of the curve of Figure 2-6 B refers to resistive ($m = 0$), capacitive ($m < 0$), or inductive ($m > 0$) influences. Impedance magnitude at 1 mHz equals the sum of R1, R2, and R3 because C2 and C3 block currents at low frequencies. Magnitude at 1 MHz equals to R1, because the current by-passes R2 and R3 via capacitances C1 and C2 in this case. The phase plot (Figure 2-6 C) also indicates capacitive, resistive, and inductive influences correlating to the magnitude plot. Impedance phase, as the divergence of current and voltage signal, is shown in degrees. For purely capacitive behaviour, the current is out of phase by +90°. In the Nyquist plot (Figure 2-6 D), resistances can be derived from the distance of semi-circles from the origin and the diameters of semi-circles. A semi-circle represents a RC combination in parallel. The frequency ω at the apex of a semicircle equals to

$$\omega = \frac{1}{RC}, \tag{2-17}$$

which can be used to estimate the capacitance C [Hamann 1985].

Cell Impedance Sensing

Impedance analysis is not restricted to electrochemical measurements monitoring anode and cathode processes in an electrolyte, but can also be applied to biology. The most prominent application in this field might be the determination of body fat with bio-impedance analysis. Here, impedance analysis of the human body connected to electrodes elicit information on water content and ratio of muscle/fat tissue due to different response characteristics to the stimulating signal.

Cells can also be investigated by EIS *in vitro* to analyse metabolic activity or cell-substrate interaction. This *cell impedance sensing* is performed either on cells that are suspended in culture medium or on cells cultured directly onto a sensor. Adherent or cultured cells are sensed on a single electrode against a (distant) counter electrode. In Figure 2-7 A, cells are shown that cover an electrode of 250 µm in diameter on a commercially available impedance sensing system (Applied Biophysics, Troy, USA) that is described in detail below. The cultivation of single cells on so called *microelectrodes* of diameters down to 5 µm (Figure 2-7 B) is less common. Another type of electrode is the *interdigitated electrode* that comprises both electrodes, working and counter electrode, as finger-like structures next to each other (Figure 2-7 C).

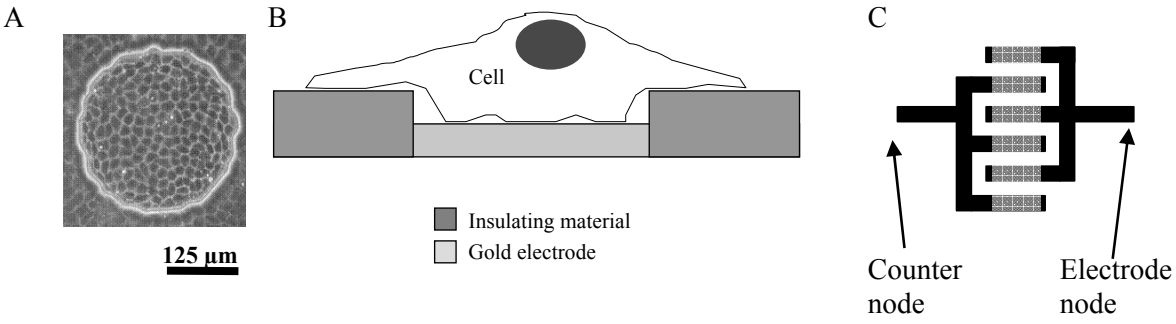

Figure 2-7: Cell Impedance Sensing. (A) Confluent cell monolayer on a large circular electrode [Wegener 2006]. The rim around the electrode indicates the electrode boundary. (B) Schematic drawing of a single cell, placed on an electrode. (C) Interdigitated electrode composed of three fingers each. Black electrode areas are insulated whereas grey areas represent the activate electrode area.

Impedance sensing of cells at a fixed frequency with phase-sensitive detection was first described in 1984 as electrical cell impedance sensing (ECIS) [Giaever 1984]. Lung fibroblasts were cultured on electrically wired Petri dishes, and an AC voltage was applied to a single sensing electrode integrated in the dish. The resulting voltage was measured using a lock-in amplifier.

Giaever and Keese developed a commercially available measurement system for Electric Cell-Substrate Impedance Sensing (Figure 2-8). It was communicated as a cell morphology biosensor using planar gold electrodes and was employed for the determination of micromotion, metastasis activity, and adhesion processes as well as for wound-healing assays [Giaever 1991, Lo 1995].

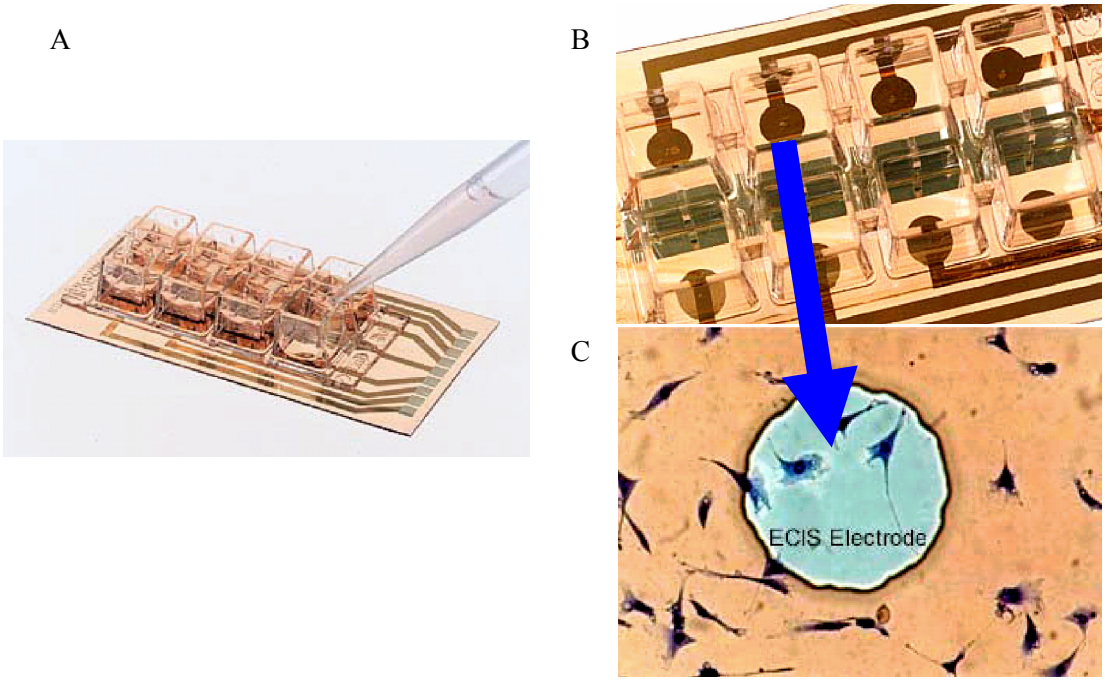

Figure 2-8: ECIS™ sensor device. (A) Loading of the 8-well sensor. (B) Closer image on culture wells and (C) on an integrated electrode. Each well is equipped with an electrode of 250 µm in diameter and a large counter electrode (black stripe along the centre) [Applied Biophysics 2004].

2.2.2 Cell-Substrate Modelling for Impedance Analysis

The impedance change of a cell layer located on a metal microelectrode in response to a sinusoidal signal is determined by a number of elements as wires, the electrode-electrolyte interface, the electrolyte with non-adherent cells in suspension, and the adherent cells. In addition, one has to take into account that the cell layer is very heterogeneous. For instance, partial coverage and the quality of the sealing between cells (gaps and junctions) influence the system response. Moreover, the composition of the cell membranes loaded with different pores, ion channels, and transporters strongly define electrical characteristics. But also the effect of the cell's interior consisting of an aqueous cytosol and membrane-equipped organelles have to be considered. Below, these elements are addressed in detail with respect to their contribution to impedance measurement results.

Wires and Connectors

Whereas the resistance of wires is low and therefore negligible, stray capacitance and stray inductance of wires has a higher relevance for modelling cell-substrate interaction. Stray capacitance can affect the accuracy of the measurement particularly at low frequencies and for high impedance samples. In contrast, stray inductance is mostly discernible for low impedance samples at high frequencies [Bio-Logic 2007].

Electrolyte

The resistive component of this impedance is given by

$$R_{electrolyte} = \frac{s}{A\,\kappa} \tag{2-18}$$

with length s of the current path, area A, and electrolytic conductivity κ. Usually, the impedance of the cell culture medium is below 100 Ω and therefore negligible.

Electrode-Electrolyte Interface

Various models of charge distribution at the electrode-electrolyte interface and its spatial arrangement were published. The recent model of the electrical double layer is based on the work of Helmholtz published in 1879 [Geddes 1972]. According to Helmholtz, a double layer manifests as ions tightly bind to the electrode surface, and a counter-layer of oppositely charged ions builds up in the solution (Figure 2-9 A). In 1910, Gouy proposed an arrangement of a diffuse and a fixed layer taking thermal motion of ions into account (Figure 2-9 B). In 1924, Stern added the possibility that the negative charge in the fixed layer could overbalance the positive charge of the electrode (Figure 2-9 C). Another modification of the model was performed by Gouy, who introduced an exclusively diffuse layer (Figure 2-9 D). Following this

model, charge separation induces a linear potential drop close to the electrode, bordered by the inner Helmholtz plane. Then, the potential declines exponentially with distance from the electrode. The actual charge distribution depends on the type of metal and electrolyte used.

However, non-ideal metal electrodes are not sufficiently described by a capacitive electrode-electrolyte coupling. Due to electrochemical reactions on the surface some charge leaks across the interface (faradaic currents) experiencing a charge transfer resistance and a Warburg impedance (Figure 2-9 E). The latter is related to diffusion of ions from the bulk electrolyte to the interface [Ehret 1997].

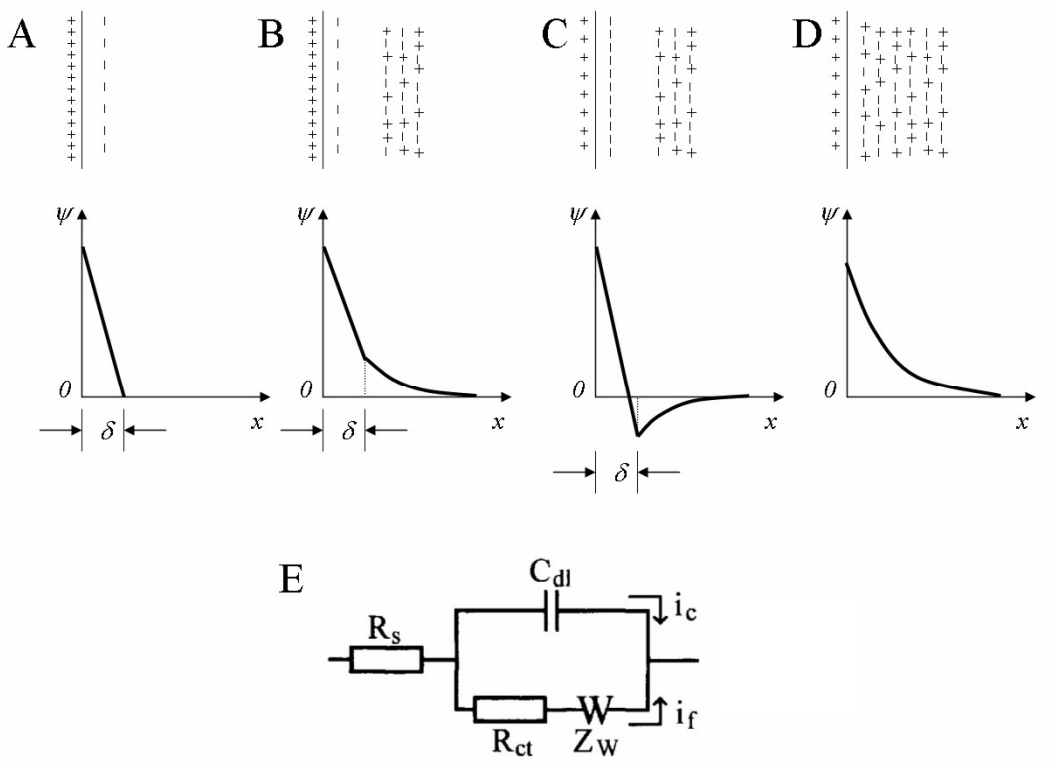

Figure 2-9: Electrode-electrolyte interface. (A) - (D) Sketches of electrochemical double layers after [Geddes 1972]. Charge distribution at the electrode interface region is shown as (+) and (-) and as a potential ψ over distance x. The distance δ indicates the Helmholtz plane. (E) Electrochemical equivalent circuit for a metal electrode submersed in electrolyte with R_S resistance of the solution, C_{dl} the double layer capacitance, R_{ct} the charge transfer resistance, and Z_W the Warburg impedance [Ehret 1997].

Interface Impedance Modelled by the Constant Phase Element

Experiments reveal that the model presented in Figure 2-9 E do not accurately fit data of typical electrodes used in impedance analysis. Indeed, it was only found to be a suitable description when perfectly smooth mercury electrodes are used [McAdams 1995]. A comparison of the circuit simulation and real data of a rough surfaced Ag/AgCl ink electrode is given in Figure 2-10. The Nyquist plot format was chosen to focus on high frequency data where the impedance behaviour differs most.

Many attempts have been performed before to describe the impedance of rough metal-electrolyte interfaces, but failed to model the system correctly because too many variables were used, or assumptions were questionable.

Then, real impedance data was modelled more accurately by an empirically developed element that lacks a physical background which brought up controversial discussions. The constant phase element (CPE), also described as *constant phase angle* or *distributed circuit element,* was first applied in 1984 by Van den Eeden [McAdams 1995] as a model for electrode surfaces. The term *constant phase* refers to the angle ϕ of the impedance locus against the *Z'* axis in the Nyquist plot, as illustrated in Figure 2-5. This constant phase angle impedance was often observed on solid metal electrodes over a limited frequency range and was, most likely, referred to surface roughness effects.

The empirical equation for the CPE is given as

$$Z_I = K\left(j\omega\right)^{-\beta}, \tag{2-19}$$

where K is a measure of the magnitude of Z_I, and β a fractional power constant related to the grade of surface roughness with $0 < \beta < 1$. A value of 1 equals to a perfectly smooth surface. β is associated with the phase angle by

$$\phi = \beta\pi / 2 \tag{2-20}$$

or

$$\phi = 90° \beta \tag{2-21}$$

[McAdams 1995, Fricke 1932].

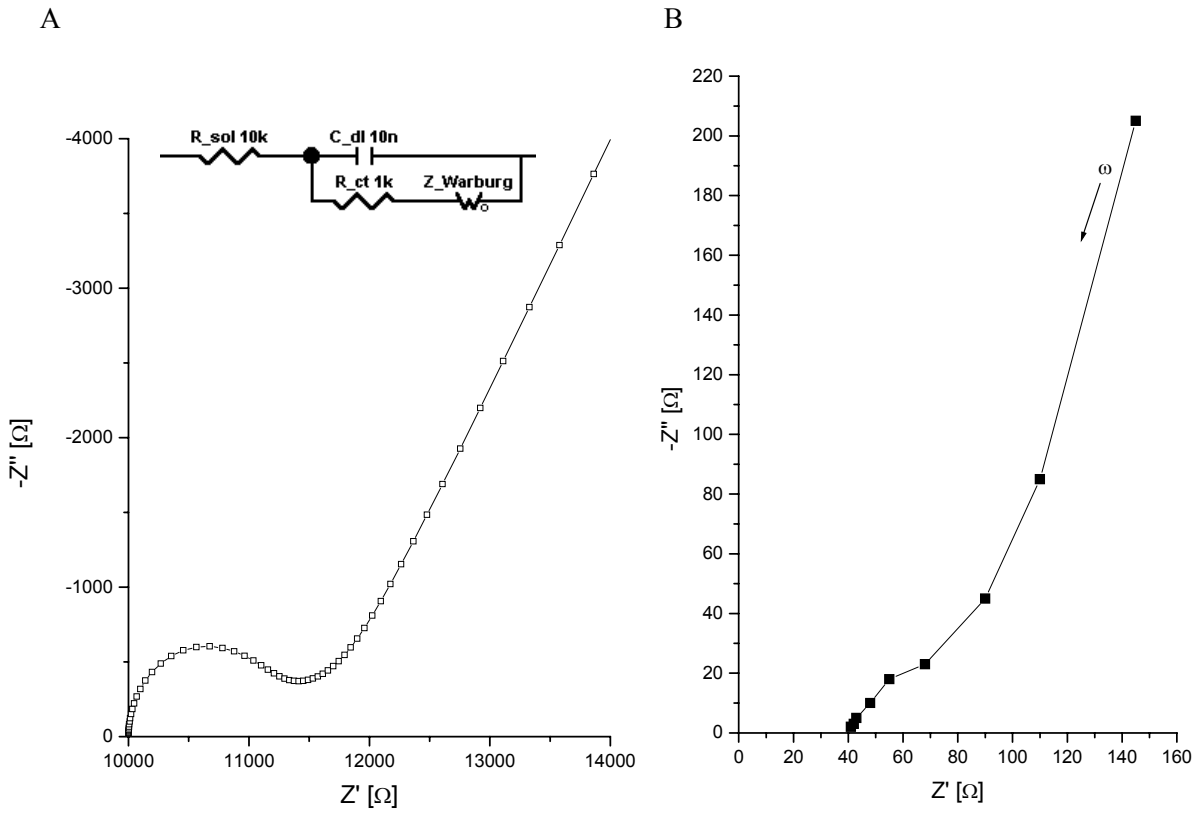

Figure 2-10: Impedance locus for Warburg impedances; according to Figure 2-9 E. (A) Simulation result of the equivalent circuit (inset) for an ideal, smooth electrode. (B) Impedance result of a real-world porous electrode. Both diagrams after [McAdams 1995].

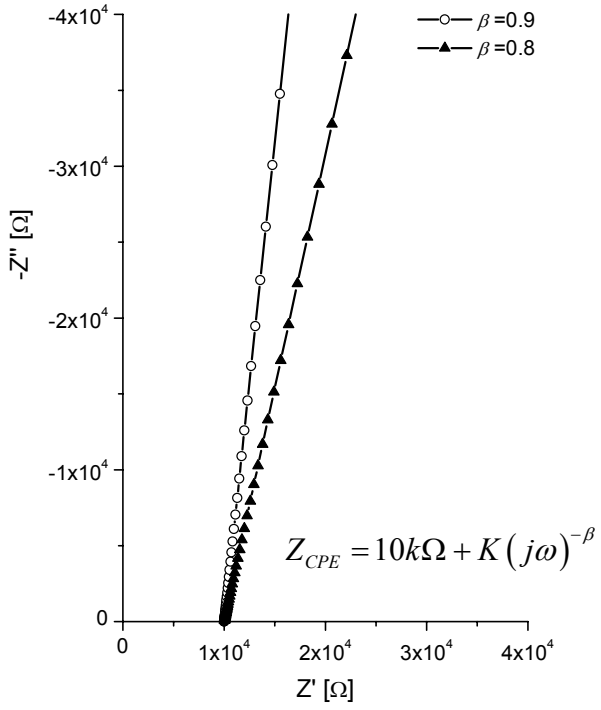

Figure 2-11: Constant phase element in the complex plane. CPE impedance locus for different fractal dimensions β.

The empirical description of the rough surface by the CPE finally received support from Mandelbrot's work on fractal geometry [Mandelbrot 1983]. According to the fractal concept, a single parameter, the fractal dimension *D*, is capable of characterising a rough surface without the need of a detailed description. Using these concepts the following expression was derived [Nyikos 1985]:

$$Z_I = R_{total} + A\left(Z_S\right)^{\beta} \tag{2-22}$$

where Z_S is the anticipated interface impedance in the absence of surface effects, β is a fractional power ($0.5 < \beta < 1$) related to the fractal dimension of the electrode surface, A is a proportionality constant which contains all frequency-independent factors, and R_{total} is the resistive influence of the electrolyte and leads. At high frequencies Z_I is dominated by C_{dl} and therefore equation (2-22) approximates to

$$Z_I = R_{total} + K\left(j\omega\right)^{-\beta} \tag{2-23}$$

where

$$K = A\left(C_{DL}\right)^{-\beta} \tag{2-24}$$

[Nyikos 1985].

Homogenous Layers on an Electrode

In impedance analysis, coatings are often modelled as *RC elements*, composed of a capacitance and a resistance in parallel. The capacitance *C* comprises dielectric properties of coating material and electrolyte, the distance, and the sensing area. The resistance *R* is a measure of sealing quality. These RC elements are characterised by a time constant τ with

$$\tau = RC\,, \tag{2-25}$$

where the time constant τ is related to the frequency domain by

$$f = \tau^{-1}\,. \tag{2-26}$$

The influence of slight changes of the RC element components is shown in Figure 2-12. Three circuits are simulated over a frequency range from 1 Hz to 10 GHz. The electrode is simplified in all cases to a 1 nF capacitor *C*, and the coating capacitances *C1* and *C2* are both set to 100 pF. Only the coating resistors *R1* and *R2* are varied. Simulations in a Bode plot (Figure 2-12 A+B) illustrate that RC elements are reflected as impedance phase maxima. Analysing two RC elements in series (red line) reveals that the RC element with the larger time constant clearly dominates over the smaller one.

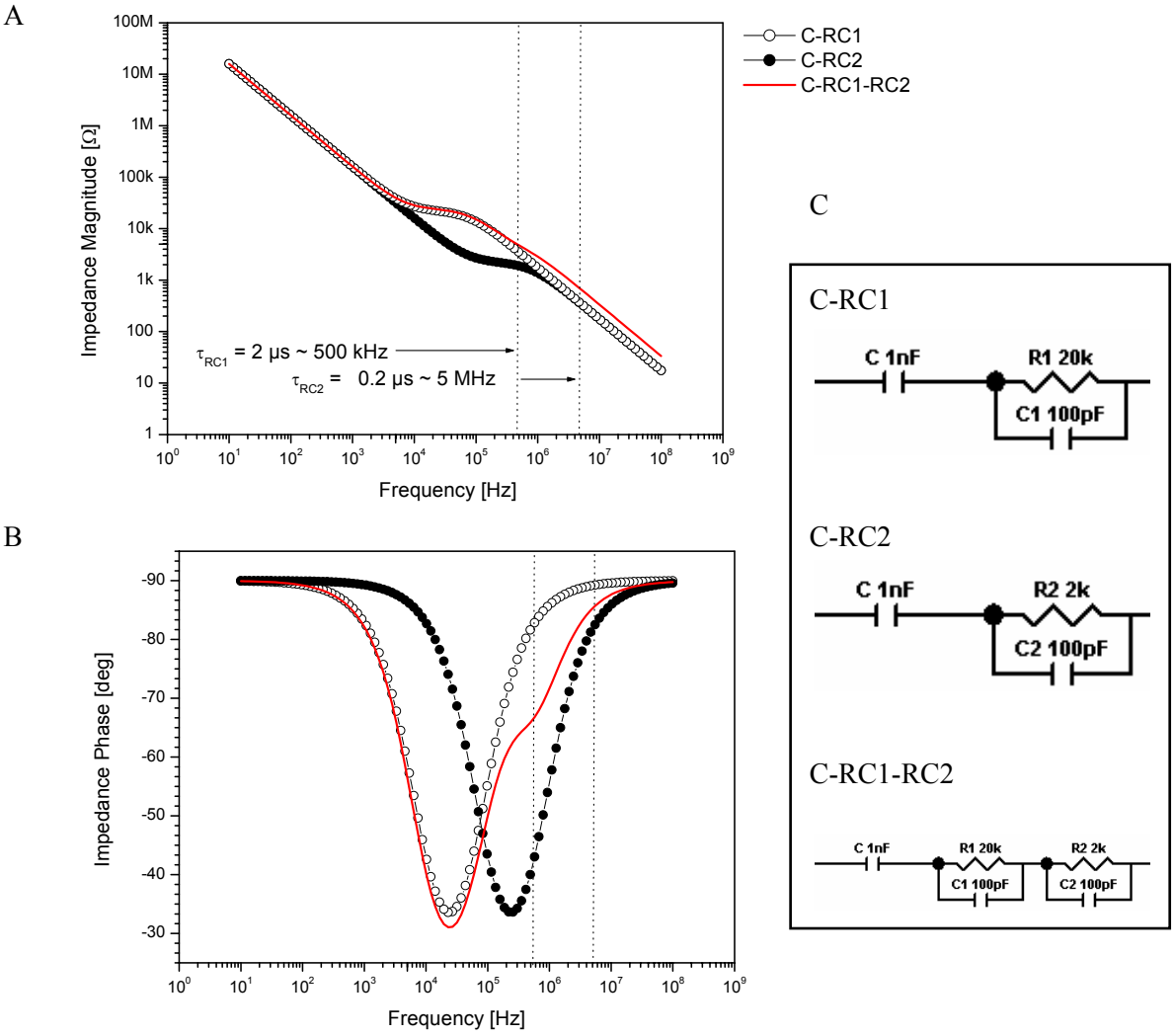

Figure 2-12: Impedance analysis of RC elements. (A) Magnitude plots and (B) phase plots of a (C) simulation circuit.

Confluent Cells on Electrodes

Another type of coating with very heterogeneous properties is represented by biological cells, that adhere as a tight layer to the electrode. This confluent cell layer also blocks currents and cause an increased electrode impedance [Schwan 1963].

A schematic illustration of a group of cells attached to a microelectrode is shown in Figure 2-13 A. The counter electrode is integrated into the sensor surface and therefore currents must not necessarily pass the confluent cell layer. Thus, the cell/substrate gap can also permit currents beneath the cell layer.

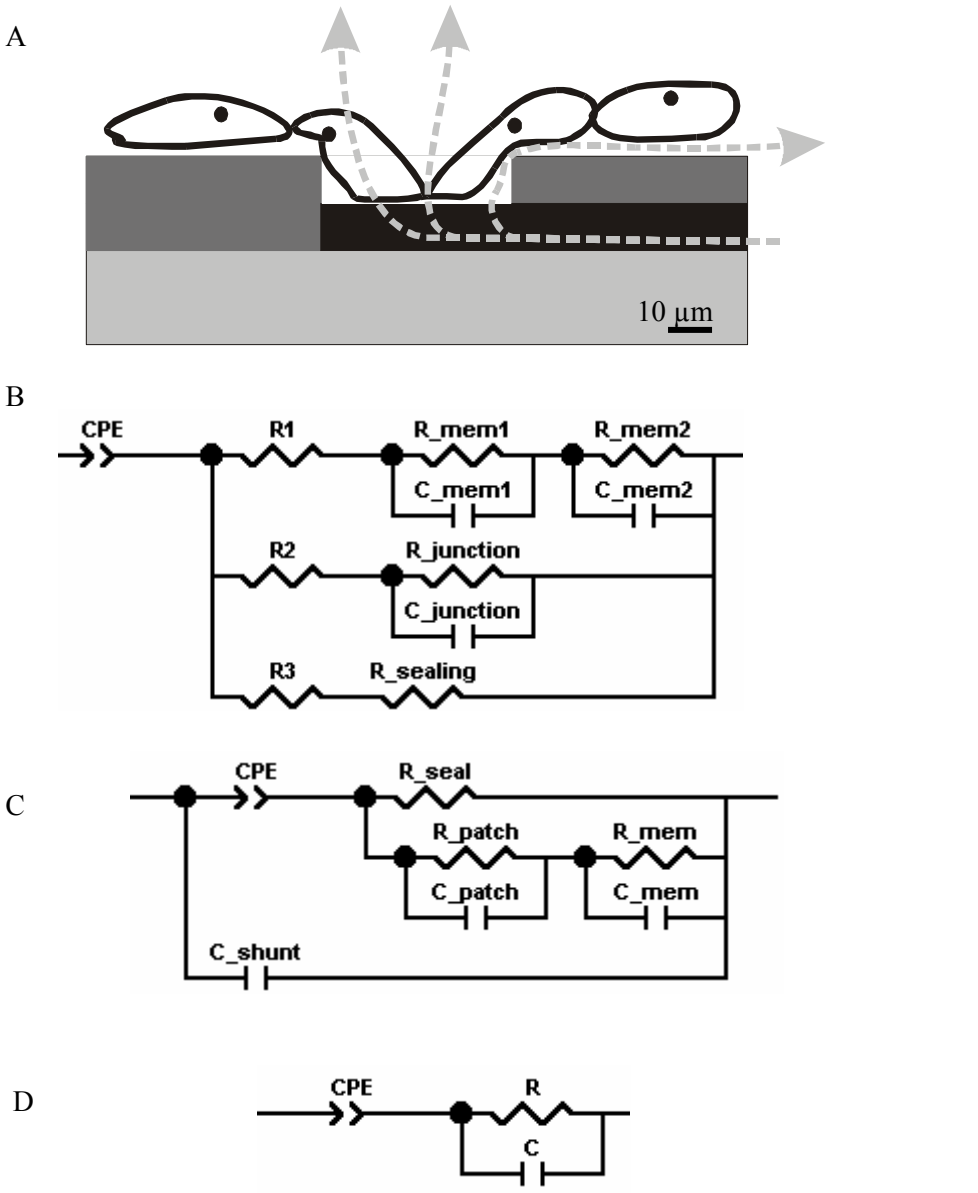

Figure 2-13: Confluent cells on a microelectrode. (A) Schematic illustration with cells on a microelectrode (black) and insulation layer (dark grey) on glass substrate (light grey). Arrows show possible current path between working and counter electrode. (B) Equivalent circuit of current path that enter the sensor surface through the electrode on the right. Three current path refer to the arrows of part (A). R1 to R3 consider electrolyte resistances. (C) Circuit used for simulation of the neuron-electrode contact [Buitenweg 1998]. (D) Simplified equivalent circuit for modelling impedance data.

A variety of current pathways between electrode and counter electrode are imaginable focusing on analysis. Some are depicted as arrows in Figure 2-13 A. Currents may pass through the cells across the basal and the apical cell membranes, through the junction between two cells, or may bypass cells via the cell/substrate gap between sensor insulation and basal cell membranes.

This situation leads to the equivalent circuit presented in Figure 2-13 B. The electrode impedance is modelled as a CPE. Miscellaneous resistances of e.g. the electrolyte or adsorbed protein layers are recognised as resistances R1 to R3 specifically for each branch although they are presumably small against membrane or sealing resistance. The sealing quality of the cell layer is represented by the resistance $R_{sealing}$ depicted in the bottom branch.

A simulation of a neuron on small gold electrode was developed by [Buitenweg 1998], shown in Figure 2-13 C. Cell membranes are considered as single RC elements (indices *mem* and *patch*). Moreover, a shunt capacitance counts for the capacitive coupling of the lead structures and the culture medium. The total impedance was defined as

$$Z_{total} = \frac{Z_{sh} Z_{CE}}{Z_{sh} + Z_{CE}} \tag{2-27}$$

with

$$Z_{sh} = \frac{1}{i\omega C_{sh}} . \tag{2-28}$$

and

$$Z_{CE} = Z_{electrode} + \frac{R_{seal}(Z_{mem} + Z_{patch})}{R_{seal} + Z_{mem} + Z_{patch}} . \tag{2-29}$$

Where index *CE* stands for the cell-electrode interface. Again, this is a model for simulation purposes, but not suitable for modelling real-world impedance data.

In summary, the physical situation of a cell layer covering an electrode is a complicated mesh of resistive and capacitive reactances. This needs to be simplified for successful, accurate impedance data modelling to a simplified representation as shown in Figure 2-13 D. A similar model with an additional electrolyte resistance placed in series to the RC element was already published in literature [Hillebrandt 2001].

Information Content of Cell-Substrate Modelling

With EIS, particularly in addition to optical microscopy, changes of the permeability and morphology of the cell layer due to biochemical signals can be monitored in real-time. A major application is the evaluation of the barrier function of a cell layer, which is normally performed by applying a DC voltage over the culture that is supported by a water permeable membrane. Using electrically wired impedance chambers as solid supports of the culture is advantageous, because cells are then in a more physiologically relevant condition [Wegener 1996].

The barrier function is determined by the ion permeability of the cell layer and measured as a *transepithelial or transendothelial resistance* (TER) with the unit Ωcm². TER values of epithelial or endothelial tissue are of high scientific interest, because epithelial cells cover all inner and outer surfaces of living organisms. In animals, they build up a highly selective permeability barrier between blood and tissue, e.g. the blood-brain barrier or the barrier between blood and cerebrospinal fluid. Values are in the range of 20 to 10,000 Ωcm² [Powell 1981, Hartmann 2007].

The TER parameter can easily be measured by EIS [Kottra 1984, Wegener 1996], when the area of the sensing electrode is adjusted to the kind of tissue leakage used in the experiment in order to keep the absolute resistance measured by the impedance spectrometer in a reasonable range. For example, large gold electrodes (0.45 cm²) were used for high resistant MDCK-I cells, and small electrodes (0.03 cm²) for cells that do not form tight junctions [Wegener 1996].

Impedance analysis on biological materials was reported for several more applications: Estimation of microbial biomass [Harris 1985], detection of protein adsorption to supported lipid bilayer [Stelze 1989], microbial metabolism [Palmqvist 1994], investigation of changes in membranes of biological cells in suspension [Matanguihan 1994], monitoring of enzyme reactions [Hintsche 1994], and detection of immunological reactions [DeSilva 1995].

In contrast to EIS, single frequency impedance sensing stimulates the sample at a fixed frequency rather than over a wide frequency range. This method only focuses on monitoring impedance and phase changes with time and is therefore suitable for monitoring dynamic processes like cellular motion, adhesion, and detachment processes.

2.2.3 Electrophysiological Recording of Action Potentials

Electrogenic cells generate action potentials (see Chapter 2.1.2) that can be recorded applying electro-physiological methods. Upon exposure to harmful chemicals and toxins, cells display altered electrical activity and therefore, registration of the electrical activity is an interesting sensing principle. Very sensitive and specific sensor systems can be designed using *intra-* and *extracellular recording* because they take advantage of the cells' highly specialised biochemical pathways.

Intracellular Recording

Intracellular recording is performed using an electrolyte-filled micropipette that is inserted into the cell. Successful puncture forms a tight sealing between electrode and membrane. The membrane potential of the cell equals the potential between electrolyte and culture medium and can therefore be registered as the *transmembrane potential*.

Monitoring currents through single channels using the *Patch-Clamp-Technique* involves no direct puncture of the cell membrane, moreover a membrane patch is clamped to a microelectrode. This is caused by a light suction through the electrode in order to build up a tight sealing [Hamill 1981]. In this case, the interior composition is maintained stable what is not always the case for other intracellular recordings and also whole-cell Patch-clamp recordings as cytosol may leak off. The non-puncturing patch-clamp recording allows direct monitoring of ion currents even at the level of single ion channels but has only limited relevance for multi-site recording. Additionally, impedance characteristics can be determined by applying this method. Fragility of the cell-electrode contact limits the duration of the experiment for all intracellular techniques to 2 to 3 hours of observation. Visual control is necessary to approach the cell with the electrodes.

Extracellular Recording

Disadvantages of the intracellular recording are addressed by applying *extracellular recording* methods. Cells are monitored using microwires placed in their vicinity, or cells were seeded on planar electrode arrays that were introduced in the 1970ies by Guenther Gross [Gross 1977].

Extracellular recording on microelectrode array (MEA) chips offers non-invasive and long-term monitoring of a large number of electrogenic cells. In contrast to the direct measurement of potentials using intracellular recording, extracellular recording involves capacitive coupling of cells to the electrode (see Figure 2-13 A). Here, local field potentials (LFP) between the basal cell membrane and the electrode are measured that evolve from ion currents across the membrane (see Chapter 2.1.2). Technically, the LFP is amplified against the counter electrode potential and is recorded as a so-called *spike* (Figure 2-14). Analyses of several parameters

derived from spike registration elicit information on the cell culture. Electrical activity therefore manifests in spike rate, amplitude, duration, shape, propagation characteristics, and synchronicity of the culture for instance.

A sensor typically comprises 60 electrodes that allow analysis of whole cell networks leading to an extended number of parameters because cell activity is also analysed cross-referentially. Therefore, applications were mainly developed in neural or cardiac research, as the detection of novel pharmaceutical compounds (drug discovery) or the evaluation of known compounds (safety pharmacology) [Stett 2003].

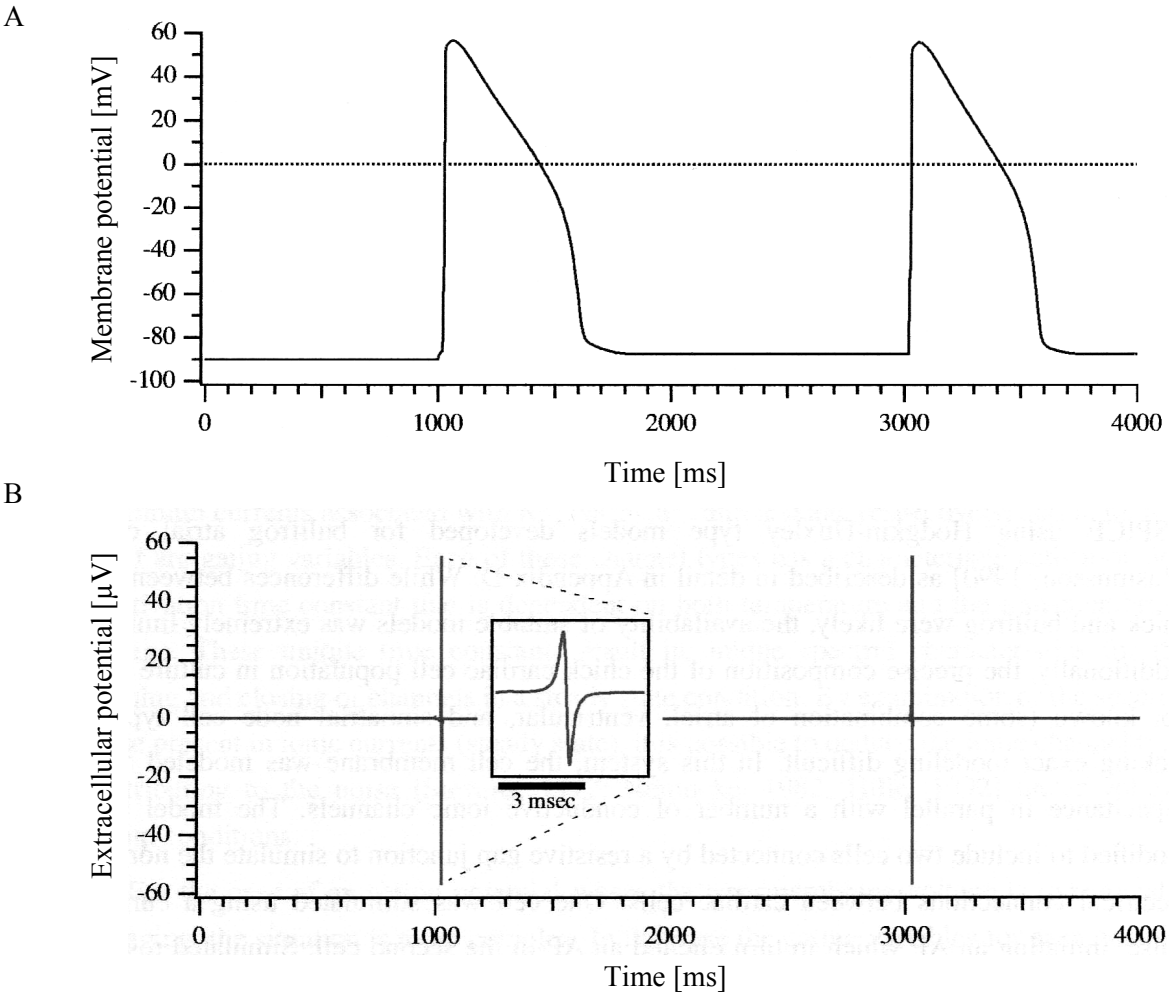

Figure 2-14: Action potentials are recorded extracellularly as so-called spikes. (A) Action potentials of cardiomyocytes simulated in HSPICE published by [Borkholder 1998]. (B) The second derivative of the action potential represents a close approximation to real extracellular spikes recordings - after [Borkholder 1998].

Coupling of Cells to Planar Microelectrodes

Successful extracellular recordings depend to a large extent on the quality of the cell-surface coupling (see Figure 2-13). A poor sealing of the cell-substrate gap causes leak currents that bypass the cell layer and weaken the detection of ion movements. Compared to the amplitude of an action potential measured across the membrane, extracellularly recorded LFP are rather small. Even for a tight sealing, a cardiac action potential of approximately 60 mV is extracellularly monitored as spike with a peak-to-peak amplitude rarely exceeding 2 mV.

Sealing quality can be expressed by a *sealing resistance* or a *sealing resistor* that hinders currents to circumvent the cell barrier. In contrast to neurons, cardiomyocytes form a tight monolayer on the chip surface and consequently provide a high sealing resistance R, resulting in an excellent signal-to-noise ratio.

The quality of the sealing also affects the shape of the extracellular signal [Borkholder 1998]. Impedance analysis was applied to estimate the sealing resistance.

A simultaneous application of extracellular recording and impedance analysis was published by [Rutten 2002]. The electrical activity of neurons can be stimulated *in vitro* by applying low voltage signals across working/counter electrodes. Cells were found to be sensitive only for a certain amplitude range of the stimulus signal, which varied with sealing resistance. Below that range, cells were not successfully stimulated while cell-destruction occurred above that range [Rutten 2002]. Reliability of electrical stimulation may be enhanced by prior determination of the sealing resistance using impedance analysis.

Microelectrode Arrays

A microelectrode array (MEA) incorporates dozens of microelectrodes integrated on a glass substrate. Electrodes are sized 10 to 30 µm in diameter and connected via insulated leads to peripheral pads that allow electrode monitoring.

In Figure 2-15 A, a commercially available MEA chip is shown (Multichannel Systems, Reutlingen, Germany). Electrodes are integrated in the centre of the glass substrate. A containment ring is placed around the array in order to provide a dish for the cell culture at a volume of approximately 1 ml. Generally, electrodes are coated with an impedance reducing material (see Figure 2-15 D) to improve the signal-to-noise ratio as titanium nitride, indium tin oxide, or platinum black.

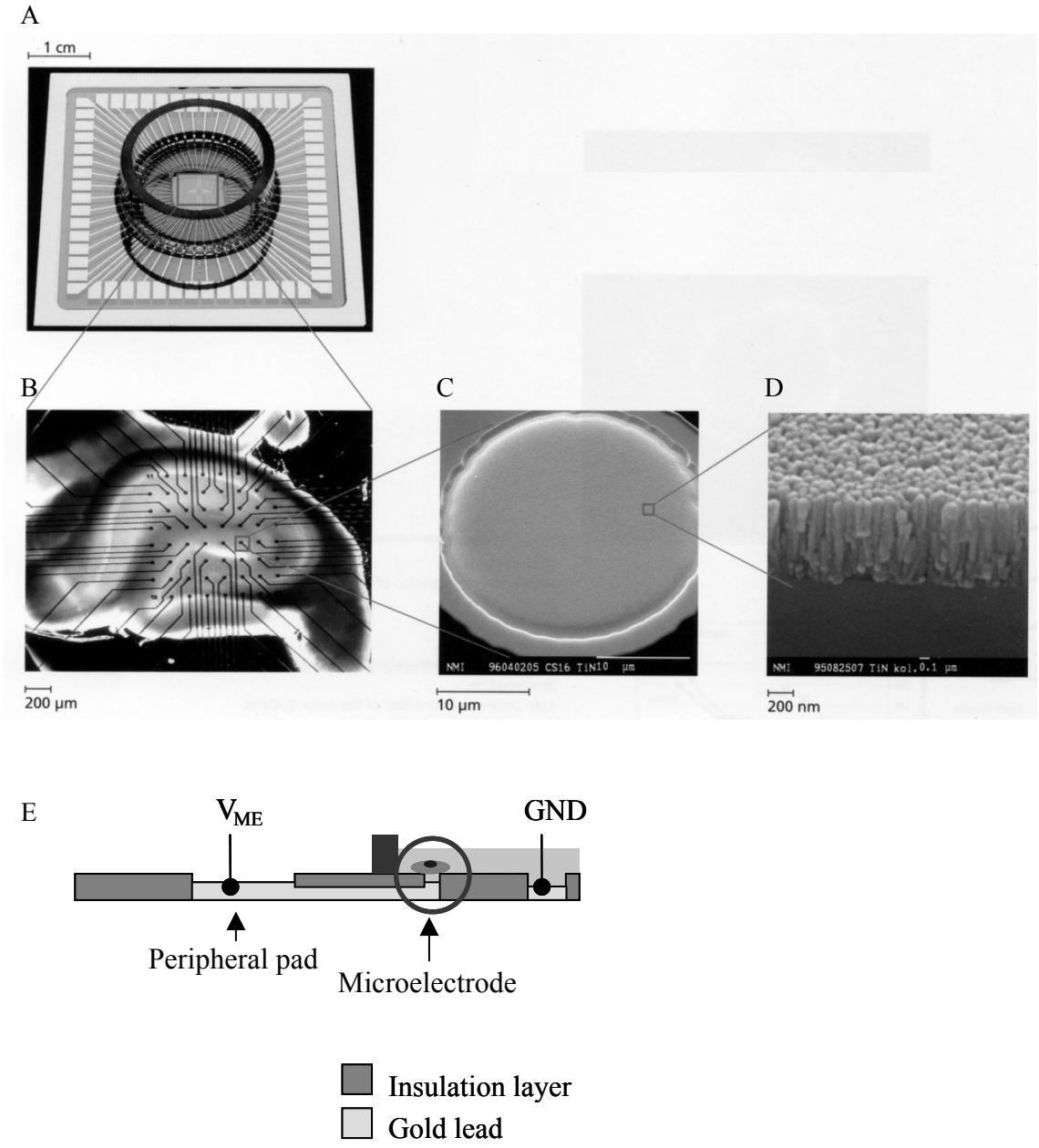

Figure 2-15: Commercial MEA sensor. (A) Whole device (Multichannel Systems, Reutlingen, Germany). (B) A brain slice positioned on the microelectrode array. (C) Scanning electron micrograph of a single microelectrode. (D) Titanium nitride coating on electrode [NMI 2003]. (E) Schematic cross-section of a MEA sensor. The cell/electrode contact is marked by a circle. Cells were incubated in culture medium (light grey) inside the containment ring. The electrode potential was differentially amplified against a counter electrode (GND) via insulated gold leads connecting microelectrodes to peripheral pads.

The cross-sectional sensor architecture is depicted in Figure 2-15 E. Cellular signals are transduced by a differential amplification of the electrode potentials of a cell-covered microelectrode and a cell-free counter electrode (GND). Electrically insulating material (Si_3N_4, SiO_2) covers the majority of the sensor at a layer thickness of 600 to 1000 nm and is only removed at electrode sites.

The number of electrodes is not limited as the following examples show. A MEA chip was manufactured in CMOS technology with integrated multiplexing structures connecting 16 x 16 electrodes [DeBusschere 1998, 2001]. Another sensor involved the integration of light addressable electrodes resulting in a MEA chip with 3600 electrodes. Electrodes were addressed by focussing a laser beam on a photo conductor connected to an underlying indium tin oxide lead. Using this technique, extracellular recording of cardiomyocytes has been successfully performed [Bucher 2001].

2.2.4 Other Methods

In this chapter some other techniques investigating cell-substrate interaction will be presented in short. The addressed techniques offer additional insights and help to understand the phenomena inherent to the interface of cells and substrate.

Minute changes in cell monolayers were quantitatively measured using *THz differential time-domain spectroscopy* [Liu 2007]. This technique may become a powerful method when *in-situ* monitoring has been made feasible. So far, cells have to be extracted from the culture medium.

Real-time extracellular attachment to and detachment from metal surfaces can also be investigated by the *Quartz Crystal Microbalance* technique (QCM) [Gryte 1993, Reiss 2003, Li 2005]. As cells adhere to the quartz crystal, resonance properties – as frequency and bandwidth - change due to mass load and viscous dissipation. For instance, specific integrin-mediated adhesion of human ovarian cancer cells (OV-MZ-6) to distinct ECM proteins immobilised on gold-coated quartz crystal resonators were observed [Li 2005].

Forces at the cell-substrate interface were determined at high lateral resolution by using *Traction Force Microscopy*. Here, dynamics of cellular movements was visualised by pattern recognition of deformations in polyacrylamide substrates. For example, fibroblasts were monitored on collagen I [Munevar 2001] or endothelial cells on peptides carrying the RGD sequence [Reinhard-King 2003]. Other methods capable of imaging cell adhesion on solid substrates are *Total Internal Reflection Aqueous Fluorescence* and *Reflection Interference Contrast Microscopy* [Reiss 2003].

An important technique to determine the width of the cell-substrate gap is the *Fluorescence Interference Contrast* (FLIC) microscopy. This method allows measurement of the distances of biological materials to a silicon substrate with an accuracy of a few nanometers [Braun 1997]. It takes advantage of the interference of incident and reflected light above a mirror. The standing modes of the electromagnetic field above the surface of silicon modulate the excitation and the emission of a fluorescent dye, which is inserted into the cell membrane [Sorribas 2001]. Experiments revealed that cells compress the laminin cushion during adhesion [Zeck 2003]. Thus, the actual gap width is a measure for a balanced force system of repulsion and attraction. From these results one might expect that the protein binding force to the substrate is crucial and should be at least as strong as the laminin/integrin binding force.

2.3 Cell-Based Lab-on-Chip Systems

This section focuses on whole cell biosensing approaches realised *en miniature*. Devices that apply mechanical and electrical principles to sense biological material are called Biological Micro-Electro-Mechanical Systems (BioMEMS). Miniaturisation offers to use BioMEMS as *point-of-care* instruments and for the operation at a patient's bedside. Another main advantage is the simple implementation of an automated assay procedure to perform experiments with reproducible (statistically confirmed) results at reasonable cost for material and manpower. BioMEMS are designed to work with certain target structures, as molecules or cells. Here, selected BioMEMS are presented that investigate suspended or adherent cells.

2.3.1 Cell Suspensions in Microfluidic Systems

Cells that are suspended in culture medium are in a specific physiological state, different from that of adherent cells. They are less sensitive to shear forces and show a different gene expression pattern. Due to their small size (5 - 15 µm in diameter) and general robustness suspended cells have been in use with microsystems for twenty years.

In combination with suspended cells, BioMEMS were used to discriminate different cell types, to monitor cellular activity, to quantify DNA, or to insert DNA molecules into cells. In Figure 2-16 a selection of processing steps that were already implemented in BioMEMS is presented. Sample transport was realised by various methods that, for instance, take advantage of electrokinetic or electroosmotic properties of cells. During transition, cells were sampled, captured, and sorted (e.g. for viability criteria for instance). Depending on the application, cell membranes were disrupted or lysed for harvesting cellular DNA or proteins [Bashir 2004, Dittrich 2006].

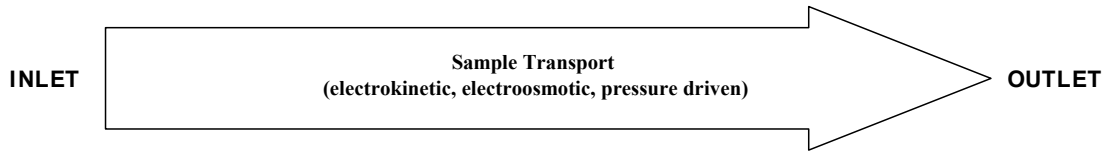

Sample Preparation	Selective Capture	Viability Control	Cell Lysing	Detection of DNA, Protein
Sorting, Trapping Filtration Electrophoresis Centrifugation	Antibody based	Optical Electrical	Electrical Mechanical Chemical	On-chip PCR Nanopores Nanowires Cantilevers

Figure 2-16: Optional processing steps for cells in suspension inside BioMEMS. After [Bashir 2004].

Sample preparation often includes cell sorting by fluorescence-activated discrimination or electrical field-based separation or simply by centrifugation and filtration. Electrophoresis has

limited applications for manipulation of cells because most biological cells have similar electrophoretic mobility [Andersson 2003]. Nevertheless trapping of *E.coli* from blood samples using dielectrophoresis has been reported to result in an enrichment factor above 30 [Bashir 2004].

Selective antibody based sampling and viability detection with impedance and fluorescent techniques (steps 2 and 3 in Figure 2-16) serve to select specific subsets of viable cells for further analysis.

Cell treatment steps target the release of DNA and proteins by electrokinetic fluid actuation, thermal cycling, sonication, electroporation, or pressure application [Andersson 2003]. Analysis of DNA and proteins was performed by various techniques that, in case of DNA, include amplification by polymerase chain reaction (PCR) or antibody based protein detection on cantilevers. Another kind of cell treatment involves the insertion of DNA molecules into living cells by electroporation using electric field pulses, puncture by microneedles and microteeth, or cell fusion by pulsed electric fields (electrofusion).

Electrochemical Impedance Spectroscopy Analysis

Impedance sensing on cell suspensions has been applied to monitor acidification of culture medium due to metabolic activity and also to sort cells [Gawad 2001]. A silicon/PDMS-based microfluidic device that allows single cell capture, positioning, and drug injection for high throughput drug discovery studies is shown in Figure 2-17.

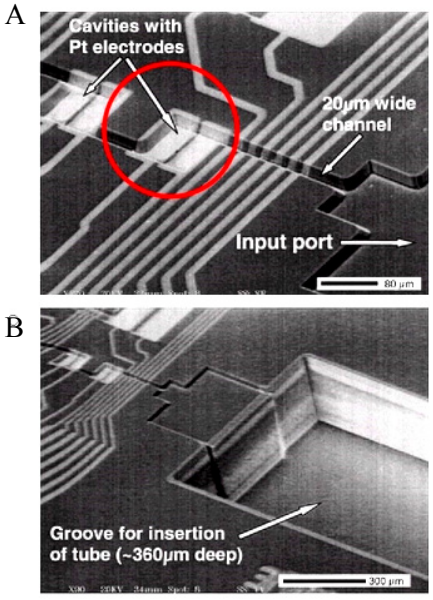

Figure 2-17: BioMEM investigating bacterial suspensions. Scanning electron micrographs of the cell-based biosensor published in [Gomez 2001]. (A) The bacteria suspension is transported via the channels into measurement cavities (circle; 530 x 850 x 12 µm³) where impedance sensing on interdigitated electrodes is performed. (B) Insertion port for macroscopic tubing and measurement chambers. Scale bars indicate 80 µm (A) and 300 µm (B).

The device employs low conducting cell culture medium to detect changes in ionic strength induced by the metabolic activity of bacteria. Impedance spectroscopy was performed on a

interdigitated electrode in a silicon chamber. Because only few (100…1000) bacteria were necessary for detection, the sensor was supposed to be useful in early detection of food spoilage [Gomez 2001].

Electrical impedance spectroscopy was also used for single cell characterisation of bovine chromaffin cells and red blood cells. Sensitivity was sufficient for the discrimination between both cell types based on their characteristic impedances [Andersson 2003]. In a different cell sorting approach, erythrocytes were distinguished from cells with nuclei removed (ghost cells). In this case, the real part of the impedance was monitored at two different frequencies at cell transit times of 1 ms [Gawad 2001].

2.3.2 Long-Term Culture Conditions in BioMEMS: Adherent Cells

The analysis of adherent cultures provides insight to functional behaviour that is more related to *in vivo* situations. But, as stated above, adherent cells are more sensitive to shear stress and malign culture conditions than suspended ones. Furthermore, they are plated directly onto the sensor device and need to grow there for long periods of time. This long-term cultivation *on-chip* raises a number of additional challenging issues. Three issues are important to mention: In order to avoid degradation of cells, only biocompatible materials must be used for BioMEM device realisation. Silicon dioxide and nitride (SiO_2 and Si_3N_4) as well as PDMS materials are widely used for cell-based approaches [DeBusschere 2001, Buitenweg 2002]. Adherent cells are very sensitive to shear stress and start to detach from the surface when the shear stress exceeds the physiological range of 2 to 14 dyn/cm^2 [Park 2003, Zantl: personal communication]. Therefore, shear stress of flowing medium inside BioMEMS has to be minimised. And, adherent cells owe a limited tolerance to unstable culture conditions. Parameters that might cause viability impairment of cells comprise the availability of oxygen and nutrients (inorganic salts, amino acids, glucose, serum) and factors as temperature, osmolality, and pH value.

To estimate the availability of oxygen in closed BioMEMS, the oxygen consumption of cardiomyocytes and the maximum solubility of oxygen in culture medium have to be taken into account. Those were estimated to approximately 2 to 10 pg / cell / hr [Spier 1982] and 8 ng / µl at 37°C [DeBusschere 1998].

The pH value is maintained within a narrow range around the cell specific optimum by using either a CO_2-dependent bicarbonate buffer system or a synthetic HEPES buffer. The importance of osmolality arises in sample injection. The osmotic strength of the sample must be adjusted to limit osmotic stress across the cell membrane. Although cells are tolerant to osmolalities in the range of 260 to 320 mOsm/kg, consistency within ± 10 mOsm/kg should be maintained to avoid interference with cellular function. Sample preparation is an important problem that was mainly disregarded yet [Freshney 1994, DeBusschere 1998].

2.3.3 Multi-Parameter Sensing of Adherent Cells

Multi-parameter sensing was performed with the *"PhysioControl-Microsystem"* that includes interdigitated electrode structures and sensors for temperature, oxygen, and pH [Brischwein 1996, Otto 2003]. A detailed analysis of the cellular microenvironment is feasible as changes in pH value, oxygen concentration, or glucose levels can be used as indicators of tumour growth [Henning 2004].

Another device represents a cell-based biosensor for electrogenic cells with on-site signal processing using a CMOS architecture. The system comprises a silicon chip with two closed culture chambers attached. Sixty-four sensing electrodes in each chamber and integrated circuitry allow for extracellular recording, temperature control, signal buffering, and signal multiplexing on-chip. By doing this it was demonstrated that mammalian cells can be cultivated inside a handheld, portable device of limited volume [DeBusschere 1998, 2001].

An outlook to the future perspective of BioMEMS is provided by the last example (Figure 2-18). The so-called cell culture analogue is an *in vitro* device that simulates the exposure of mammalian cells to chemicals. The design is based on a model that simulates molecular mechanisms of a chemical or its metabolite inside an organism, the so-called physiologically based pharmacokinetic (PBPK) model. The microfabricated cell culture analogue device contains tissue culture compartments that are interconnected with each other. Different tissue types represent some of the basic metabolic properties of the specific organ the cells originate from. Blood is mimicked by circulating medium. In pharmaceutical research, existing theoretical PBPK models can be analysed using this technique and secondary effects, caused by metabolites, may be identified [Park 2003].

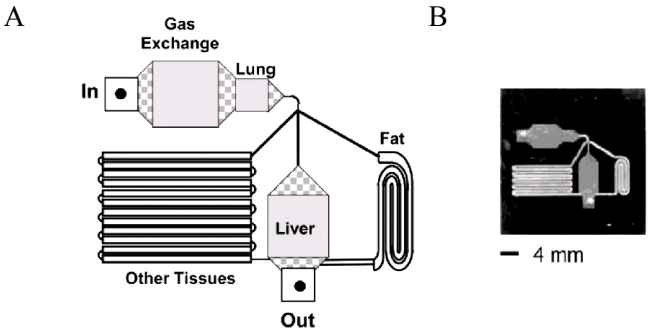

Figure 2-18: Cell culture analogue. (A) Schematic diagram of the different tissue compartments. Circulating culture medium is applied through the nozzle (*In*), transported along an oxygen supply and passes three compartments before it leaves the chip at the nozzle (*Out*). According to a PBPK model, the 1 x 1 inch wide chip ensures that certain flow rates feed the chambers. The fat chamber contains no cells, but holds back circulating fluids. (B) The actual size of the chip [Park 2003].

The perspectives of cell-based biosensing shown in this chapter are the basic motivation for this work. Two different kinds of biosensing were investigated. On the one hand, the usage of microelectrode arrays for impedance-based analysis of cell-substrate interaction was investigated. On the other hand, miniaturisation of sensors for monitoring electrical activity facilitate compound screening in a highly attractive field of medical and pharmaceutical research. In collaboration with an industrial partner this project aimed at the integration of cells inside a microfluidic chamber in combination with silicon based fluidic channelling and automated fluid dispensing.

Both were single projects that mounted in a biosensor platform combining both sensor principles capable of monitoring cell-substrate interaction and electrical activity in a single device.

3 Materials and Methods

3.1 Biological Material

3.1.1 Ovarian Cancer Cells

Tumour cells used for experiments determining cell-substrate interaction have been established from a patient afflicted with an ovarian cystadenocarcinoma. The resulting cell line, OV-MZ-6, has already been studied with respect to its integrin-mediated adhesion profile to different ECM proteins [Hapke 2001, Li 2005]. Cells were maintained in a nutrient mix based on Dulbecco's Modified Eagle Medium (DMEM; Invitrogen, Karlsruhe, Germany) supplemented with 10 % foetal bovine serum (FBS; Invitrogen). Additionally, Gentimycin (Invitrogen), HEPES (Invitrogen), Arginin (Sigma, Taufkirchen, Germany), and Asparagine (Sigma) were supplied. Detailed protocol descriptions for medium preparation and cell culture are given in Chapter 7 (Appendix).

Cultivation started with thawing cells from cryoconserved cultures. The additive dimethyl sulfoxide (DMSO; Invitrogen) present in the freezing medium was removed by several washing steps in the centrifuge (n = 1300 rpm, t = 5 min) at various temperatures and serum concentrations. First, cells were rinsed in ice cold medium without serum supplement and centrifuged at 4 °C. Washing continued using medium containing 10 % FBS (4 °C), 0 % FBS (37 °C), and finally 10 % FBS (37 °C). The centrifuge was operated at room temperature for the last two steps. Finally, cells were seeded on tissue flasks at a concentration of 10,000 cells per ml and incubated (37 °C, 5 % CO_2 in O_2).

Cell cultures were split every 4-6 days by adding 0.025 % ethylene diamine tetraacetic acid (EDTA; Biochrom, Berlin, Germany) dissolved in phosphate buffered saline (PBS; Invitrogen). After 5 minutes incubation time, cells were transferred into blue caps and centrifuged (n = 1300 rpm, t = 3 min). The supernatant was discarded and the cell pellet was re-suspended with medium/10 % FBS. Finally, cells were added to tissue flasks at a concentration of 10,000 cells per ml and cultured as described before.

For experiments, only cells of a certain developmental stage were considered. Cells must not be split more than 12 times after thawing and must be at least two weeks in culture. Only cultures with confluency rates between 70 % and 90 % were used for experiments [Reuning, personal communication], because adhesion properties change when cells have no space to adhere to and thereby enter the lag phase of their development.

Cells were applied to biosensors precoated with a *multiadhesive protein* (see Chapter 2.1.1). fibronectin (Roche Applied Science, Mannheim, Germany) was coated at a concentration of 10

to 50 µg/ml for at least 2 hours at 37 °C. After rinsing, cells were added as a suspension of 450,000 – 600,000 cells per ml medium/0 % FBS and placed into a table top incubator. Cell-substrate interaction was only observed under serum-free conditions because serum also contains multiadhesive proteins that mediate adhesion and therefore might cause artefacts.

Cell Viability Assays

Cell viability was quantitatively analysed either using the MTT assay that was introduced in Chapter 2.1.3 or by trypan blue staining. Trypan blue is an intense dye that enters the cell upon application. Living cells are able to remove the dye, whereas dead cells do not and therefore appear blue coloured. The substance (0.4 %, Invitrogen) was supplied to the culture medium at a concentration of 10 % v/v and incubated for 10 minutes. Cell counting revealed a ratio for dead versus alive cells.

The MTT assay is a more precise method [Hendrickx 2003] and allows a more comfortable read-out. The yellow coloured MTT solution (5 mg/ml medium) was added to the culture and converted to crystals of dark blue colour, MTT-formazan, by mitochondrial dehydrogenases in living cells. Turnover was stopped after 0.5 - 3 hours by addition of acidified isopropanol that also dissolved the formazan crystals. The cellular viability has been found to correlate to the photometric absorption at 570 nm. The spectrometric read-out was performed by an automated plate reader (BMG Labtechnologies, Offenburg, Germany) after thoroughly stirring of well plates.

3.1.2 Cardiomyocytes

Primary cardiomyocytes were prepared from rat hearts of 18 to 19 days old CD rats (E18-19, Charles River, Sulzbach, Germany). After hearts of 8 to 11 neonates were removed under sterile conditions, they were washed in ice-cold Ca^{2+}- and Mg^{2+}-free Hanks Balanced Salt Solution (Invitrogen) and chopped. Because this mixture contained not only heart muscle cells of various heart compartments but also connective tissue, several digestion steps followed to discriminate the electrogenic tissue type from others. Therefore, the tissue was incubated with 0.025 % Trypsin/EDTA (Sigma) for 4.5 min at 37 °C. Ice-cold F10 nutrient mix (Invitrogen) containing 30 % FBS (Sigma) stopped the enzymatic treatment. Dissociation of tissue was supported by performing gentle trituration. Then, cells were allowed to settle and the supernatant, containing mostly fibroblasts, was discarded. A second digestive step was performed with the remaining tissue (25 min, 37 °C). Again, trituration served to isolate cells from the tissue that were now found in the supernatant phase. After tissue residue was allowed to settle down, this supernatant was removed and stored on ice. This digestion of tissue residue was repeated until it was completely disintegrated. Cell containing fractions were collected and centrifuged (1300 rpm, 4 °C, 5 min). Then, the pellet was suspended in culture medium (F10/pen-strep/HEPES/10 %

FBS) and passed through a cell filter (40 µm pore diameter; BD Biosciences, Heidelberg, Germany). Finally, cells were transferred to culture conditions (37 °C, 5 % CO_2 in O_2). In order to separate myocytes from other cardiac cell types like fibroblasts, differential adhesion was applied. This takes advantage of different adhesion kinetics of the cell types. Here, fibroblasts are mostly settled to the bottom of the culture flask within 120 minutes, whereas myocytes remain in suspension. After differential adhesion, the supernatant was harvested. Then, cells were seeded to a density of about 6,000 cells/mm^2 on sensors pre-coated with 50 µg/ml fibronectin (Roche). After 24 hours in culture, FBS content of the nutrient mix was reduced to 3 %.

3.1.3 Bioactive Substances

Integrin Ligands and Control Peptide

Adhesion of OV-MZ-6 cells can be reversed in the presence of the integrin $\alpha_v\beta_3$-directed cyclic peptide c(-RGDfV-) [Aumailley 1991], because it acts as a competitor for the $\alpha_v\beta_3$/ECM interaction. Whereas the peptide c(-RADfV-) with an exchanged amino acid had no affinity to the integrins and therefore served as a control peptide. The lyophilised stock proteins were diluted with PBS, and aliquots were stored at -20 °C for up to 3 months. Prior to the experiment, peptides were prepared with medium/0 % FBS to a concentration of 250 - 500 µg/ml.

Photodynamic Therapy with Hypericin

Hypericin (Sigma) was used as photosensitising agent for Photodynamic Therapy (PDT) of OV-MZ-6 cells. Stock solution was prepared with DMSO and kept frozen at –20 °C. Hypericin working solutions were prepared with medium/10 % FBS at concentrations between 10 nM and 1 mM.

Prior to photoactivation, adherent cells were incubated with hypericin for at least 12 hours. Culture vessels were wrapped in aluminium foil to protect the photosensitiser from light. Shortly before photoactivation started, hypericin was exchanged against medium/0 % FBS. Photoactivation was performed by broad band illumination at a fluence rate of 16 mWcm^{-2}. The rate was determined using a power meter (Model 815-SL, Newport Research, USA).

Detachment of Tumour Cells

Loosening of the cell-substrate interaction or removal of cells was induced either by addition of 0.025 % EDTA (Biochrom) in PBS, 0.025 % Trypsin/EDTA (Sigma), or by applying mechanical stress to the cells using a Pasteur pipette.

Isoproterenol Treatment of Cardiomyocytes

Isoproterenol bitartrate (Sigma) is a well-known drug for enhancing the heart rate by accelerating spike generation in cardiac pacemakers (positive chronotropy). Isoproterenol binds to the β-adrenergic receptors and triggers a number of functional activations that in turn enhance the entry of calcium through L-type calcium channels (see Figure 2-3). The increased intracellular calcium concentration causes a higher spontaneous beat rate [Aravanis 2001].

Isoproterenol solution was always freshly prepared with F-10 medium/3 % FBS in various concentrations before the onset of the experiment. A typical concentration range was 10 pM to 100 nM.

3.2 Sensor Chip Design and Processing

3.2.1 Microelectrode Array Biosensor for Impedance Spectroscopy

Overview

This section focuses on the fabrication of a Microelectrode Array (MEA) chip prototype. Chips were used to study cell-substrate interaction of tumour cells with electrochemical impedance analysis.

The sensor device shown in Figure 3-1 comprised the glass chip carrying the microelectrode array and a printed circuit board (PCB). Because both parts were assembled by the so-called Flip-Chip technology (see page 57), the sensor was referred to as *Flip-Chip MEA sensor*. The devices were characterised by several requirements. For example, the sensors were supposed to be re-used and must therefore stand autoclaving conditions. Additionally, multiadhesive proteins that are necessary for cellular attachment must be able to adsorb to the sensor surface. The MEA were integrated on glass wafers that were fabricated in cooperation with GeSiM (Gesellschaft für Silizium-Mikrosysteme, Grosserkmannsdorf, Germany) based on own computer-aided design (CAD) drawings. The PCB were ordered from an external supplier (Schwind Elektronik, Ulm, Germany).

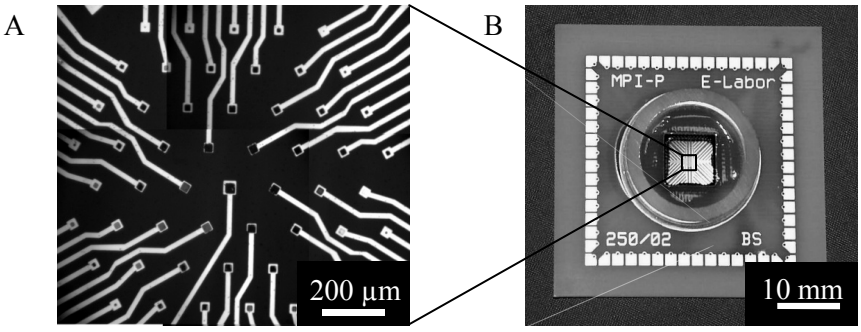

Figure 3-1: The Flip-Chip MEA biosensor. (A) Microelectrode array (MEA) with differently sized electrodes. (B) Biosensor depicted in a top view. The MEA is represented by a small rectangular in the chip centre.

This kind of sensor assembly had several advantages. Due to the small chip size, 45 sensors were manufactured from a single 4″ wafer at several different designs resulting in reasonable production costs per sensor. This approach was appropriate for initially experiencing the manufacture process of MEA sensors.

Chip Layout and Processing

A single chip comprised 60 microelectrodes with diameters from 5 to 40 µm. Each electrode was connected to a single peripheral pad. This pad was later bonded to the PCB and covered an area of 200 µm x 300 µm. Pads were located at a distance of 500 µm from each other all around the chip edges. Fabrication of the chips required CAD drawings of the gold leads structure and, separately, the electrode openings of the whole wafer. The drawings were transferred to chromium masks (Delta mask, Enschede, Netherlands) or photo emulsion masks. The wafer was then processed by a photolithographic procedure called *lift-off* process that is described below.

The substrate, a 550 µm thick 4″ glass wafer (TE-DGS D263 T; Schott Desag, Mainz, Germany), was spin-coated with 1400 µm positive standard photoresist and exposed to illumination through a darkfield mask (Figure 2-1 A). Subsequent developing released the unexposed areas (B). The whole wafer was then coated by evaporation of 10 nm chromium as adhesion layer and 100 nm gold (C). In the following lift-off step (D) the exposed photoresist was removed by solvent rinsing leaving the structured glass substrate. The lift-off process is schematically shown in Figure 3-2.

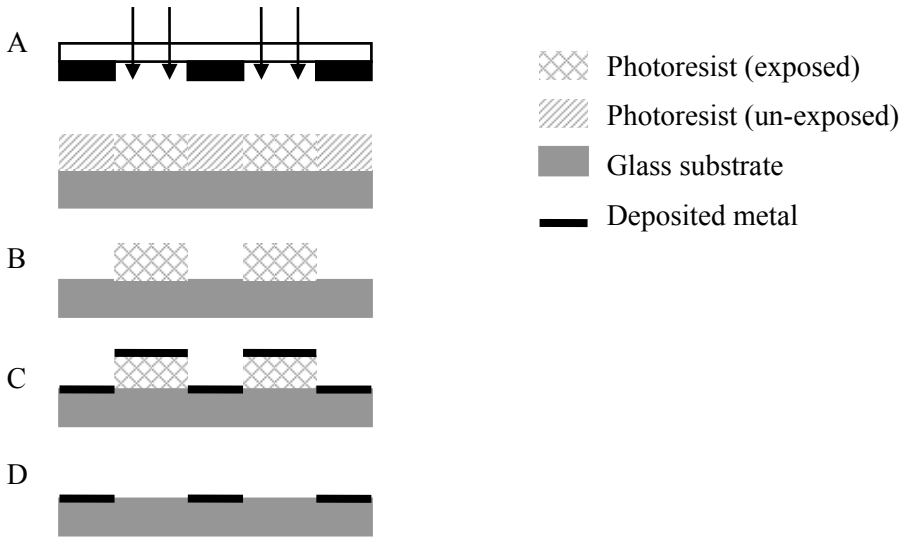

Figure 3-2: Lift-off process. (A) Exposure of photoresist on glass through a dark field mask. (B) Removal of unexposed resist. (C) Metal deposition on whole substrate. (D) Release (or *lift-off*) of gold structure by solvent rinsing.

Printed Circuit Board

The wafer was then insulated with 770 nm SiO_2 and/or Si_3N_4 using Plasma Enhanced Chemical Vapour Deposition (PECVD). At last, the insulating layer on the microelectrodes was opened. Again, photoresist was spin-coated on the wafer and electrodes were released by exposure through a dark-field mask in a second photolithographic step. Reactive ion etching was

performed on the whole wafer, etching away the insulation layer at previously defined electrode sites. Finally, the photoresist coating was removed and the wafer diced into 45 single chips, sized 11 mm x 11 mm. Before dicing, a protective coating was applied and removed after sawing.

The PCBs measured 50 mm x 50 mm and were structured with gold leads on both sides. A square aperture in the centre was 10 mm by 10 mm wide. The MEA chip was glued onto the backside with the MEA facing the aperture. Thereby, the peripheral pads on the glass chip were bonded to the inner gold lead terminations on the backside of the PCB. These terminations were connected to the large pads forming a ring on the PCB front side (see Figure 3-1 B). Hence, each pad offered a low ohmic electrical connection to a single microelectrode of the centre array and was therefore used by the measurement equipment during experiments.

Flip-Chip-Technology

This technology was applied to finally assemble the biosensors. It involves flipping a (micro)chip onto a circuit board that was prepared before with precisely applied polymer glue spots on electrical contacts. It is used in electronic packaging industries for bonding small series production [Lau 1996].

First, a stencil printer (SP-002; ESSEMTEC, Switzerland) was equipped with an appropriate stencil. This was a 150 µm metal stencil that allowed pasting silver glue (H20E-PFC; Polytec, Waldbronn, Germany) spots precisely on the inner gold lead endings on the PCB. Glue was spread over the stencil after visual alignment of the PCB and the stencil. The next step involved camera-aided alignment of the bumps and counterpads on the glass chip (Fineplacer-145 pico; FINETECH, Berlin, Germany) using a X-Y working table. Once the MEA chip and the PCB were perfectly aligned, the MEA chip was removed from the alignment position and placed onto the PCB. This was the actual flipping process, comprising a 180° turn of the chip that was fixed by a vacuum suction to a rotatable arm of the Fineplacer instrument. The chip flipping must be very precise to ensure proper bonding.

Sensor Architecture

A cross section of a ready-to-use biosensor is shown in Figure 3-3. The MEA chip is shown in transverse section with the gold lead connecting microelectrode to peripheral bonding pad, and the insulation layer detailed. The silver glue bonding was the central element (circle) that connected the MEA chip and the PCB. The bonding site was encapsulated by an underfill resin (U-300, Polytec) that was finally coated by biocompatible poly(dimethylsiloxane) (PDMS; Sylgard® 184, Dow Corning, Wiesbaden, Germany). Therefore, glass rings served as boundaries to prevent the PDMS from covering the MEA. The outer ring (1) also served as a containment for culture medium during incubation of cells.

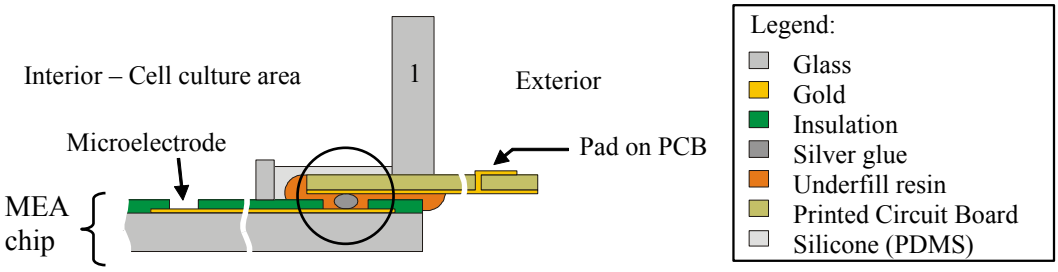

Figure 3-3: Biosensor architecture. Figure describes a cross-section through a MEA chip (bottom) bonded to a printed circuit board (PCB) by Flip-Chip-Technology. A glass ring (1) served as a containment between cell culture area and exterior.

3.2.2 Microelectrode Array Chip for Extracellular Recording

Overview

This MEA chip design was different from the one described in section 3.2.1 and fabricated to be used for monitoring extracellular activity, exclusively. The chip was planned to be combined with an attached microfluidic unit, and therefore it is subsequently referred to as the *microfluidic MEA chip*. Some design rules have been changed, compared to the Flip-Chip MEA sensor. The culture chamber, for example, is now obsolete, and instead the challenge of a properly sealed fluid system arose. The prior barrier between electrical pads and wet cell culture area was now removed due to the attachment of the microfluidic unit. Therefore, the whole sensor was immersed in culture medium during cultivation periods. Other changes refer to the size of the sensor and the number of electrodes. Both were reduced to ensure handy insertion. Additionally, the sensor required an impedance reducing coating on the working electrodes. Again, the sensors were fabricated in cooperation with GeSiM (Gesellschaft für Silizium-Mikrosysteme).

Sensor Chip Layout

In Figure 3-4 A the chip and the microfluidic unit are shown. The culture medium entered the system on the left and was transported along a microchannel to the chip, depicted on the right. Cells were located on the MEA that is detailed by an inset. The MEA was a 2 x 8 array of microelectrodes sized 40 µm x 40 µm and a large electrode (250 µm x 400 µm) that served as a counter electrode. The distance from one microelectrode to another was 200 µm (centre-centre). Electrodes were connected to large, contact pads (1). The chip was also fabricated using the lift-off process as described in Chapter 3.2.1. To ensure proper sealing a PDMS gasket was applied

onto the insulating layer around the MEA by stencil printing. Photographs of the sensor are given in Figure 3-4 B and C.

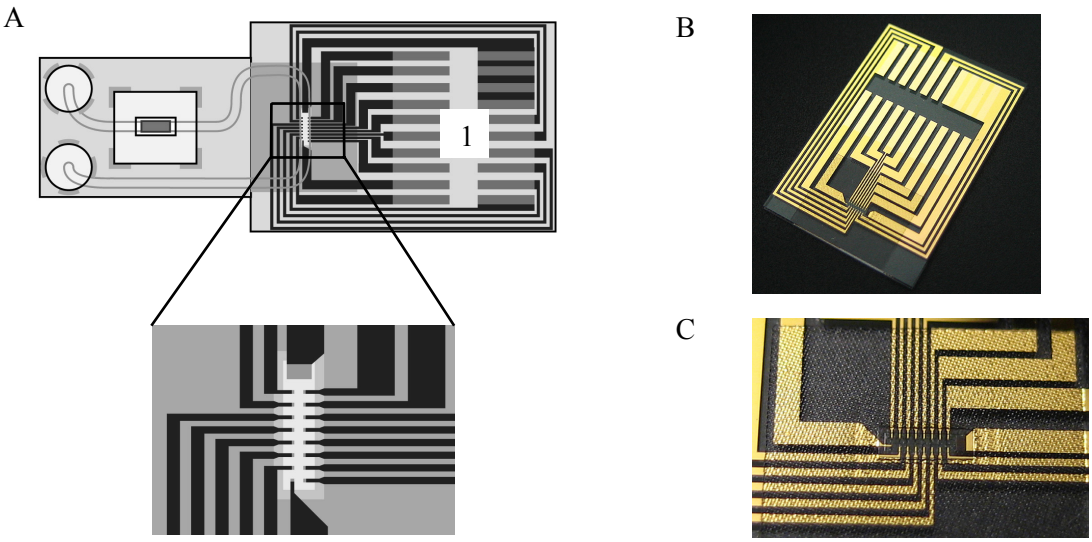

Figure 3-4: MEA chip for the use in an external microfluidic unit (*microfluidic MEA chip*). (A) Chip (right) attached to the microfluidic unit (left). Dimensions were 19 mm x 13 mm for the chip and 2.5 mm x 0.5 mm for the MEA. Inset shows magnified view of the MEA. (1) shows the pad region connected to electronics during experiments [GeSiM 2006]. (B) Image of the sensor chip. (C) Enlarged view on the sensor array surrounded by the silicon gasket for sealing purposes.

Deposition of Platinum Black

Platinum black was applied to the gold electrode surfaces as an impedance reducing coating. Pt^{3+} ions were supplied by Kohlrausch's platinising solution containing 10 mM hexachloroplatinic acid IV (Sigma) and 0.4 mM lead citrate II (Sigma) and deposited under ultrasonic conditions at DC voltages below 5 Volts (a more detailed description of this procedure is given in Chapter 7. Figure 3-5 gives the structure of the surface as an SEM image.

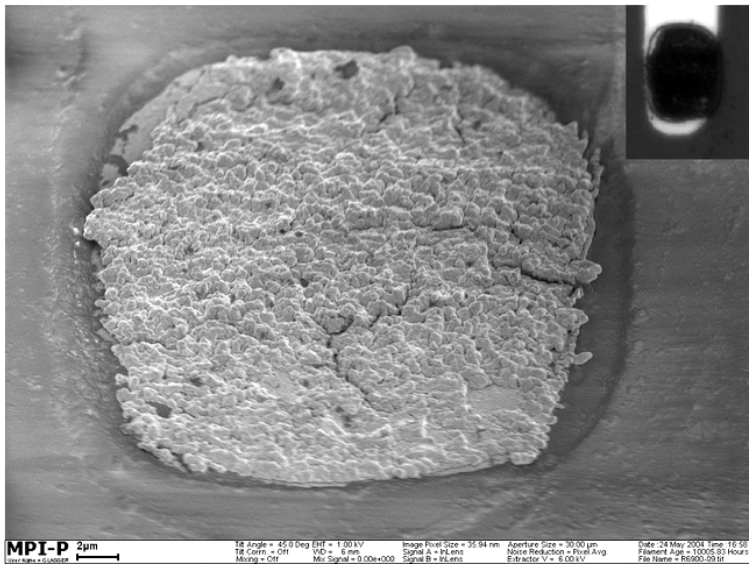

Figure 3-5: Platinum black coated microelectrode. SEM image of a 40 µm electrode with a scale bar of 2 µm. In the inset, a micrograph obtained by conventional light microscopy of the same electrode is shown.

3.2.3 Fluidic Chip

Overview

The main functions of the fluidic chip were delivery of culture medium and test substances to cardiomyocytes during extracellular recordings. The integrated microchannel with an on-chip injector has the strong advantage to enable fluid transport at low dead volumes and times. Hence, the chip was positioned beneath the microfluidic MEA chip described in Chapter 3.2.2. The fluidic chip was also manufactured by GeSiM (Gesellschaft für Silizium-Mikrosysteme).

General Fluidic Concept

A schematic cross-section given in Figure 3-6 shows the MEA chip aligned to the microfluidic unit. Culture medium entered the microchannel on the left. Test substances were added to the medium flow through the injector. The injector was loaded by an external micro-machined pipette that was operated in an automated dispenser machine *NanoPlotter* (see Chapter 3.3.2). Typical volumes applied were in the range of 10 µl. The pipette served as an interface between substance libraries based on multiwell plates and the microfluidic system. During rinsing the injector was left empty, and a ground sieve prevented the intrusion of air into the channel [Fiehn 1994, Howitz 1999]. After passing the injector, the fluid stream was transported to the cell culture located on the up-side-down oriented MEA chip. Finally, the medium with test agents left the chip and was discarded.

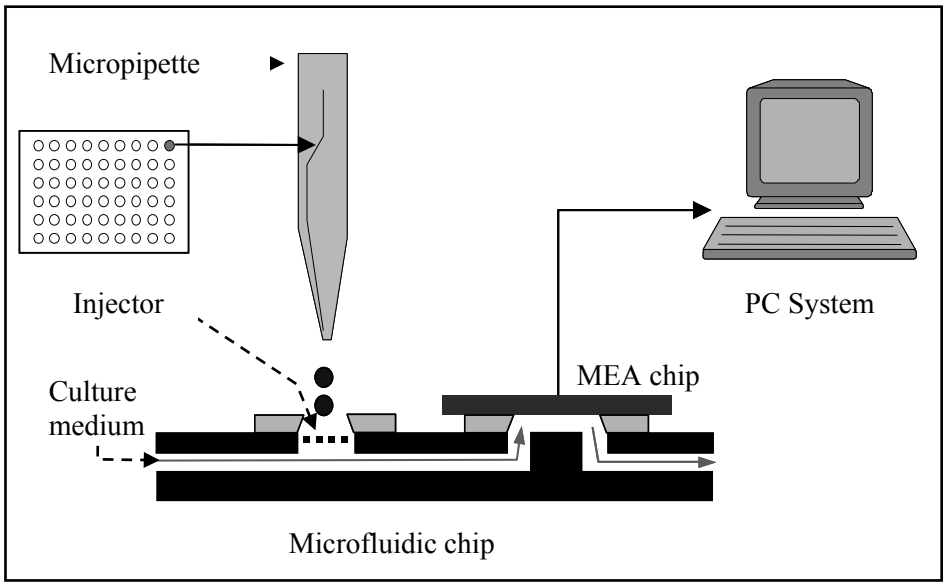

Figure 3-6: MEA chip aligned to microfluidic chip. Culture medium was transported along the chip from the left side to the right. Test substances were sucked into the micropipette and transferred from a multiwell plate to the injector. Here, substances entered the culture medium stream and were moved to the cell culture located on the MEA chip. A blocking structure on the bottom of the channel guided the fluid into close vicinity to the cells. Cellular responses were displayed on a PC system.

Chip Architecture

The chip was composed of a bilayered arrangement of 1 mm thick optical glass underneath a three-dimensionally structured silicon wafer of 0.4 mm depth. Glass and silicon were assembled by anodic bonding. The fluidic channel of 0.2 mm height was realised by a silicon etching step (anisotropic KOH-etching) applied to the back of the silicon chip [Howitz 1999, Richter 1999]. On top 100 nm platinum was deposited in order to ensure proper electronic grounding of the chip. The total volume of the microchannel was about 1.86 µl. The fluidic chip is shown in Figure 3-7:

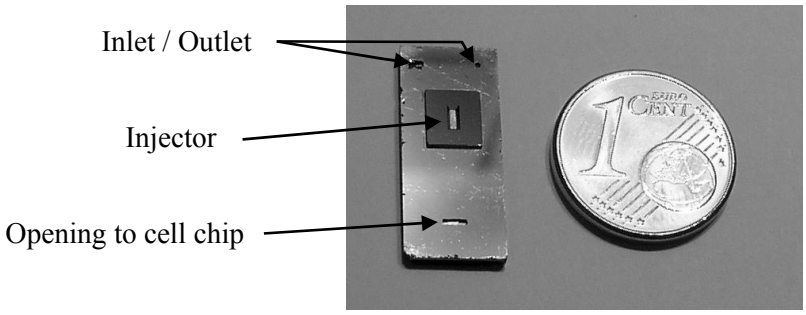

Figure 3-7: Microfluidic chip

Injector

The injector represents a device for rapid drug application into the microchannel with the benefit of preventing air intrusion. Because the injector is located near to the cell chip, drug screening with low dead volumes and short sample/rinse cycles was feasible. The orifice (2 × 0.5 mm²) of the injector port shown in Figure 3-8 A was equipped with a sieve plate that was etched in silicon by anisotropic KOH-etching. Pores were 50 µm in diameter. The transition of a drop representing the test substance is given in Figure 3-8 B with culture medium (L1) and test substance (L2).

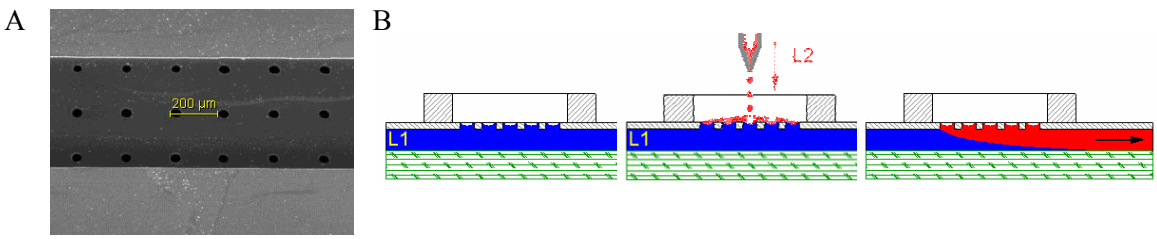

Figure 3-8: Injector port in detail. (A) Electron micrograph of the injector. (B) Working principle of the injector. [GeSiM 2006]

3.2.4 Sensor Chip with Integrated Fluidic Unit

Overview

For this third type of sensor a microfluidic silicon chip was irreversibly attached to a MEA. Holes and channels were etched into the silicon chip to obtain cell culture chambers and fluidic paths for nutrient supply. In contrast to the prior fluidic chip design, culture medium was guided across the cell culture at a distance of 300 µm. Because this sensor was used in the platform it is referred to as the *platform sensor*. During experiments, the sensor was inserted into a sample holder and covered by a lid that provided a PDMS sealing layer, fluid supply nozzles, and a PCB for contacting sensor pads. The sensor is schematically depicted as a cross section in Figure 3-9.

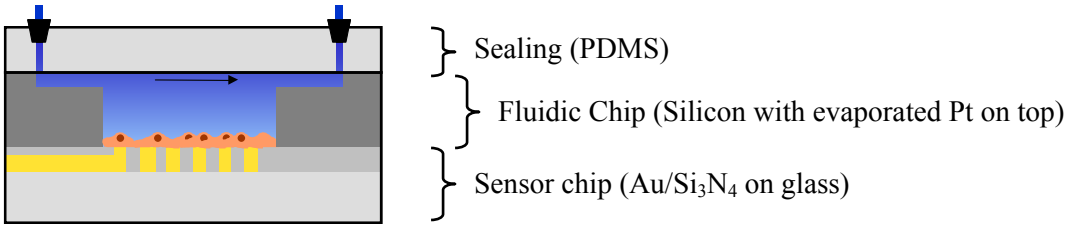

Figure 3-9: Platform sensor covered by the sealing lid. Cells were cultured on the sensor chip. Culture medium was supplied via connectors on top and passed the cell chamber in the direction indicated by the arrow.

Two separate fluidic paths were integrated on the silicon chip, one for test substance application, the other as a reference path for cells that were not subjected to any test substance (control experiment). Each path contained two cell culture chambers in series that were equipped with a MEA and/or various impedance electrodes.

Sensor Chip Layout

The glass MEA sensor was fabricated by a lift-off process as described before (see Chapter 3.2.1). Four impedance arrays and two microelectrode arrays permitted impedance analysis and extracellular recording. The CAD drawing is given in Figure 3-10. The impedance electrode array consisted of two types of working electrodes (30 µm and 300 µm in diameter) opposing large counter electrodes, and an interdigitated electrode couple. The microelectrode array was composed of 11 electrodes, arranged in a pattern of 200 µm distance to each other (centre-centre). Two counter electrodes served as a reference node separated from the impedance counter electrode. Array electrodes were coated with platinum black as an impedance reducing coating.

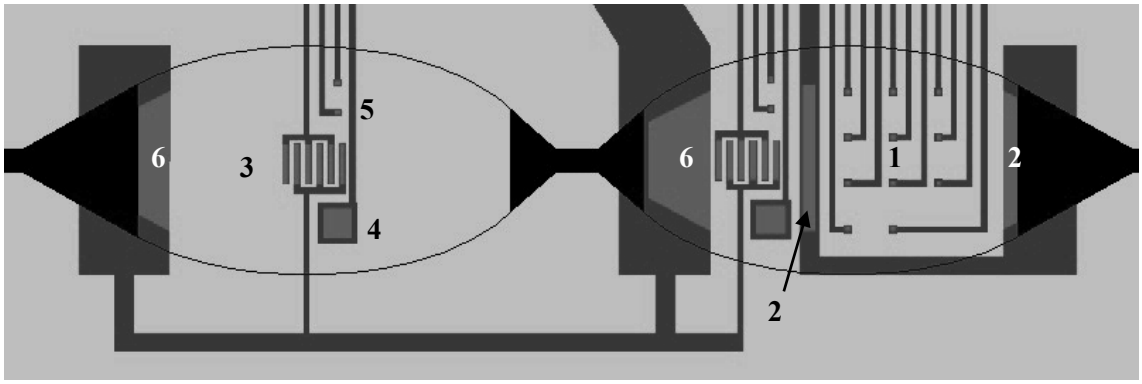

Impedance electrode array:
(3) 1 Interdigitated electrode
(4) 1 Large electrode (250 µm)²
(5) 2 Microelectrodes (30 µm)²
(6) 2 Counter electrodes

Microelectrode array:
(1) 10 Microelectrodes (30 µm)²
(2) 2 Counter electrodes

Figure 3-10: CAD drawing of electrode structures on the biosensor. The image displays one fluid path with two culture chambers aligned. Active electrode structures are shown in light grey, passivated structures in dark grey, and black counts for etching borders of the fluidic chip. Hollow black structures were etched through the whole silicon chip, whereas solid black structures represent the channel at a depth of 200 µm.

Fluidic Chip Processing

The fluidic channels (200 µm deep) were etched into a 500 µm thick silicon specimen (sized 23 x 23 mm) by anisotropic KOH-etching. The chip surface was coated with platinum for proper grounding. Bulk etching was performed to carve out culture chambers that had a volume of about 10 µl each.

Assembly of Sensor Chip and Fluidic Chip

The platform sensor is depicted in Figure 3-11. Both parts were assembled using glue (Endfest® 300, UHU, Brühl, Germany). Fluid channels led to four culture chambers located in the centre of the sensor where the electrode arrays were located. Electrodes were connected to the peripheral pad region on the left and on the right of the glass chip.

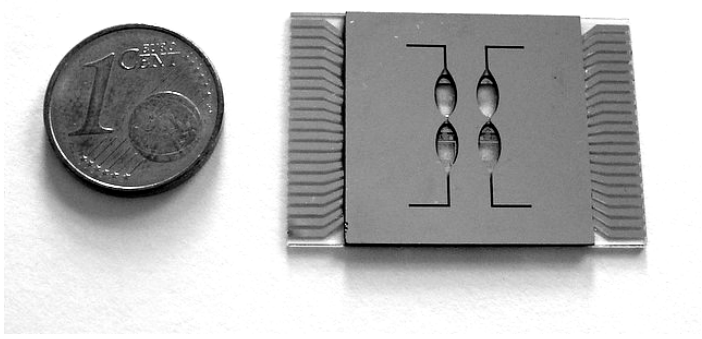

Figure 3-11: Prototype of the assembled biosensor.

3.3 Hard- and Software Tools

3.3.1 Devices for Impedance Analysis

Impedance analysis can be performed over a range of frequencies (Electrochemical Impedance Spectroscopy, EIS) or on a single frequency (single frequency impedance sensing). Whereas EIS is used for modelling physical systems, single frequency impedance sensing is an appropriate method to determine real-time impedance changes.

Electrochemical Impedance Spectroscopy

Broad band impedance analysis was performed using a commercial impedance spectrometer (IM6, Zahner, Kronach, Germany) that was operated in the two electrode mode with the working electrode and the input from the reference/counter electrode connected to the frequency analyser. The cell/culture medium system was excited by a sinusoidal signal of 10 mV in a frequency range of typically 1 Hz to 1 MHz. Data analysis, modelling, and fitting algorithms were performed in ZVIEW (Scribner, USA).

Single Frequency Impedance Sensing

A system capable of single frequency impedance sensing was developed. Stimulation was done by a 1 V sinusoidal signal of a fixed frequency chosen between 50 Hz and 120 kHz. As a reference source, a sine oscillator module was used (SOM-1, Femto, Berlin, Germany). Changes in impedance were detected in real-time by a dual phase lock-in amplifier (LIA-BV-150 H, Femto). The impedance was calculated from three voltage outputs ranging from 0 to 10 Volts. The impedance *magnitude*

$$R = \sqrt{\left(X^2 + Y^2\right)} = U_{Signal} \tag{3-1}$$

is the vector product of the *in phase* component

$$X = U_{signal} \cos\theta = Z' \tag{3-2}$$

and the *quadrature* component

$$Y = U_{Signal} \sin\theta = Z'' \,. \tag{3-3}$$

The phase shift between reference source and sample signal is given by

$$\theta = \arctan\frac{X}{Y} \,. \tag{3-4}$$

Four parameters were set either manually or digitally to control the lock-in amplifier: Sensitivity, coarse phase shift, fine phase shift, and the time constant.

Incubating System for Flip-Chip Sensors

During experiments physiological conditions such as humidity, pH value, carbon dioxide concentration and temperature had to be maintained on a stable level. For impedance analysis experiments, a table top incubator (Mini-Inkubator S, Zeiss, Jena, Germany) was used. The sensor was inserted into a transparent cell culture chamber (Figure 3-13 A) that was connected to a CO_2 controller (CTI controller 3700, Zeiss) and a temperature controller (Tempcontrol 37-2 digital, Zeiss) via flexible tubing. Evaporation of the culture medium was reduced by guiding the air stream through a humidifier (see Figure 3-13 B).

Microscopy

Optical observation of cells cultured on Flip-Chip sensors was performed using a light microscope with phase contrast filters (Axiovert 40, Zeiss). Time-lapse imaging was accomplished by a CCD camera (XC-ST50CE, Sony, Japan) and a PCI frame grapper card (PXC-200, Stemmer Imaging, Puchheim, Germany).

Multiplexing Electrodes

Impedance sensing focused on the observation of just a single electrode. To overcome this limitation, a PC controlled 16 channel multiplexer was realised for usage in the biosensor platform. The multiplexer PCB is shown in Figure 3-12.

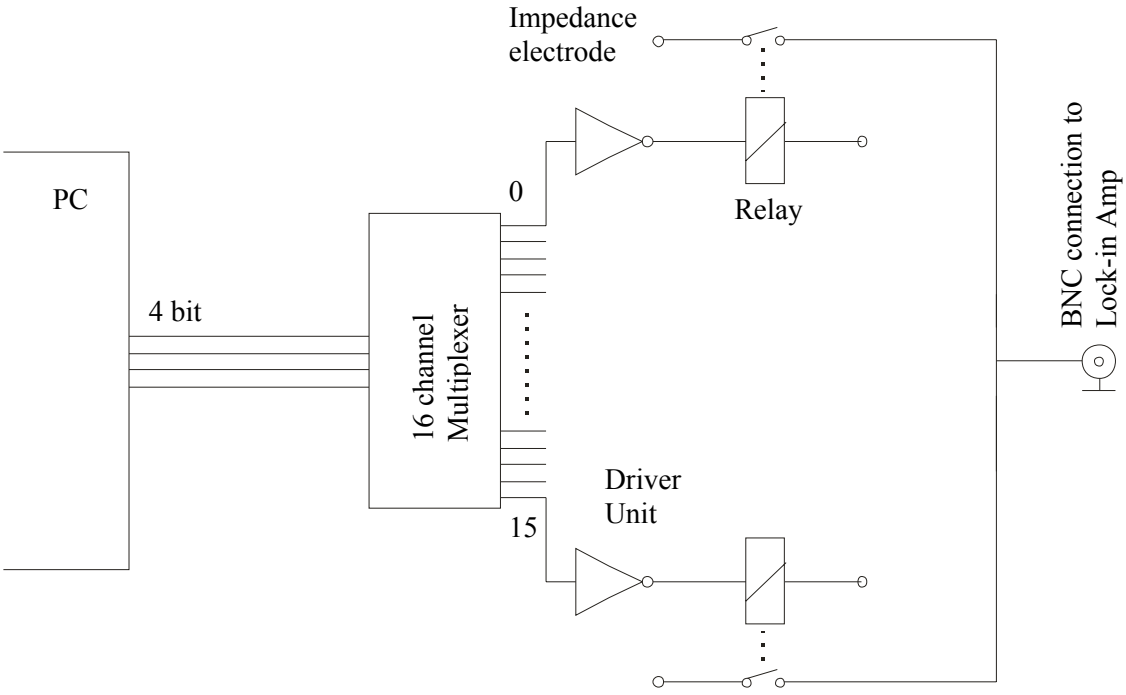

Figure 3-12: Impedance channel multiplexer. The impedance electrode was connected via a relay controlled line. The particular relay was activated via a 16 channel multiplexer unit. A 4 bit scheme transmitted via 4 digital lines allowed to control the relay.

Using this device, any single electrode of the impedance array (see Figure 3-10) can be observed and measured sequentially. For each electrode a set of specific lock-in parameters (sensitivity, coarse phase shift, fine phase shift, time constant) had to be transmitted, which was performed by the application software described in Chapter 3.3.3.

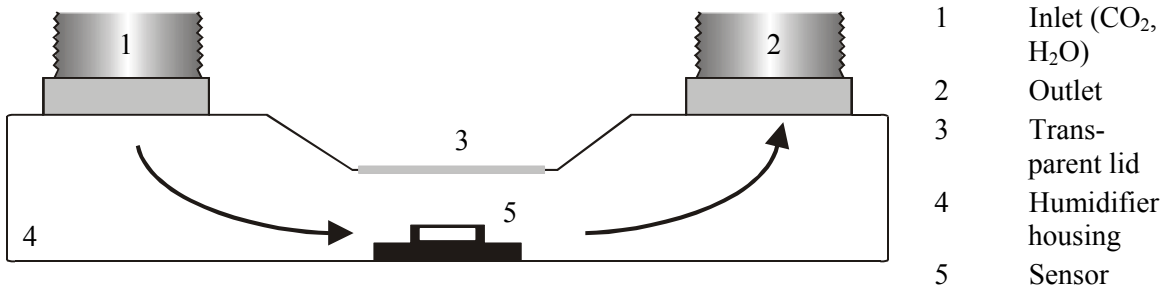

Figure 3-13: Sensor incubation system. Incubation ambience is provided by an humidifier, a CO_2-controller and a thermostat (not shown) located upstream of the tubing inlet (1). The gas stream circulates around the MEA sensor that is located on the bottom. The sensor is accessible be removing the lid.

3.3.2 Devices for Extracellular Recording

Sample Holder for Sensor and Fluidic Chip

The first microfluidic biosensing system was exclusively used for extracellular recording. The (microfluidic) MEA sensor and the fluidic chip, described in detail in Chapters 3.2.2 and 3.2.3, were set into an aluminium sample holder during experiments. The holder is given as a CAD drawing in Figure 3-14.

The MEA sensor was attached to the fluidic chip by means of a mechanical clamp mechanism. The PDMS gasket printed on the MEA chip ensured leak-free operation. Cells were continuously fed with cell culture medium using a peristaltic pump (IPC-N, Ismatec) and 190 µm wide biocompatible tubing (Pharmed, Ismatec, Wertheim, Germany). The pad region on the MEA chip was contacted by springs that led to a socket integrated on a printed circuit board. The holder was kept at a physiological temperature of 37° C controlled by a heating circulator (ME-26, Julabo, Seelbach, Germany).

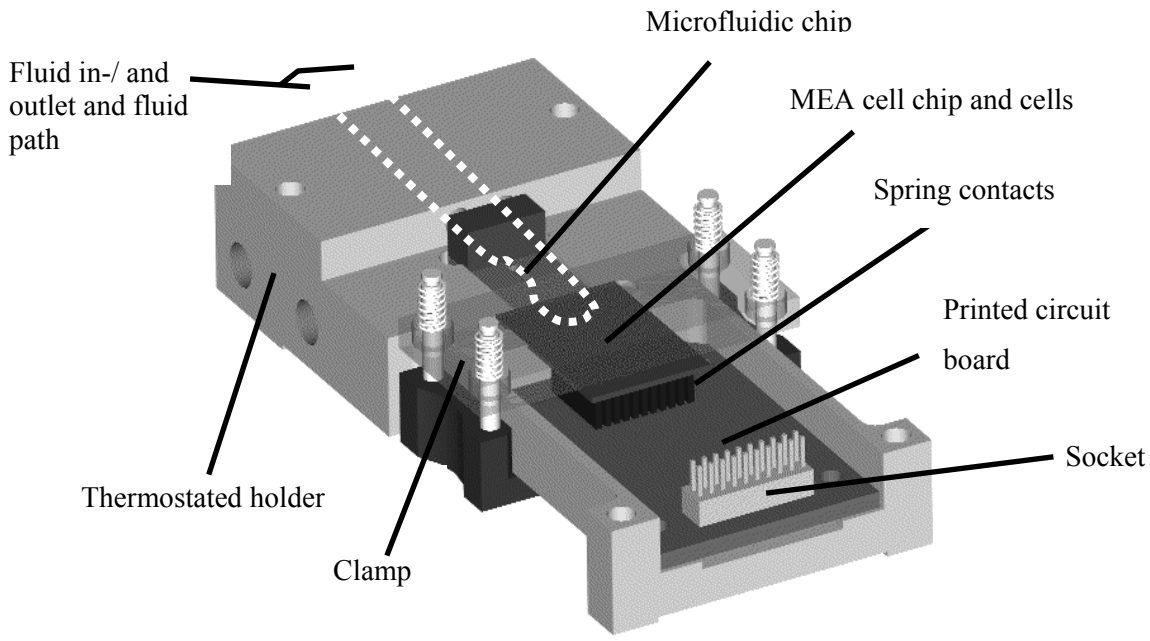

Figure 3-14: Sample holder of the first microfluidic concept given as a CAD drawing. The MEA cell chip was clamped onto the microfluidic unit with cells orientated downwards. Culture medium was supplied along the (white dotted) fluid path. Electrical signals were acquired from MEA chip pads via spring contacts, printed circuit board, and surface mounted socket [GeSiM 2006].

Computer-Controlled Fluid Dispenser

Test substances were applied to the injector opening of the fluidic chip manually or by using a fluid dispenser (Nanoplotter 1.2; GeSiM) shown in Figure 3-15 A. During experiments the sample holder was caged by a housing connected to electrical ground in order to shield the electronic circuitry from noise pickup. Sample holder and housing were mounted on the working table (Figure 3-15 B).

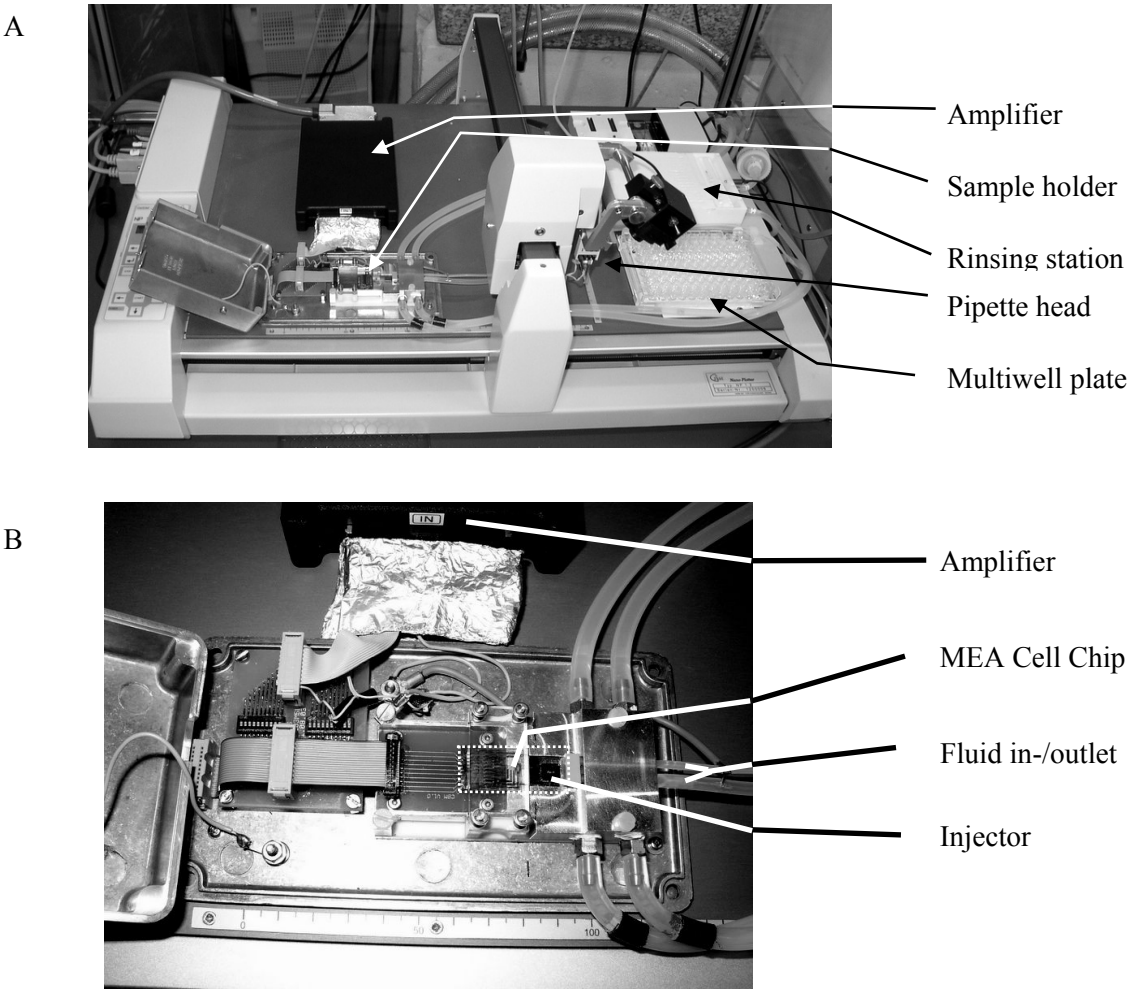

Figure 3-15: Fluidic dispenser with the sensor setup mounted on top. (A) Dispenser and (B) Sample holder.

Precise positioning of a micropipette (SPIP A-010; GeSiM) within the range of the working table was achieved by computer-controlled linear drives. During operation, the pipette tip was first moved to a defined well on the multi-well plate to aspirate a 5-10 µl load of a test substance. Then, the pipette was moved to the sample holder and the test substance was dispensed into the injector. Finally, the pipette was rinsed in a washing station to remove residual test substance from the tip.

Within the centre of Figure 3-16 (circle), the pipette tip is positioned above the injector, ready to dispense a test substance into the fluidic chip. Application software (np8; GeSiM) provided implemented functions for precise coordinate addressing of the pipette head and various other operations.

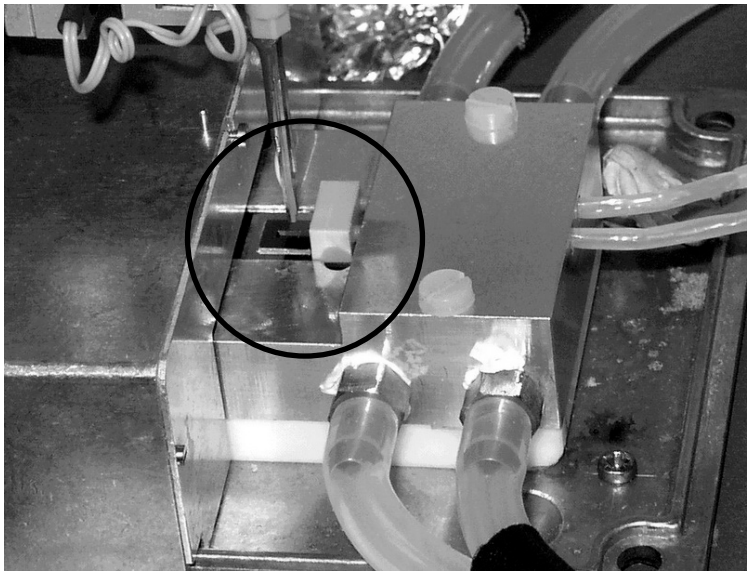

Figure 3-16: Fluid injection using the Nanoplotter. The micropipette is about to apply a substance onto the injector of the microfluidic chip (circle). Large tubing in the foreground guide thermostated water through the sample holder and culture medium is transported in the small tubing on the right. The sample holder was thermo-insulated from the ground plate of the shielding cage by a sheet of Teflon.

Data Acquisition and Processing

The output of the MEA chip (see Chapter 3.2.2) was fed into a 64 channel differential input filter-amplifier (F-64; Multi Channel Systems MCS GmbH, Reutlingen, Germany). The device was characterised by a low cut-off frequency of 200 Hz, a high cut-off frequency of 5000 Hz, and a voltage gain factor of 1200. The amplifier output was connected to a PCI data acquisition card (MCCard; MCS) on a standard PC system. Data analysis was performed with the application software MCRack (MCS).

Second Generation Recording System

The commercially available recording system described before was not used in the second approach, the biosensor platform. Amplification of the local field potentials had to be performed in close vicinity of the sensor to reduce pickup of noise. Therefore, a multichannel amplifier was developed and manufactured. In Figure 3-17 the amplifier PCB is shown. It was mounted onto the multiplexing board inside the aluminium box. The PCB was realised at similar specifications as the commercially available amplifier, except for the number of channels that was reduced to 20 and for the gain factor that was slightly increased compared to the amplifier previously used. Due to a central hole (diameter 13 mm) in the circuit boards, optical observation through the aluminium box was made feasible.

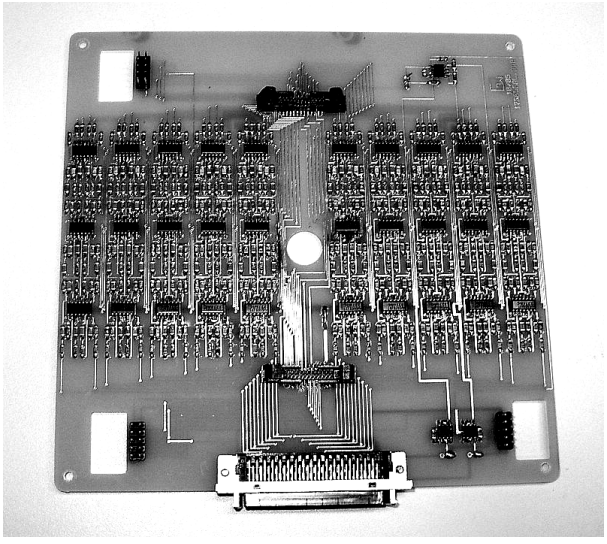

Figure 3-17: Filter amplifier board. 20 channels were differential input filter-amplifier differentially amplified against a reference potential (differential input filter-amplifier). The board was sized 165 mm by 165 mm and mounted inside the aluminium housing with the electrode multiplexer board beneath. In the centre, the circuit board includes a central aperture for optical observation using a light microscope.

3.3.3 Concept and Components of the Biosensor Platform

The biosensor platform allowed to measure cell impedances and record cellular activity at the same time. Additionally, optical observation offered visual control of cells and fluid chambers. After the sensor and the transducing systems have already been described in detail (Chapters 3.2

and 3.3), the rest of this chapter focuses on the sensor holder, the optical observation equipment, and the application software. But first, an overview of the system concept is provided.

System Concept

The core concept of the screening system is shown in Figure 3-18. Signal acquisition is displayed following the processing pathway from the biosensor source via sample holder and set-up electronics to final data display and storage. Multichannel signals were drawn in bold lines.

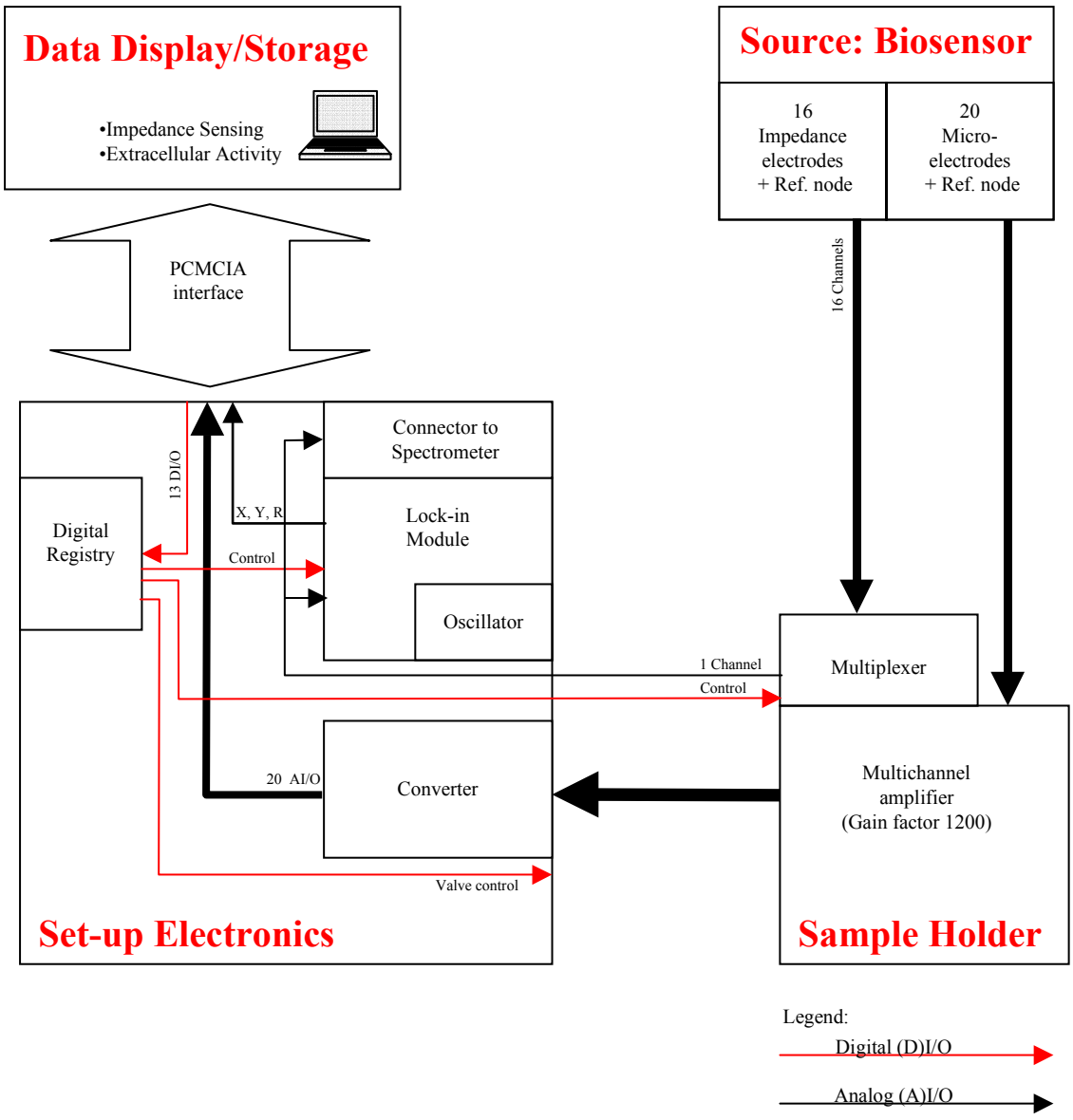

Figure 3-18: Schematic concept of the biosensor platform. Signals originated from the biosensor (top right) and were first processed in the multichannel amplifier and the multiplexer unit located beneath the sensor holder. Then, signals were transferred to the electronic setup and displayed on screen.

The electrodes of the biosensor were connected to the multiplexer board and multichannel amplifier. As described above, both were located in an aluminum housing close to the sensor holder. The output of these devices, the single multiplexed impedance channel and the 20 amplified microelectrode channels, were connected to the external set-up electronics.

A rack was assembled what contained a lock-in amplifier, power supplies, and a converter board, as the drawing of the front panel shows (Figure 3-19 A). Multichannel signals first enter the converter board, where channels were rearranged according to the specifications of the commercial amplifier (F-64; MCS, Reutlingen) which was used for compatibility reasons. The multiplexer output was connected to the lock-in amplifier that encoded the impedance as in-phase component *X*, quadrature component *Y*, and impedance magnitude *R*, as described in equations (3-1) to (3-3). The input of the lock-in amplifier was also guided to a connector for an external broad band impedance analyser. Digital registry was used for controlling the lock-in module, the multiplexer, and also an external valve.

A B

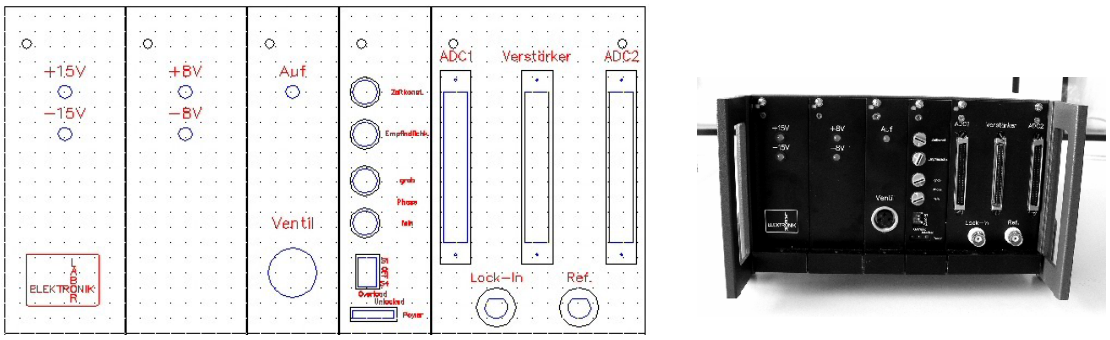

Figure 3-19: Set-up electronics. (A) Drawing of set-up electronics front panel. Rack includes power supplies, external valve control, lock-in amplifier, and converter boards. (B) Photograph of the device.

The rearranged multichannel lines and the three impedance channels *X*, *Y*, and *R* were then transferred to the PC system. Therefore, two 16-channel data acquisition cards (DAQcard 6062E, National Instruments, Munich, Germany) were connected to the PCMCIA interface of a notebook (Latitude 610, Dell, USA). The cards worked as an A/D converter, accomplished data acquisition at 500 kilosamples per second, and offered 16 digital control channels. Cards were controlled by LabVIEW (National Instruments) based software.

Sensor Holder of the Biosensor Platform

Cells were grown and cultured on the sensor chip outside the measurement system in culture medium located in petri dishes (Figure 3-20 A). When used for experiments, the sensor was set into the temperature controlled sample holder (see lower square in Figure 3-20 B). It was

covered using a lid (upper square) that carried a printed circuit board to connect sensor pads to peripheral electronics and that sealed the measurement cell. The closed cell chamber is shown in Figure 3-20 C+D.

A plain PDMS layer on the lower surface of the polymethyl methacrylate (PMMA) lid sealed the top side of the platform sensor. Furthermore, fluid supply nozzles fit onto the outer terminations of the integrated microchannels. A peristaltic pump (IPC-N; Ismatec, Wertheim, Germany) transported cell culture medium via microchannels to the cell chambers at flow rates of 10 to 100 µl/min. Sterility of the fluidic system was provided by Teflon coated silicone septa on supply vessels and autoclavable tubing (Pharmed; Ismatec).

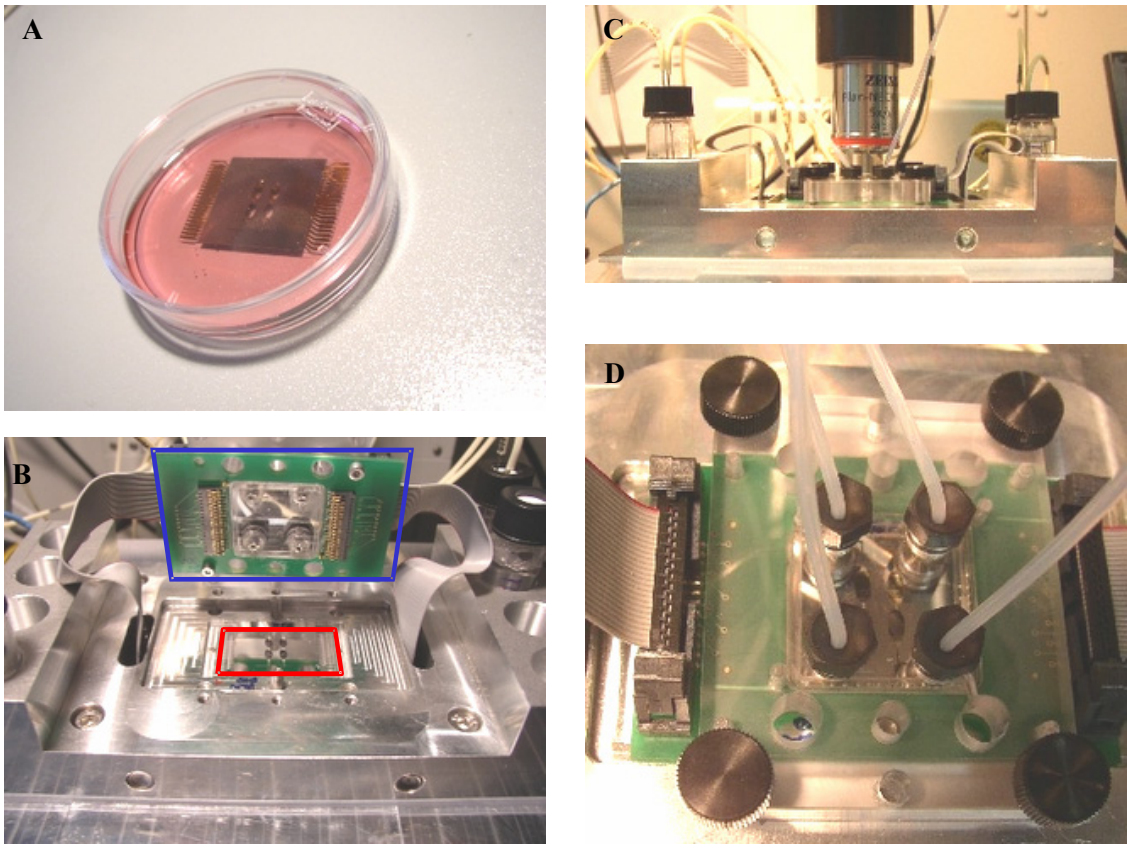

Figure 3-20: Sample holder of the sensor platform. (A) Sensor chip immersed in culture medium. (B) The sensor (bottom square) was placed on the sample holder. The lid is hanging above (top square). (C) Side view on sample holder with mounted cell chamber and the microscope objective. (D) Top view through the PMMA lid onto the sensor.

Optical Observation System

Optical observation of the cell culture within the platform sensor was performed by a light microscopial setup composed of a zoom objective (Opto Sonderbedarf, Gräfelfing, Germany), a CCD camera (XC-ST50CE; Sony), and a frame grapper card (PXC-200; Stemmer imaging,

Puchheim, Germany). Illumination was provided by a broad band light source (HBO 50 35W; Zeiss, Jena, Germany) that coupled light into the system by a beam-reflector. A polarisation unit was used to improve the image contrast.

Application Software

The LabVIEW application software displayed, processed, and stored data acquired from extracellular recording and impedance analysis. Moreover, control of the lock-in amplifier was performed using LabVIEW functions via digital channels of the data acquisition cards. The software was based on the work of a diploma student who implemented a routine to efficiently process high volume data as are obtained from extracellular recordings [Steininger 2005].

The application software contained three major panels; The control bar (see dashed rectangle in Figure 3-21) indicated information on the status and the signal output of the lock-in amplifier. Additionally, it controlled display parameters, spike detection parameters, impedance recordings, and extracellular recordings. Two specific screens were programmed for analysis of extracellular recording data or impedance sensing data, respectively. Screenshot images of the operating surface are given in Figure 3-21 A and B. Operations that were integrated in the software are listed below.

- Protocol: Observations or present parameter settings were written as comments stored with precise time information.
- Data storage: Spiking activity or impedance changes were recorded as data files in ASCII format (termination was performed manually or automatically by a count-down-mode).
- Spike detection: Threshold values were set manually for each electrode channel to allow determination of the spike rate (spikes per time). Spike counting was ceased for a defined time period after a spike event was recorded to prevent artefacts as multiple counting of the same spike.
- Replay tool: Analysis of extracellular recordings was performed by reviewing data as single spike trains (see Figure 3-22).
- MUX controlling: The lock-in amplifier required electrode specified settings. Optimal settings for time constant, sensitivity, and phase correction values were determined during the beginning of an experiment and stored in a matrix for all electrodes. In the multiplexer mode, values for the sensed electrode were transmitted to the digital input of the lock-in amplifier (Figure 3-21 B).

A

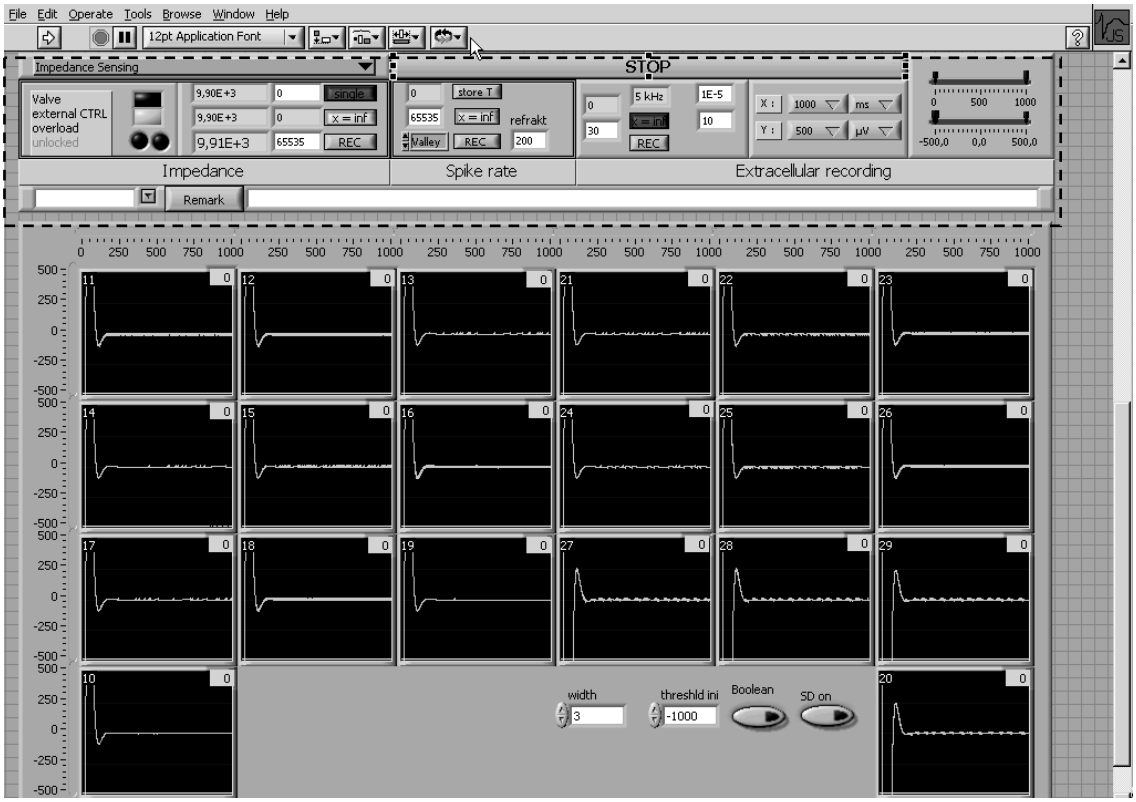

B

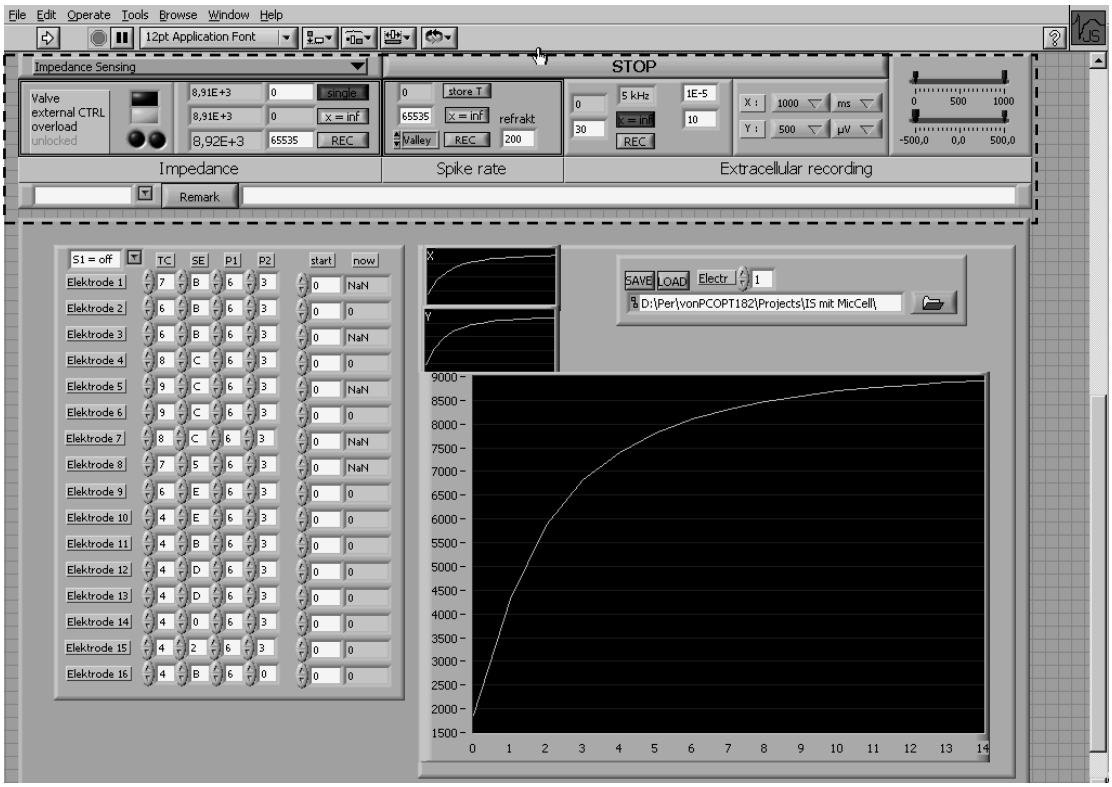

Figure 3-21: Screenshot images of the application software. (A) Screen used for the analysis of extracellular recordings. (B) Screen for impedance sensing analysis. The control bar is highlighted by a dashed rectangle.

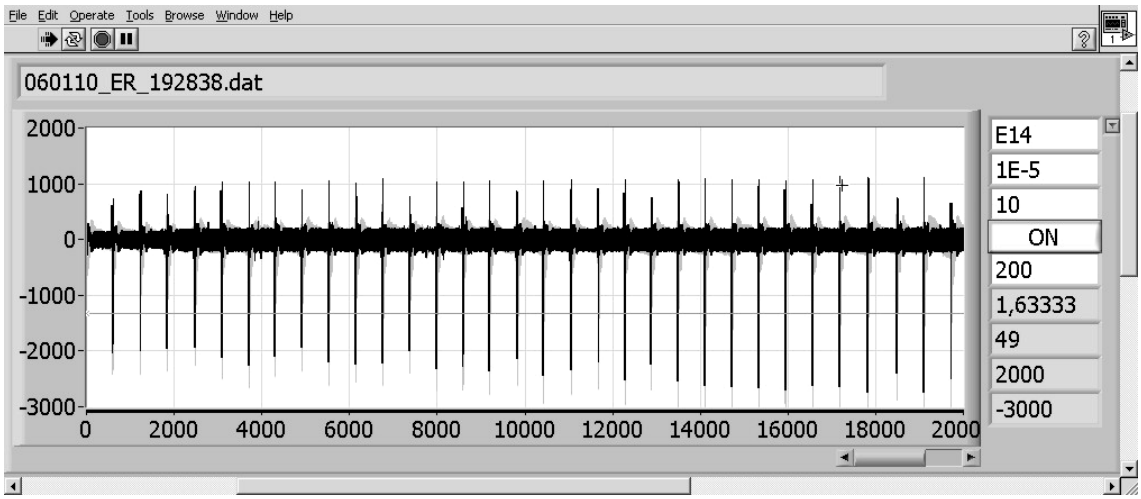

Figure 3-22: Spike train of a period of 20 seconds displayed on the replay tool.

The screen for monitoring extracellular recordings is presented in Figure 3-21 A. The amplified local field potentials were displayed in an array of 20 electrodes referring to the geometry on the MEA chip array. In Figure 3-21 B the screen is shown that was used for monitoring impedance sensing. Here, the control matrix of electrode number and lock-in pre-settings were adjusted prior to each experiment. Three graphs represented impedance parameter magnitude *R*, in-phase component *X*, and the quadrature component *Y*.

The review tool for extracellular recordings is presented in Figure 3-22. Stored data was loaded into the program and displayed as a single spike train for each electrode. Zoom functions on both axis and a bandstop filter were useful to reveal information even from data with a low signal-noise ratio and at different time scales.

4 Results and Discussion

4.1 Investigation of Cell-Substrate Interaction

Cell attachment and detachment processes of human ovarian tumour cells (OV-MZ-6) on Petri dishes or microelectrode array (MEA) chips were monitored by EIS, single frequency impedance sensing, and optical phase contrast microscopy.

Two different approaches were followed that are both related to anti-cancer strategies: Monitoring of

- the competitive binding of synthetic ligands to $\alpha_v\beta_3$-integrins on the cell membrane and
- the effect of photodynamic therapy (PDT) using photoactivated hypericin.

4.1.1 Experimental Set-up

The Flip-Chip MEA sensor (see Chapter 3.2.1) was inserted into the incubation system (Chapter 3.3.1) and placed on a microscope stage as depicted in Figure 4-1. The peripheral sensor pads on the sensor circuit board were connected to an external impedance analyser.

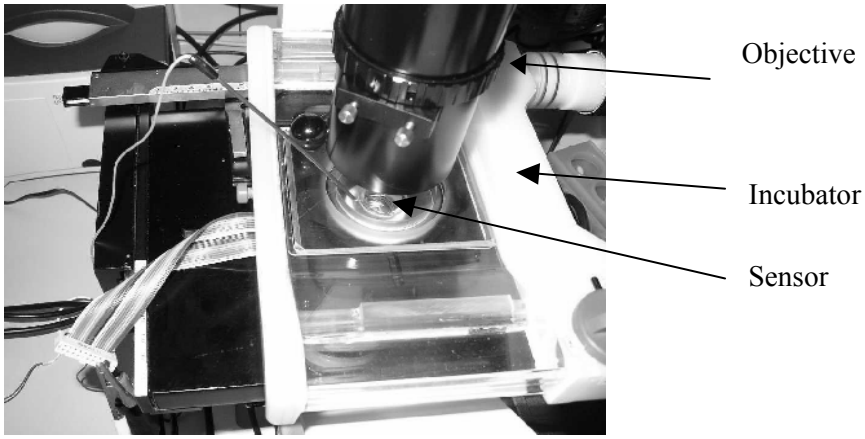

Figure 4-1: Setup used for analysis of cells on Flip-Chip MEA biosensors. Impedance analysis and optical microscopy were synchronously performed. Experiment was performed at 37°C.

4.1.2 Dynamic Cell-Substrate Interaction

Optical Characterisation of Tumour Cell Adhesion

This section focuses on visual observation of cellular behaviour during attachment and detachment. Fibronectin (Roche Applied Science, Mannheim, Germany) was applied to a proportion of a Petri dish at a concentration of 50 µg/ml diluted in PBS. Then, OV-MZ-6 cells were added at a concentration of 400,000 cells per ml and incubated for 24 hours.

Cells exclusively settled down to the area precoated with fibronectin, and no attachment was observed on the area devoid of coating (Figure 4-2). Cells in suspension appeared as spherical objects surrounded by a halo (see cells on top of Figure 4-2), whereas adherent cells revealed a flattened, darkly shadowed, and often polygonal shape. As a result, coating of multiadhesive protein was found to be crucial for successful cell adhesion *in vitro*.

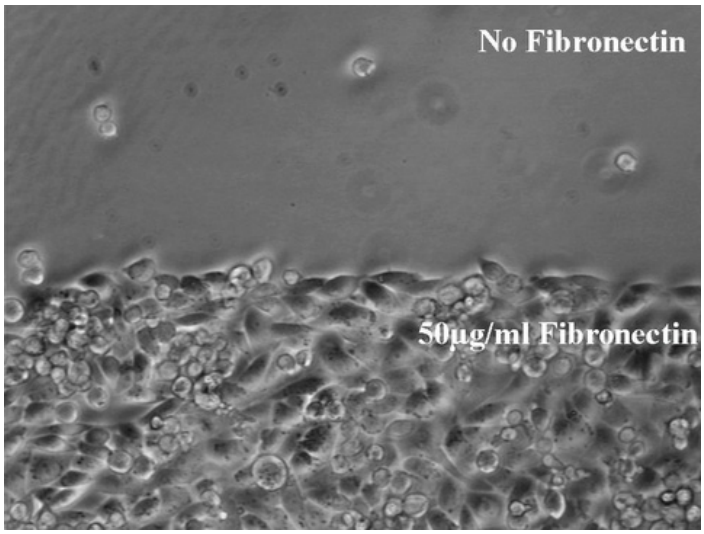

Figure 4-2: Fibronectin coating mediates cell adhesion. Phase contrast microscopy image of OV-MZ-6 cells on a polystyrene dish, partly precoated by fibronectin. The image was taken four hours after cells were applied to the sensor. Experiment was performed at 37°C.

In Figure 4-3, a group of cells was observed during a time period of about 6 hours. Time lapse imaging allowed demonstrating different stages of cellular attachment, motility of adherent cells, and even proliferation. Cell attachment was observed focusing on a proliferating cell and its offspring (red arrows). In this representative case, the proliferating cell was adherent (no image shown) before observation started. Shortly before mitosis, it changed to a spherical body (image 1) that was also observed when cells in suspension were added and started to interact with the substrate. Shortly after mitosis, the offspring cells formed focal adhesions (image 2) in analogy to (former) suspended cells shortly after attachment. After about one hour, this initial cell attachment was finished (image 5) and cells began to spread out on the surface. These two phases were related to stages of cell attachment, *cell adhesion* and *cell spreading.* Cell motility is clearly reflected by images 11 and 12 that were acquired at a time interval of 2 hours and 22 minutes.

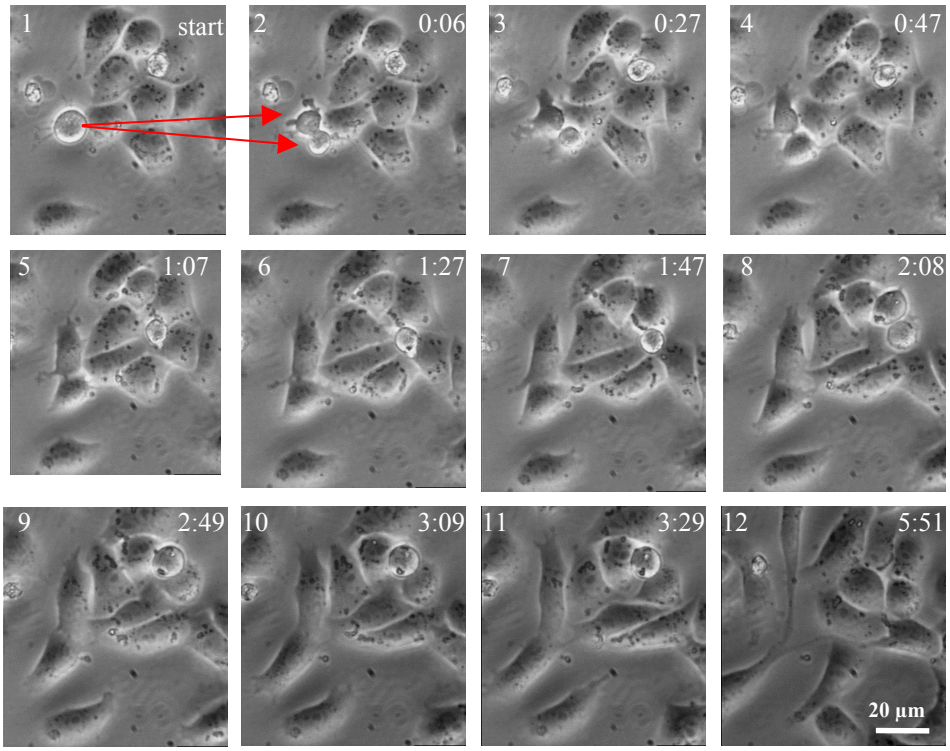

Figure 4-3: Cell attachment during cell proliferation. Micrographs show a part of a polystyrene dish laced inside the incubator and incubated with OV-MZ-6 cells. Image acquisition is indicated in the format of [hh:mm]. Especially the upper offspring cell (see arrows) started to increase its size strongly between images 4 and 6. This process is called *cell spreading*. Motile activity was particularly documented between images 11 and 12 (time interval: 2:22). Experiment was performed at 37°C.

Impedance Spectroscopy of Adherent Tumour Cells

Attachment and detachment of tumour cells at 37°C.were monitored by Electrochemical Impedance Spectroscopy (EIS) on Flip-Chip MEA sensors. Therefore, electrodes of various sizes were connected to a frequency response analyser in a two-electrode configuration and cells were seeded to the sensor surface. Cultivation of cells took place as described in Chapter 3.1.1.

The impedance spectrum of a 30 x 30 µm² gold electrode is shown during the course of a single experiment in Figure 4-4. The Bode diagram covers a frequency range of 100 Hz to 1 MHz. The initial bare electrode impedance is represented by a solid line. In this situation, only a precoating of adhesive protein was adsorbed to the electrode surface. The second impedance scan (dashed line) was recorded after the electrode was covered by a confluent cell layer as also shown in the image inset. The dotted impedance spectrum was recorded at last after the cells were removed from the sensor surface by adding 0.025% EDTA binding bivalent ions crucial for cell adhesion.

Within a frequency range of 10 to 600 kHz, cell attachment caused a substantial increase of impedance magnitude (up to +172 % at 100 kHz; Figure 4-4 A). The system response almost returned to initial values after cell detachment was induced.

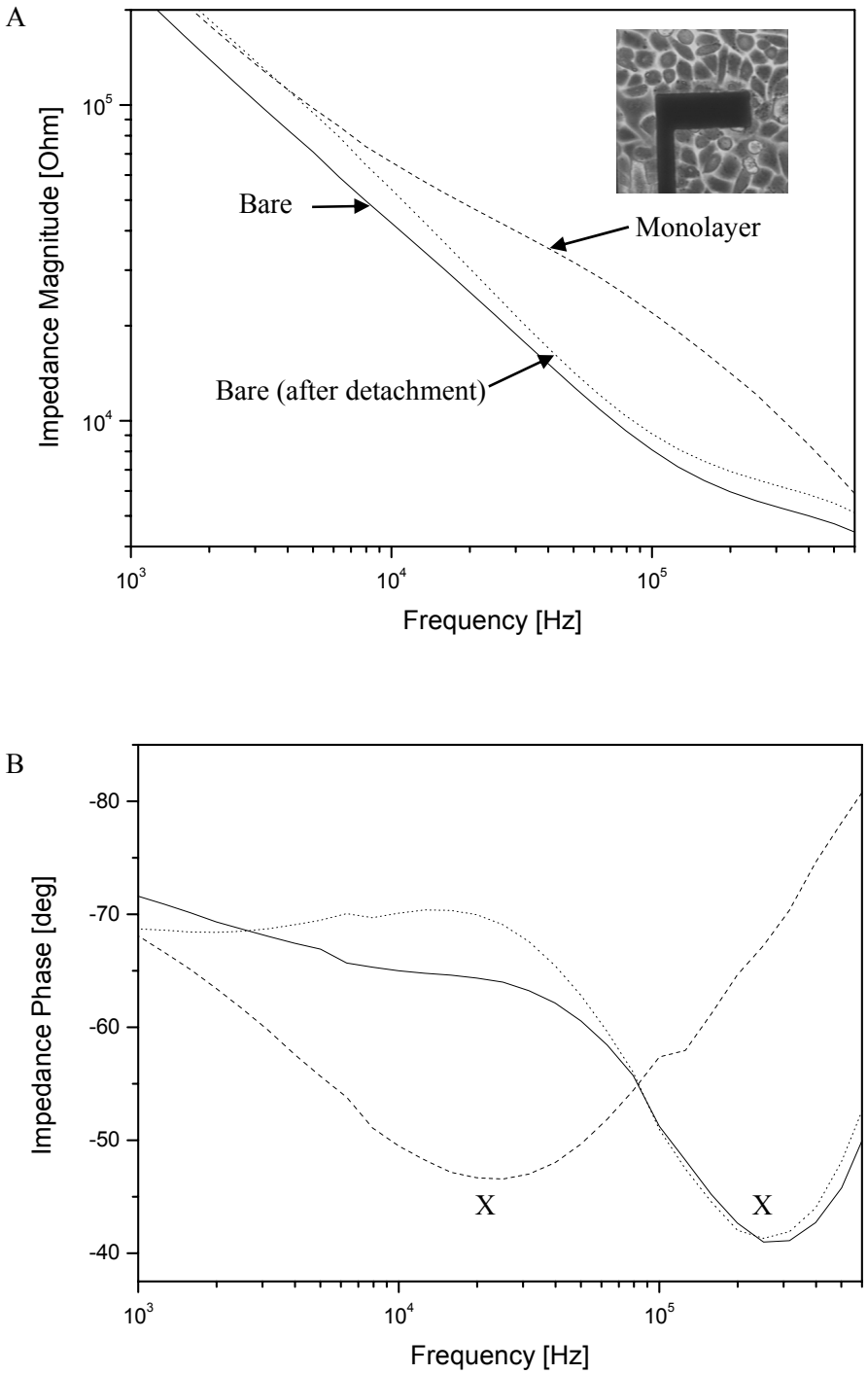

Figure 4-4: Cell-substrate interaction monitored by EIS. Data is presented as a Bode diagram with (A) magnitude plot and (B) phase plot. First, the electrode impedance of a bare 30 x 30 µm² large microelectrode was monitored (solid line; 'Bare'). Then, OV-MZ-6 cells were added that built a confluent layer after approx. 3 hours (inset image; dashed line; 'Monolayer'). Finally, cells were removed from the sensor surface by EDTA administration (dotted line; 'Bare (after detachment)'). 'X' marks in (B) refer to impedance phase maximum values for cell covered and bare sensors.

Impedance phase characteristics were also influenced by the formation of a cell layer on the electrode (Figure 4-4 B). The maximum value of the impedance phase (X in Figure 4-4) correlated well with the state of cell attachment. First, 200 - 300 kHz were registered for the initial cell-free situation. Then, after cellular attachment to the electrode, the maximum value shifted to 20 kHz. Measuring the impedance phase after removal of cells confirmed that the frequency shift of the maximum value is almost reversible.

The effect of attachment became even clearer when the impedance magnitudes of both cases were compared (Figure 4-5). Obviously, the system was not equally sensitive over the entire frequency range – a peak was found to be located at 70 kHz for the 30 x 30 µm² electrode used.

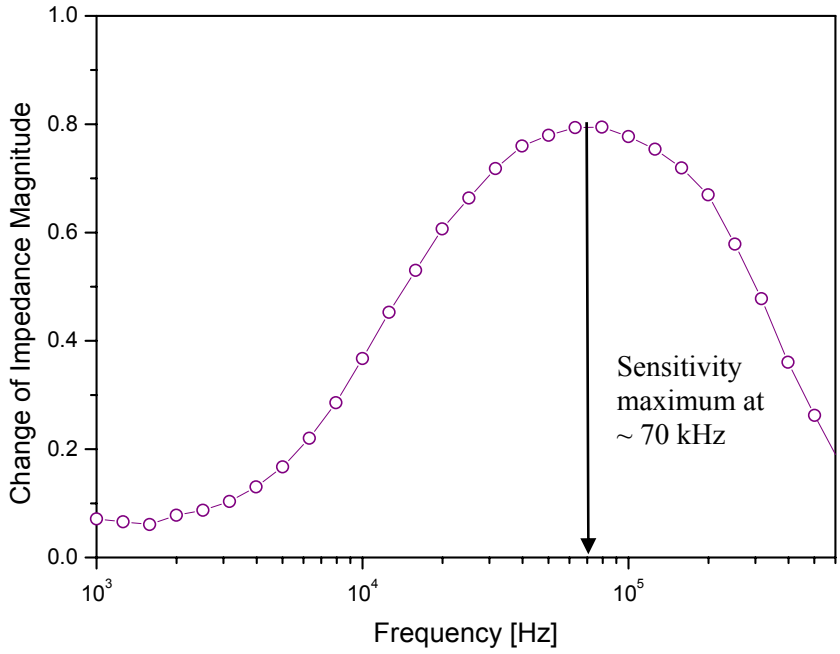

Figure 4-5: Optimal sensitivity of monitoring cell-substrate interaction. Cellular attachment was monitored by Impedance Spectroscopy and normalised to bare sensor conditions.

Analysis of Cell-Substrate Interaction

Data of several experiments investigating adhesion and detachment of OV-MZ-6 cells were analysed by equivalent circuit modelling in order to determine parameters that reflect cell-surface interaction. The model used was already presented in Figure 2-13 D and is now given again in Figure 4-6. It comprises a constant phase element (CPE) counting for the surface of the microelectrode and a RC element representing the electrode coating. An additional non-linear component in series to the resistance counting for diffusion related phenomena might increase the accuracy of modelling but would also result in a higher variance of model elements [Hillebrandt 2001].

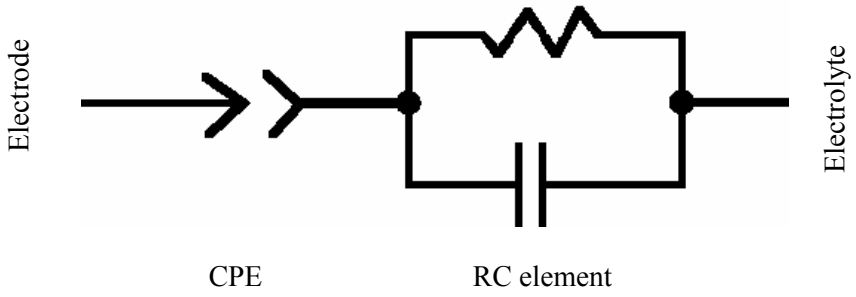

Figure 4-6: Equivalent circuit used for modelling EIS data.

The accuracy of the modelling process is illustrated in Figure 4-7 that comprises measured data (circles) and the resulting fitting curve (solid line).

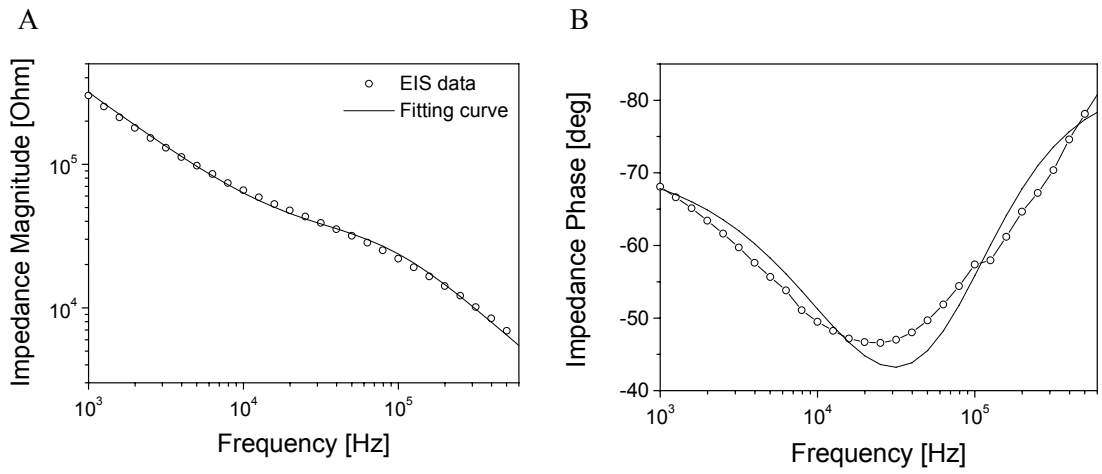

Figure 4-7: Modelling accuracy. (A) Magnitude plot and (B) phase plot of EIS data that was acquired from a bare electrode (30 µm diameter; circles) and fitting curve (solid line).

Parameter extraction revealed a correlation of the model parameter resistance *R* to cell-substrate interaction (Table 4-1), whereas CPE parameters and capacitance *C* did not correlate (Table 4-2). Resistance *R* increased strongly for monolayer formation (*Adhesion*) whereas culture medium exchange (*Control*) only caused a weak increase that can be referred to further protein adsorption from FCS supplement. That might have been tested by a control experiment by flushing without FCS. Detachment by either chemical, enzymatic, or mechanical treatment (0.025 % EDTA, 0.25 % Trypsin/EDTA, Pipette flush) led to a decrease of resistance *R*. The latter, *Pipette flush*, involved mechanical removal of cells by rinsing using a Pasteur pipette.

Table 4-1: Change of resistance in adhesion and detachment experiments. Data was normalised to bare electrode results (bare electrode = 0) in the cases of *Control* and *Adhesion* and the fitting result of an electrode covered by a confluent monolayer in the cases of *EDTA*, *Trypsin* and *Pipette flush*. Additionally, the standard deviation (SD) and number of experiments performed are indicated.

Experiment Type	Change of Resistance	SD	Experiments
Control	0.504	0.181	5
Adhesion	3.182	2.445	12
EDTA	-0.703	0.249	3
Trypsin	-0.670	0.206	6
Pipette flush	-0.625	0.312	4

Table 4-2: Change of capacitance in experiments. Number of experiments as indicated above.

Experiment Type	Change of Capacitance	SD
Control	-0.064	0.158
Adhesion	-0.034	0.506
EDTA	0.370	0.436
Trypsin	0.262	0.436
Pipette flush	0.068	0.335

Table 4-3: Change of CPE-T parameter in experiments. Number of experiments as indicated above.

Experiment Type	Change of CPE-T	SD
Control	0.256	0.169
Adhesion	-0.143	0.547
EDTA	0.393	0.250
Trypsin	0.215	0.251
Pipette flush	-0.065	0.180

Dynamic Cell Adhesion

The ongoing process of OV-MZ-6 cell attachment was monitored by EIS on the same type of electrode as previously shown (30 x 30 µm²). Cell attachment to the sensor is displayed by superimposed spectra that were acquired at interval of 20 minutes in a single Bode diagram in Figure 4-8.

During the first hour of measurement no response was observed. Then, during the following 80 minutes impedance magnitude rose and the phase maximum shifted to lower frequencies as described before. Both kinds of impedance representations show that cellular attachment to the sensor is not recorded equally over the whole frequency range. At 600 kHz, adhesion was measured already within the first hour. In contrary, during this time period no response was monitored at 10 kHz. This finding is illustrated in Figure 4-9 by normalisation of impedance magnitude values to initial bare electrode values.

The delay of the response for certain frequencies is an important finding for setting up the single frequency impedance analysis system. The frequency used for system stimulation has to be chosen carefully under consideration of the type of experiment. A cell adhesion experiment involving a bare sensor would require a higher stimulation frequency than an assay with already cultured cells on the sensor observing the detachment (e.g. invasion of tumour cells into confluent cell culture). A comparison of three different frequencies is given in Figure 4-10.

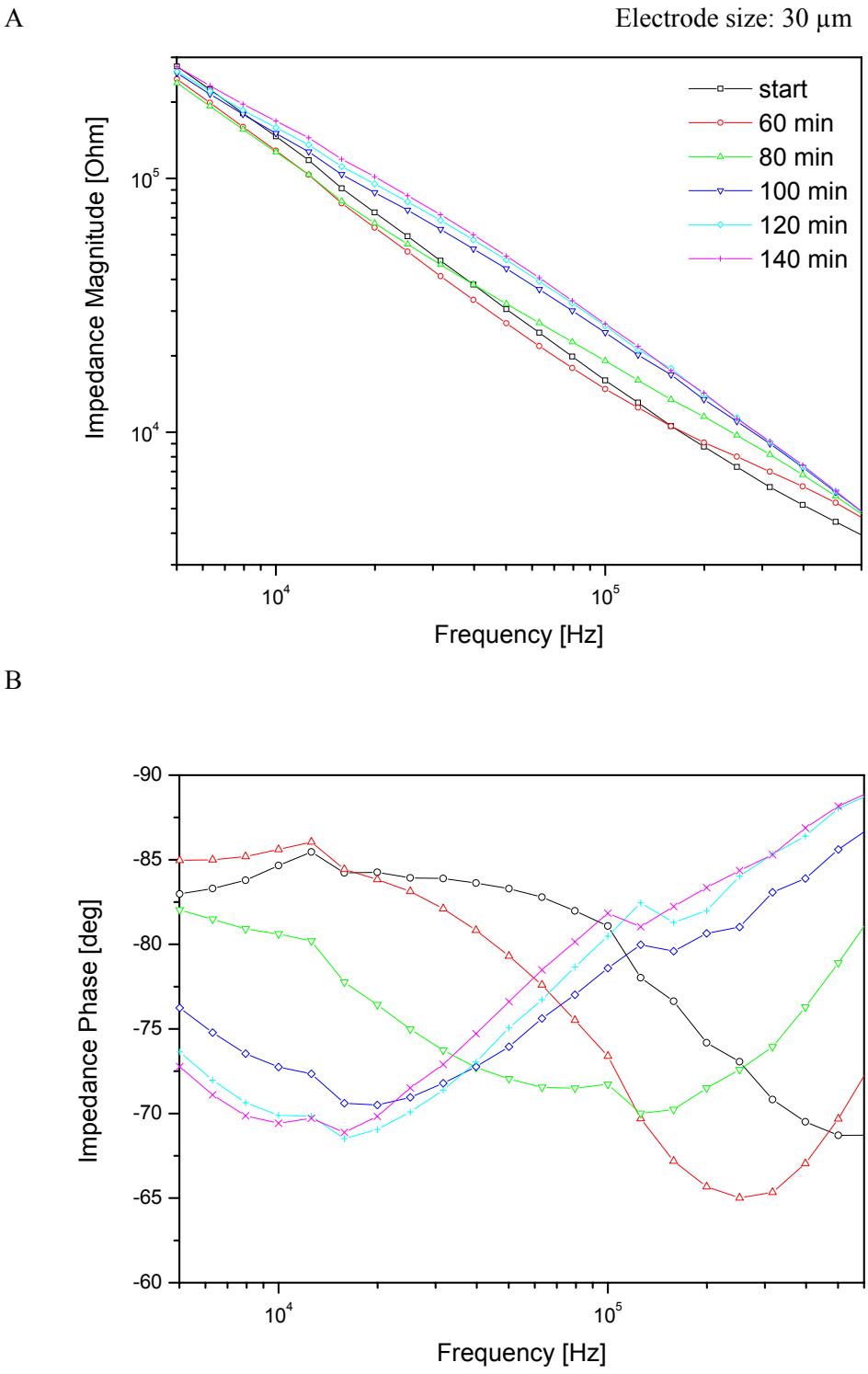

Figure 4-8: Dynamic cell adhesion monitored by EIS. (A) Impedance magnitude plot. (B) Impedance phase plot. Monolayer formation is shown on a single microelectrode at a time interval of 20 minutes. Open circles reflect the condition prior to cell addition.

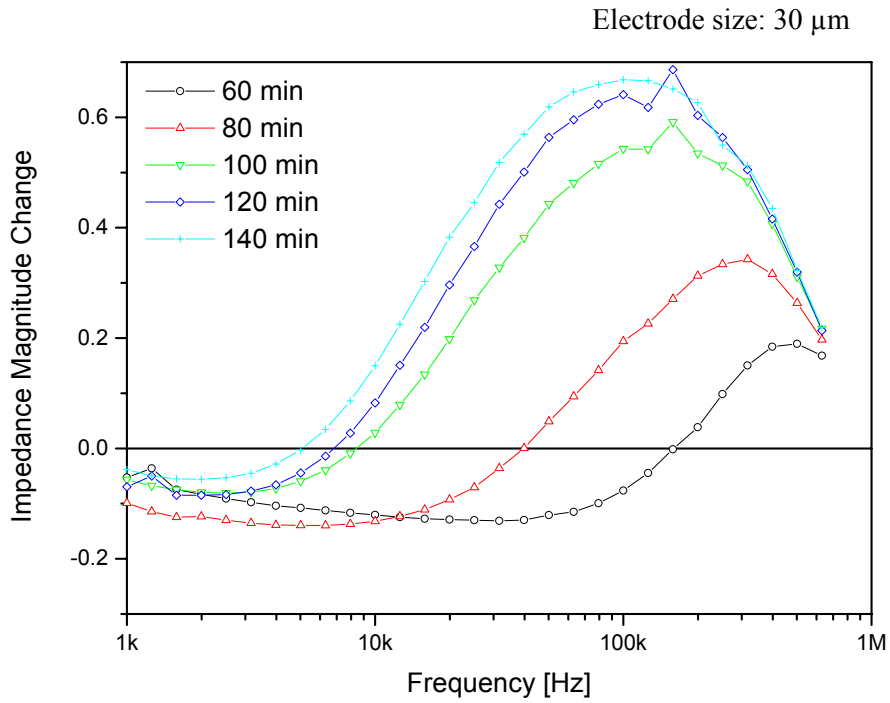

Figure 4-9: Change of impedance magnitude during dynamic cell adhesion. Cells were seeded on the sensor at time zero. Attachment was first observed at high frequencies (500 kHz). Completion of the monolayer was most sensitively monitored at 70 kHz.

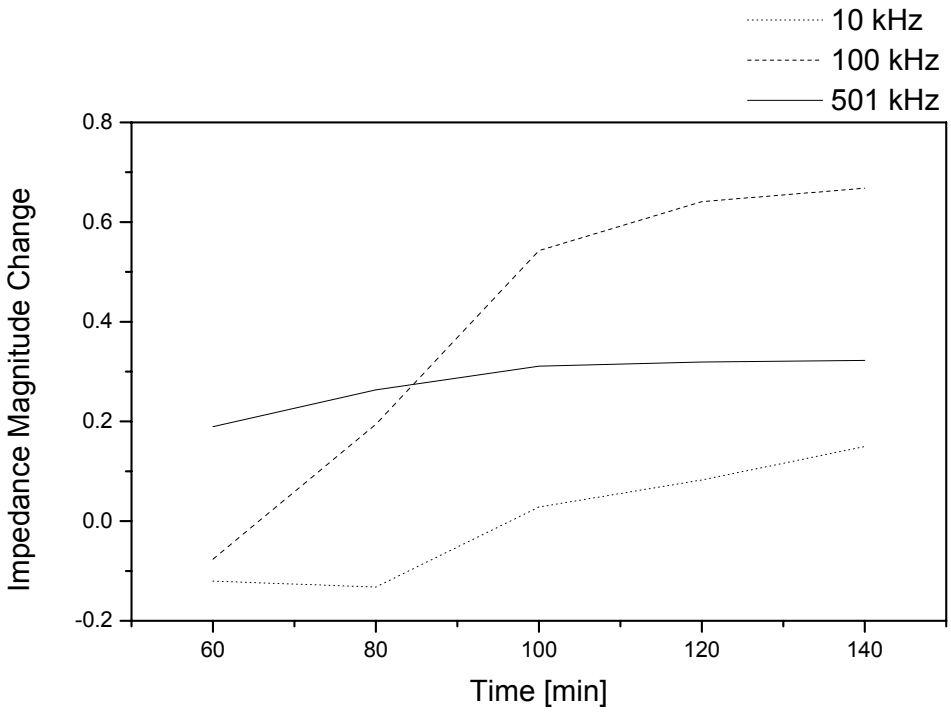

Figure 4-10: Dynamic cell adhesion evaluated for three different stimulation frequencies.

Impedance Sensing at Single Frequencies

Cellular attachment was monitored using the impedance sensing device described in Chapter 3.3.1. Because the voltage output of the system was non-linear, the system was calibrated as described in Appendix E. The sensing frequency was varied in order to confirm previous statements on frequency dependencies. Additionally, the influence of the electrode size was investigated by using differently sized working electrodes (Figure 4-11).

Previous findings for multi-frequency measurements were confirmed on electrodes of 30 µm diameter (Figure 4-11 A). The 95 kHz impedance signal showed a higher sensitivity than the 10 kHz signal. The cellular response in both experiments was monitored almost instantly which is in contrary to the case presented in Figure 4-8. Here, the signal did not change for about one hour. Presumably, the coverage of the electrode differs from experiment to experiment revealing different adhesion kinetics. Following this idea, the experiment presented in Figure 4-8 might document the situation of a bare electrode that has been covered by cells late during the course of the experiment.

Interestingly, a strong influence of the size of the working electrode was found, too. On working electrodes with a diameter of 300 µm (Figure 4-11 B), the lower frequency was found to elicit a more sensitive signal.

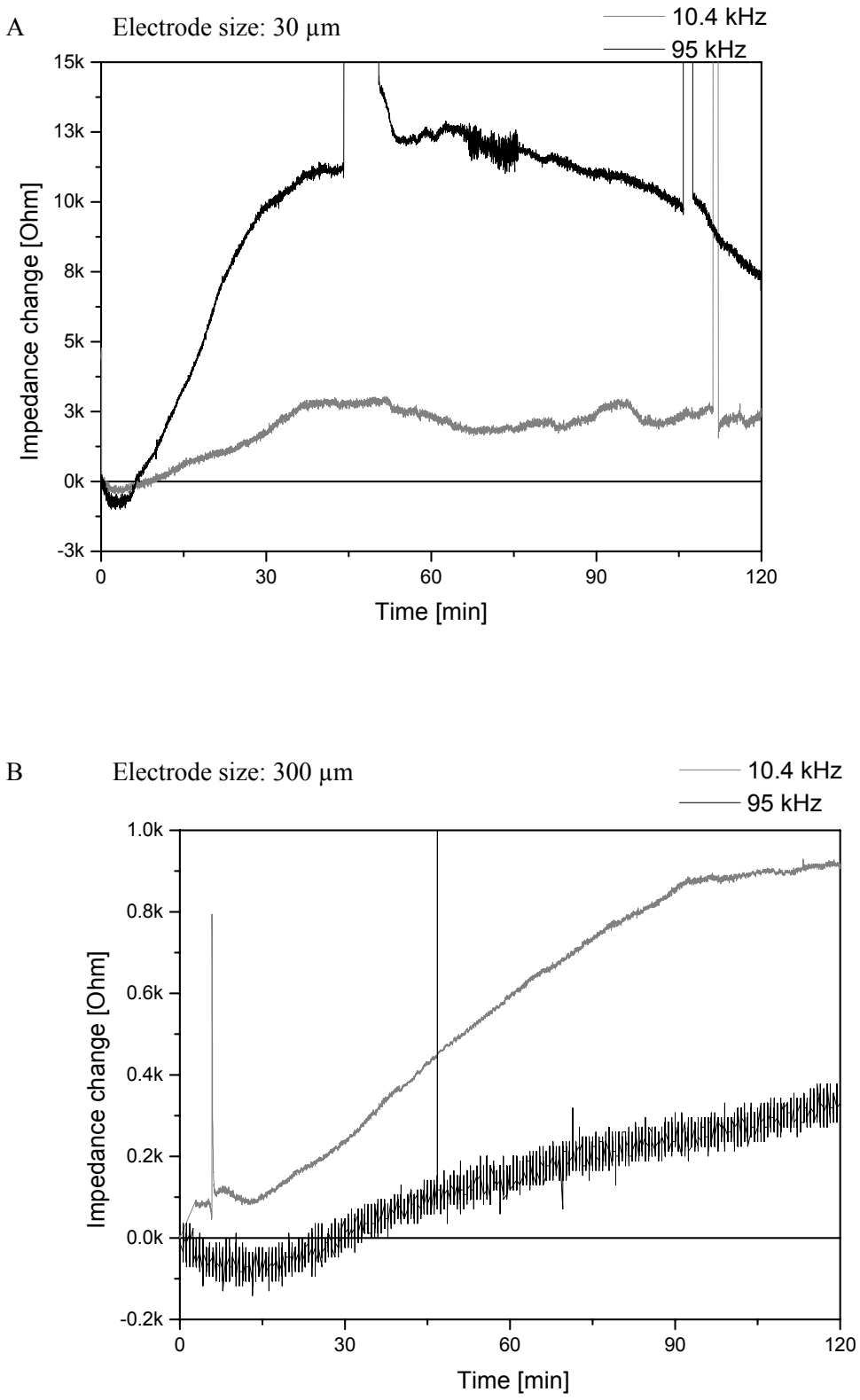

Figure 4-11: Single frequency impedance analysis for cell attachment. Cell attachment monitored by single frequency impedance analysis at 95 and 10.4 kHz. (A) 30 µm electrode size. Signal interruptions result from the transfer of the sensor to an external microscope. (B) 300 µm electrode size. Experiment was performed at 37°C.

4.1.3 Integrin Ligand Induced Cell Detachment

Investigation of cell-substrate interaction so far involved either total attachment or total detachment of cells in rather exemplary situations. These experiments only represent the spread of possible responses. This chapter now, monitors the influence of an integrin ligand that competitively binds to the tumour cells. Therefore, OV-MZ-6 cells were cultured on Petri dishes and Flip-Chip MEA biosensors until confluence. Optical microscopy, EIS and single frequency impedance sensing were performed on working electrodes sized 30 µm.

After recording of the initial electrode impedance, the integrin ligand c(-RGDfV-) or the control peptide c(-RADfV-) were added at a concentration of 500 µg/ml, and the response was monitored for a period of about 2 hours. Tumour cells started to lose contact to the substrate and detached after addition of c(-RGDfV-) (see Figure 4-12).

A 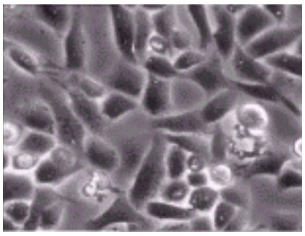 B 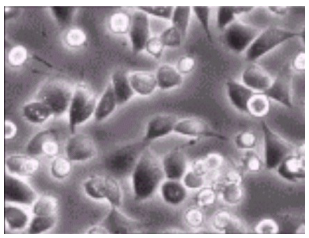

Figure 4-12: Integrin induced detachment monitored by microscopy. Images represent the same group of cells before (A) and after (B) administration of c(-RGDfV-) for 2 hours and 14 minutes. Experiment was performed at 37°C.

In Figure 4-13, impedance spectra of cells that experienced integrin ligand-induced detachment are compared to spectra of bare and confluent covered biosensors. After addition of c(-RGDfV-), impedance magnitude decreased during two hours of incubation.

The mechanism behind is supposed to be a higher affinity of the synthetic integrin ligand to the RGD binding site compared to one of the multiadhesive protein. An interesting control experiment would have been to monitor the response of un-attached cells to immobilised c(-RGDfV-) on the sensor surface.

Results of the model parameter resistance *R* for the described integrin ligand assays and other detachment processes are given in Table 4-4. No change was observed after c(-RADfV-) application, while c(-RGDfV-) resulted in an impedance magnitude decrease as seen for previous detachment assays. The response is weaker because this kind of cell detachment still leaves residual cells behind.

In summary, real-time monitoring was performed using impedance analysing techniques in a more efficient way as e.g. the manual cell-counting assay. Automatic screening of large substance libraries for their potency to induce tumour cell detachment is in principle possible with this approach, offering a true real-time assay.

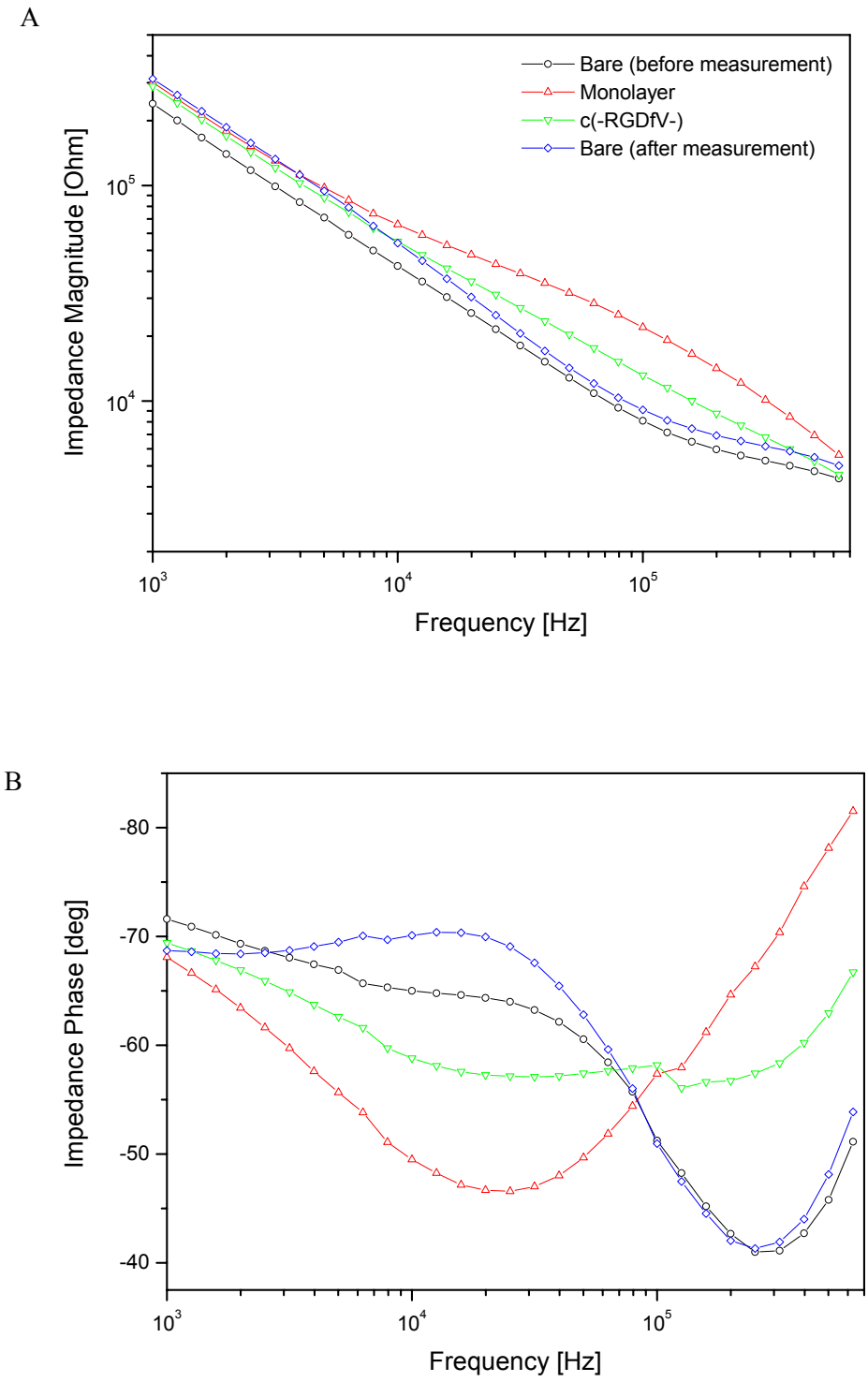

Figure 4-13: Integrin ligand induced detachment monitored by EIS. (A) Impedance magnitude for the bare electrode, the cell covered electrode, the electrode after 2 hours of incubation with c(-RGDfV-) peptides, and cell-free sensor induced by EDTA application. Legend is applicable for both diagrams. (B) Impedance phase.

Table 4-4: Fitting parameter *R* for integrin-ligand induced cell detachment. The impact of various treatments on the normalised resistance *R* is displayed: Integrin ligand c(-RGDfV-), the control peptide c(-RADfV-), chemical, and mechanical detachment methods. Values were extracted from the model circuit presented in Figure 4-6.

Experiment Type	Change of Resistance	SD	Experiments
c(-RGDfV-)	-0.374	0.498	8
c-(RADfV-)	0.010	---	1
EDTA	-0.703	0.249	3
Trypsin	-0.670	0.206	6
Pipette flush	-0.625	0.312	4

4.1.4 Photodynamic Therapy

This chapter also investigates whether impedance analysis can also be used to monitor the effect of Photodynamic Treatment or Therapy (PDT). This treatment involves local injection of a photosensitiser into tumour tissue and its subsequent irradiation. During PDT, a high proportion of cells that have taken up the photosensitiser are destroyed which can possibly be measured as an impedance decrease of the electrode/cell system.

Standard Procedure and Parameter Definition by Assaying Cell Viability

The procedure of PDT is drawn schematically in Figure 4-14. Confluent human ovarian tumour cells (OV-MZ-6) were cultured on multi-well plates and incubated with hypericin at various concentrations for at least 12 hours. Then, broad-band irradiation was performed at varying exposure times. Cell viability was evaluated by examining trypan blue or thiazolyl blue tetrazolium bromide (MTT) assays, described in Chapter 3.1.3. Incubation time was 5 minutes in the case of the trypan blue assay and 60 minutes in the case of the MTT assay.

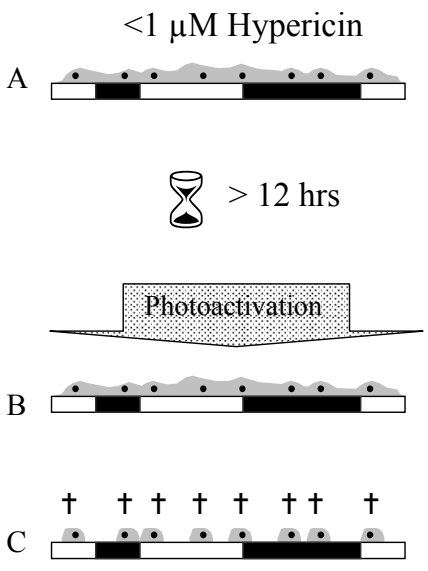

Figure 4-14: Photodynamic Therapy.

(A) Cells were seeded on the sensor chip - black areas represent sensing electrodes.

(B) The photosensitiser was incubated for at least 12 hours and subsequently photoactivated …

(C) … resulting in a decreased cell viability and gap formation on the sensor surface.

Trypan blue staining involved evaluation of the ratio of blue coloured and transparent cells by manual cell counting. In contrast, the MTT assay allowed automated plate reading and therefore cell viability was mostly assayed by this technique. The spectrometric absorption of the irradiated well content (composed of culture medium, MTT, formazan product, stopping solution, and cells) was measured at a wavelength of 570 nm and normalised to non-irradiated control wells. No visual effect was observed for irradiating cells without prior hypericin treatment.

In Figure 4-15 the effect of PDT is displayed for varied photoactivation duration and different hypericin concentrations. Cell viability was reduced up to 50 % for increasing hypericin concentrations and irradiation periods. Cells were barely impaired after treatment with 200 nM Hypericin. Due to the multiparametric character of this technique, it is difficult to confirm data by literature. Hendrickx *et al.* [Hendrickx 2003] applied similar Hypericin concentrations at a fluence rate of 4.5 mW/cm² using fluorescent lamps and received an IC-50 value of 80 nM.

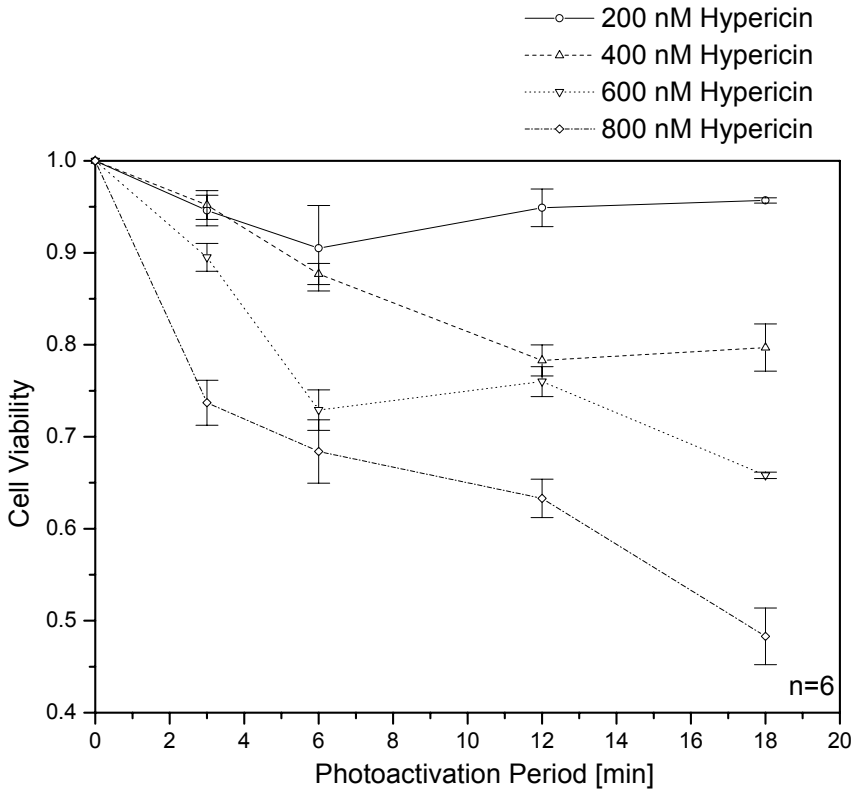

Figure 4-15: Cell viability after multiparametric PDT performed at 37°C.. Cells were treated with hypericin at denoted concentrations, subsequently irradiated at a fluence rate of 16 mWcm^{-2} for the given photoactivation period, and finally evaluated using the MTT assay. Data were normalised to non-irradiated samples.

Visual Observation

The effect of PDT on a culture of OVMZ-6 cells at 37°C was investigated visually by light microscopy. Hypericin concentration and exposure time of PDT exceeded the ones applied for the previously presented MTT assay, because the effect was supposed to be even clearer then.

After treatment (Hypericin 1 µM, 18 min photoactivation), a high proportion of cells lost contact to the substrate. Cell shape changed to a more spherical appearance and intercellular space increased (Figure 4-16 B). Cells sometimes looked like they burst and were adsorbed strongly to the sensor surface. Enzymatic digestion of residual cell matter was necessary for cleaning sensors.

On the other hand, no visually detectable destruction was evident for cells that were incubated with hypericin, but not irradiated.

A 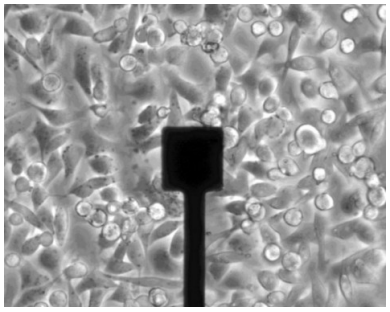 B 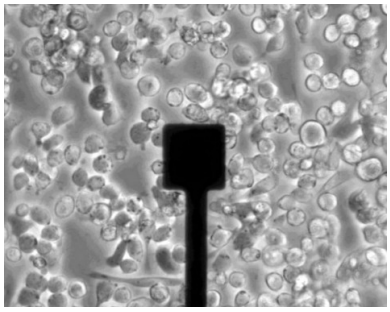

Figure 4-16: Effect of PDT monitored visually. Images of cells before (A) and after (B) photo-activation. The shadow was cast by the microelectrode.

Impedance Spectroscopy and Model Parameters

The effect of PDT was investigated by EIS on electrodes of 30 µm in diameter. Hypericin was applied at a concentration of 1 µM and irradiation lasted for 18 minutes.

Impedance spectroscopy data is shown in Figure 4-17 in a Bode plot. During photoactivation, impedance magnitude decreased for frequencies above 400 Hz and impedance phase maximum shifted by a decade to lower frequencies. Compared to detachment assays presented in Figure 4-4, these are similar characteristics.

In Table 4-5 model parameter resistance R is compared with results of previously presented experiments. Sealing resistance R was reduced which corresponded to the visually perceivable formation of gaps between the cells.

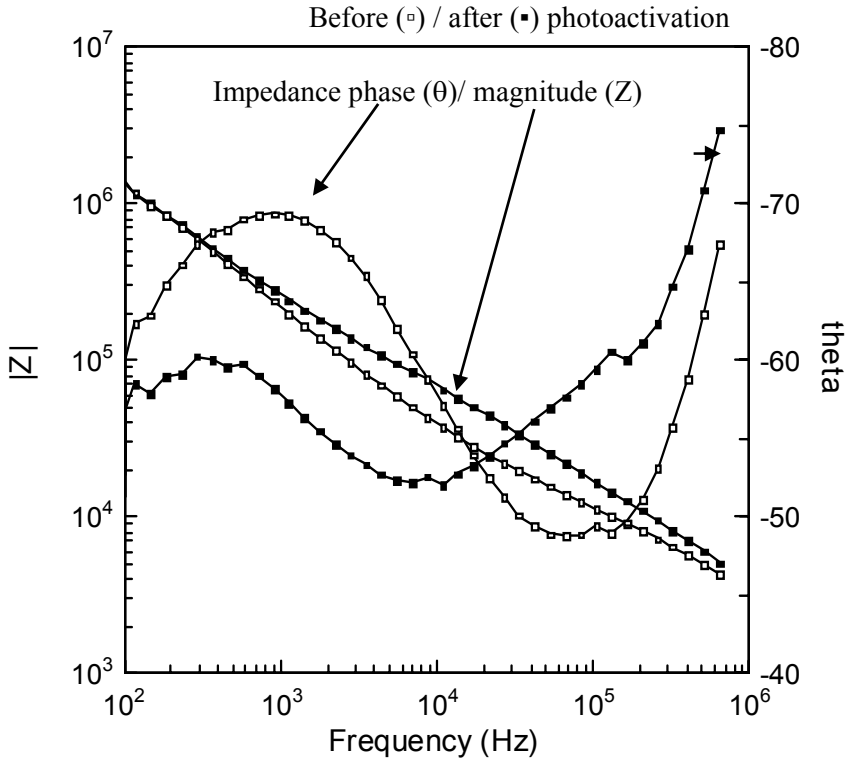

Figure 4-17: Photodynamic Treatment investigated by EIS. Tumour cells were incubated with 1 µM hypericin. The impedance of an electrode (30 x 30 µm²) was measured before and after photoactivation. The experiment was performed at 37°C.

Table 4-5: Change of modelling parameter resistance *R* for PDT and other detachment assays on microelectrodes. The circuit used for interpretation of EIS data was shown in Figure 4-6.

Experiment Type	Change of Resistance	SD	Experiments
Hypericin	-0.433	0.28	7
c(-RGDfV-)	-0.374	0.50	8
EDTA	-0.703	0.25	3
Trypsin	-0.670	0.21	6
Pipette flush	-0.625	0.31	4

Dynamic Process of PDT Monitored by Impedance Analysis

Again, cells were incubated with hypericin (1 µM) on a Flip-Chip sensor with integrated large electrodes (300 x 300 µm²) and monitored by EIS. First, the sensor system was kept in the dark and two curves were recorded in an interval of 30 minutes. These curves *Base line* and *Start PA* (photoactivation) showed that the system was in a steady state before PDT started. Then, impedance magnitude plots were recorded at an interval of 3 minutes and normalised to *Start PA* data.

Superimposed spectra are depicted in Figure 4-18. After photoactivation started, impedance magnitude decreased, reached saturation after about 12 min, and, surprisingly increased again during the late course of the experiment. It will turn out that this response is characteristic for the photoactivation of electrodes immersed in hypericin and must not necessarily be a cellular response.

The sensitivity maximum is located in the range of 16 kHz, which correlates to the results of the single frequency attachment experiment on a 300 µm electrode shown in Figure 4-11 B. The process of PDT was displayed as a single frequency representation at 16 kHz in Figure 4-19.

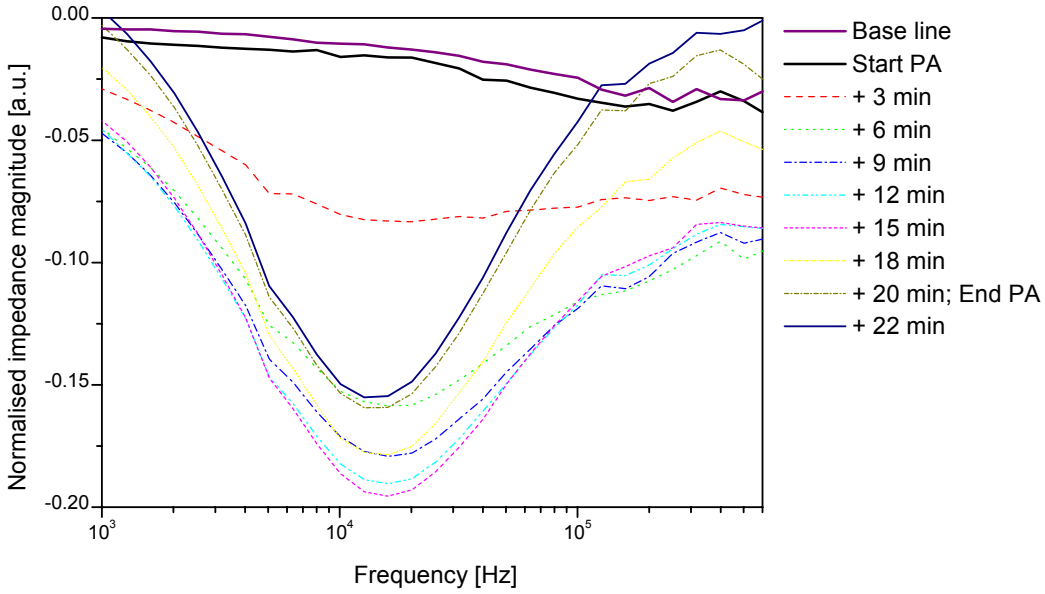

Figure 4-18: Impedance magnitude change of an 300 µm wide electrode during irradiation lasting for 22 minutes. Data was normalised to *Start PA* data. *Base line* was recorded 30 minutes before irradiation began and served as a control measurement. The experiment was performed at 37°C.

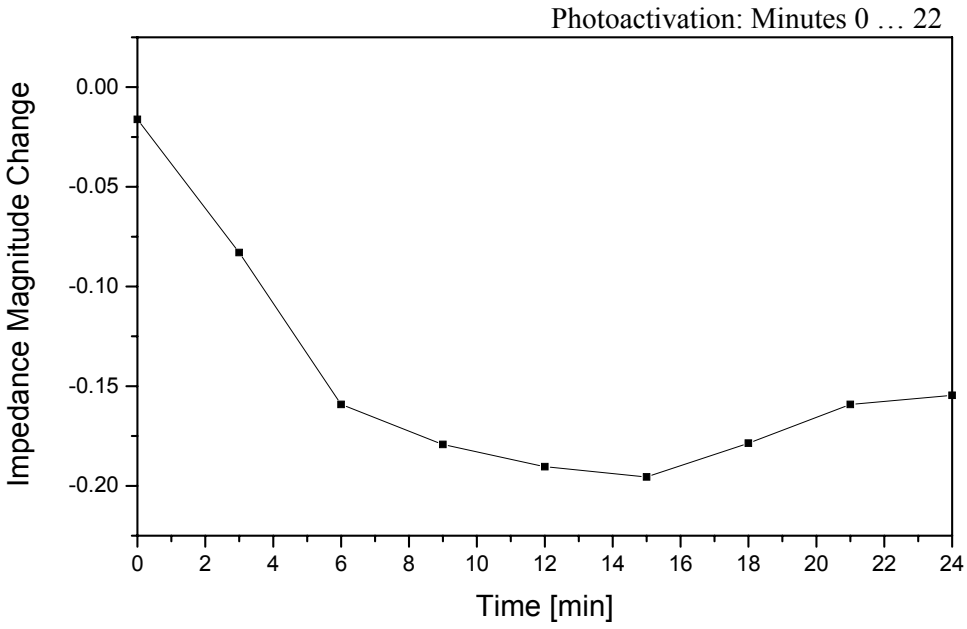

Figure 4-19: Single frequency impedance analysis of PDT. Impedance values were extracted from impedance spectra at 16 kHz on the data presented in Figure 4-18.

Single Frequency Impedance Sensing

The effect of hypericin containing culture medium on a bare, cell-free gold electrode (300 x 300 µm²) monitored by single frequency impedance sensing is shown in Figure 4-20. Irradiation of a gold electrode immersed in hypericin (1 µM) resulted in a reversible decrease of electrode impedance in the range of 100 Ω.

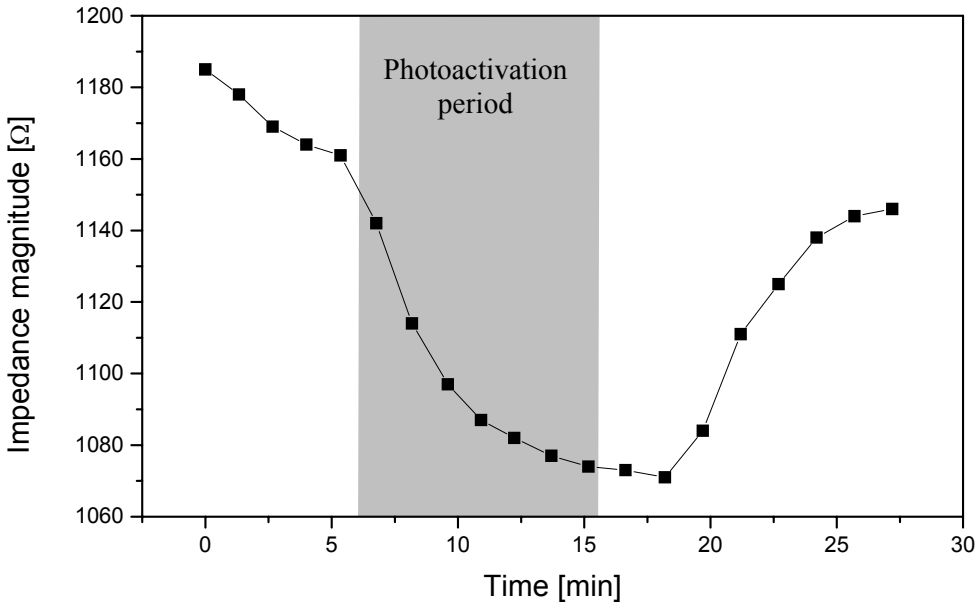

Figure 4-20: Impedance magnitude during photoactivation (using standard parameters).

Then, tumour cells (OV-MZ-6) were continuously monitored on a microelectrode (30 x 30 µm²) using the impedance sensing system, adjusted to a stimulation frequency of 95 kHz. It would have been interesting to perform these experiments also on the other electrode sizes, but unfortunately results are not available. Cells were incubated with hypericin (1 µM) and irradiated twice during a time period of 65 minutes. Despite the phases of photoactivation, the sensor was kept in the dark throughout the experiment.

The impedance magnitude of the electrode is shown in Figure 4-21. Before the light treatment began, impedance magnitude was measured between 19.0 … 20.5 kΩ. The slope of the impedance magnitude over time for the last 30 minutes before PA 1 was 0.04 kΩ / min. The first photoactivation interval (PA 1) lasted for about 7.5 minutes and induced a strong impedance magnitude decrease (slope: 0.21 kΩ / min). But interestingly, in contrast to the impedance sensing result, optical evaluation of the culture after PA 1 revealed no major changes in cell morphology. Most likely the duration of PA 1 was too short to result in sudden, visually detectable cell death. Impedance magnitude declined continuously even after termination of

PA 1 (slope: 0.13 kΩ / min) and did not reach saturation until the second photoactivation PA 2. Then, also micrographs documented visible destruction of the cells.

Provided that the correlation “decrease of impedance magnitude” and “increase of intercellular space” is valid, cells were damaged in response to PA 1 and continued to degrade after the first activation finished. During PA 2 the degradation process ceased at the maximal effect. This experiment outcome shows that fixed frequency impedance sensing can visualise processes that are beyond the scope of optical microscopy.

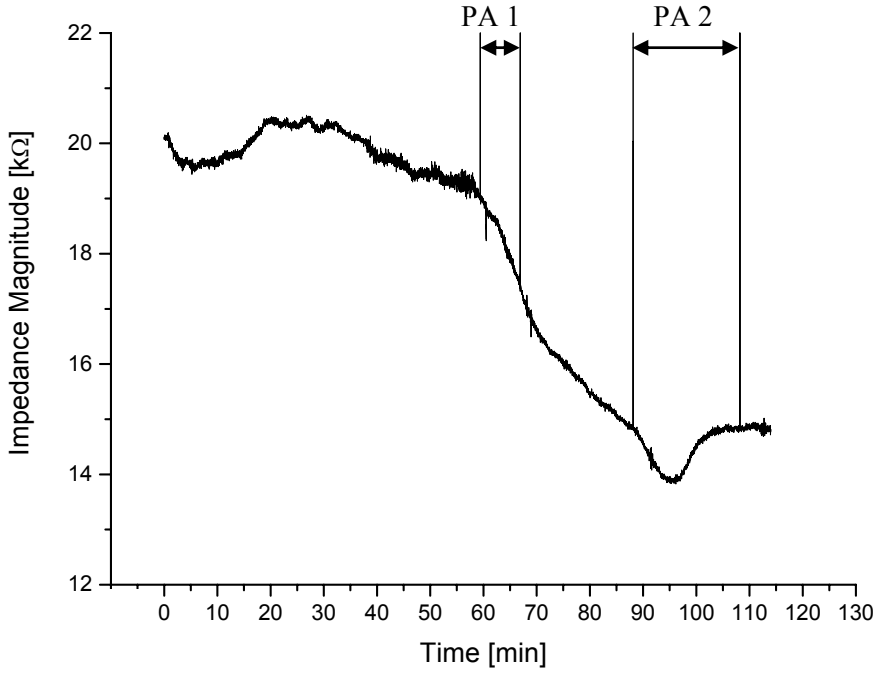

Figure 4-21: Two-phase PDT monitored by single frequency impedance sensing.
Stimulation frequency was set to 95 kHz.

4.2 Extracellular Recording from Cardiomyocytes

This chapter describes the implementation of a cell-based sensing system that was used to extracellularly monitor electrical activity of cardiomyocytes in a microfluidic flow system. A robotic dispensing machine offered automated test substance application in microlitre scale.

4.2.1 Set-up and Electrode Performance

The fluid dispenser was located inside a laminar flow bench to ensure sterile working conditions, as shown in Figure 4-22. The sample holder (see also Chapter 3.3.2) was mounted on the working table of this device. The biosensor, the so-called *microfluidic MEA chip* (see Chapter 3.2.2), and the microfluidic chip (see Chapter 3.2.3) were positioned inside. For better visualisation it is recommended to view a short video documentation attached on CD-ROM (for a list of contents see Appendix F).

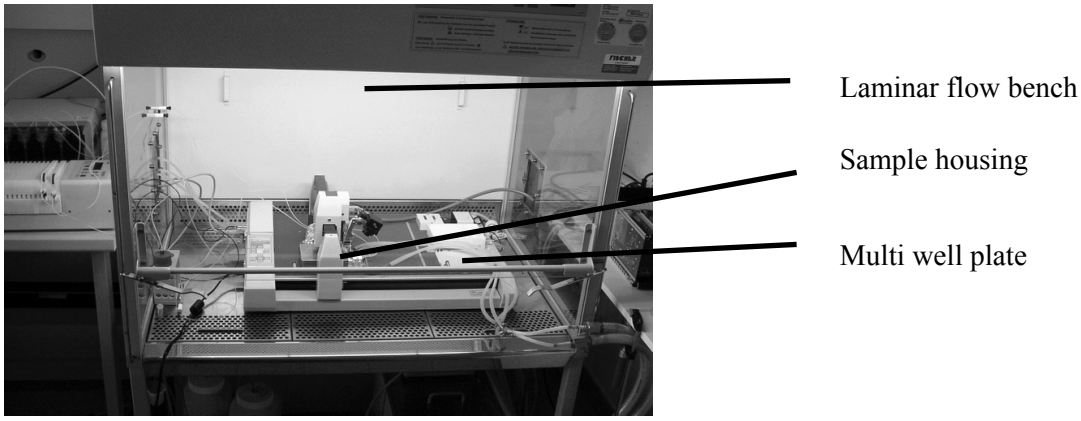

Figure 4-22: Setup used for extracellular recordings.

The noise level of the electrode was in the similar range to the commercial sensors due to deposition of platinum black. Background noise was determined to about 2000 µV peak-to-peak (pp) were measured for uncoated gold electrodes in contrast to 20 – 100 µVpp amplitudes for coated electrodes.

4.2.2 Cell Performance and Extracellular Recording

Cell Viability and Electrical Activity

Cellular activity of cardiomyocytes was investigated outside and inside the microfluidic system and compared to cells cultured on commercial available MEA devices. Sensors were covered with a confluent layer of cardiomyocytes (> 4 DIV) and signals were amplified against the counter electrode potential using the F-64 multichannel amplifier (Multichannel Systems, Reutlingen, Germany), described in Chapter 3.3.2. A peristaltic pump delivered culture medium at a constant, continuous flow rate of 0.4 µl/min.

When seeded to MEA sensors, cardiomyocytes spontaneously generated action potentials and started to contract following a quiescent period of about 1–2 days. This electrical activity was highly synchronised throughout the complete culture. After insertion into the sample holder, cells at first showed a quiescent period of about 2 - 5 minutes, presumably due to the insertion process. On commercial MEA chips (no insertion necessary) sudden electrical activity was observed. But, after a while, spikes of both systems were quite similar in shape and amplitude. (Figure 4-23 A). Often, a positive peak was displayed as an initial spike component that is not directly attributed to the recorded myocyte. It represents the ionic return flow from surrounding tissue that was previously excited [Halbach 2003, Pottek 2006]. A sharp negative peak followed and sometimes a 100 – 300 ms lasting negative but more sustained component was visible. The sharp peak was presumably caused by the cell membrane depolarisation due to reflux of Na^+ ions, while the following long-lasting Ca^{2+} influx into the cells was responsible for the second signal component.

Within the fluidic system spike shape changed considerably during long-term operation. After 10 to 30 minutes, most biosensor signals provided waveforms with decelerated time course as depicted in Figure 4-23 B.

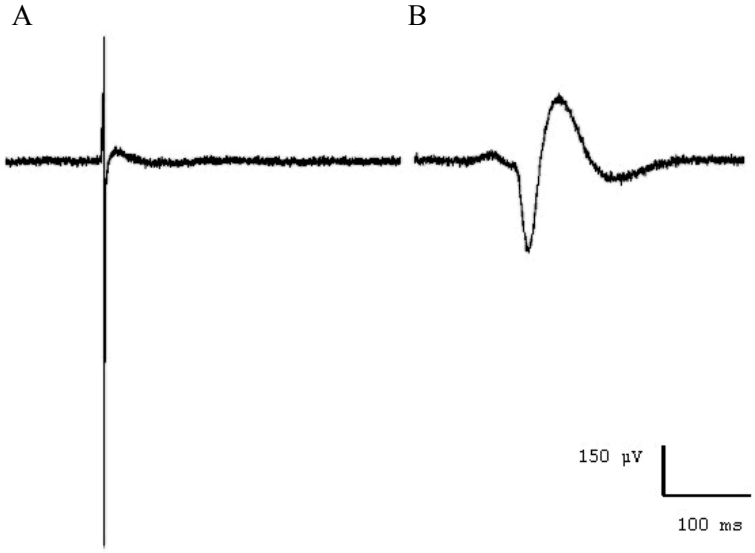

Figure 4-23: Electrical activity recorded from myocytes located within a microfluidic system. (A) Spike shortly after chip insertion. (B) Signal waveform from the same electrode 25 minutes later.

However, even with decrease of signal quality, the signal amplitude was still sufficient for a threshold-based spike detection. Cellular signals were detected for up to 6 hours inside the microfluidic system. A high synchronicity all over the sensor was observed as Figure 4-24 documents.

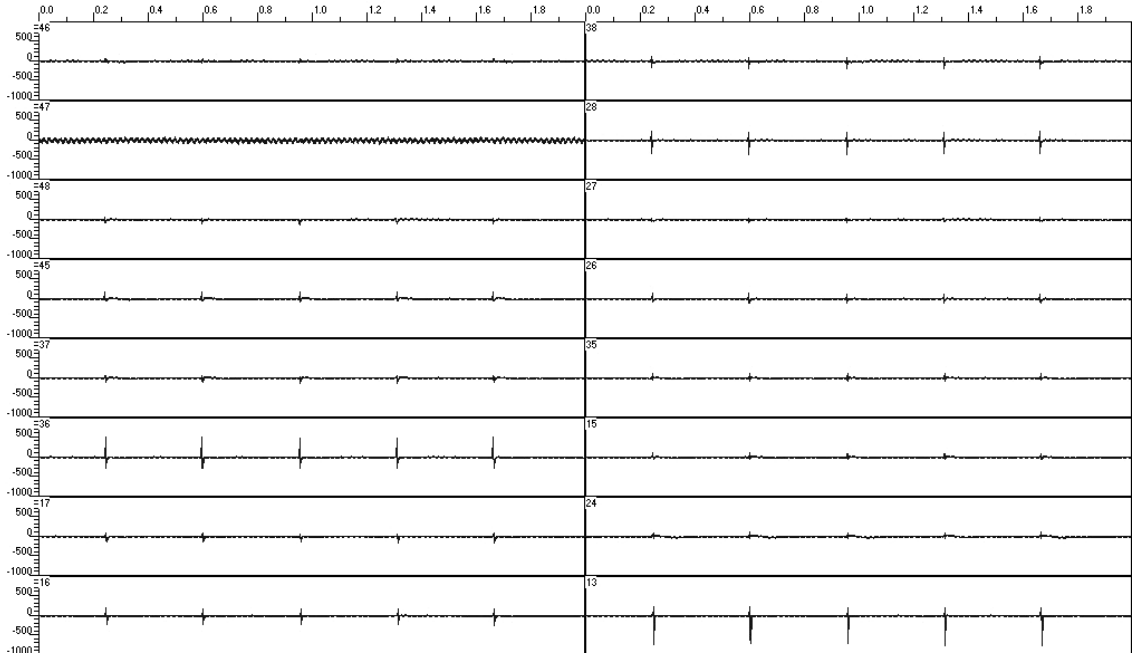

Figure 4-24: Synchronous cardiac myocyte signals. Screenshot of extracellular recordings on the microfluidic MEA chip. Axis show 2 Volts peak-to-peak over 2 seconds. The experiment was performed at 37°C.

4.2.3 Drug Screening

Drug Responsiveness and Parameter Extraction from Recorded Signals

Increasing concentrations of the β-adrenergic agonist isoproterenol in the range of 100 pM to 100 nM were applied to the screening system. Spike rate and duration were investigated over a duration of about 50 minutes. Drug application was always followed by rinsing with standard culture medium.

The time course of an experiment testing four isoproterenol concentrations is given in Figure 4-25. After each isoproterenol application, a rinsing step followed that lasted until the initially monitored base activity was reached again.

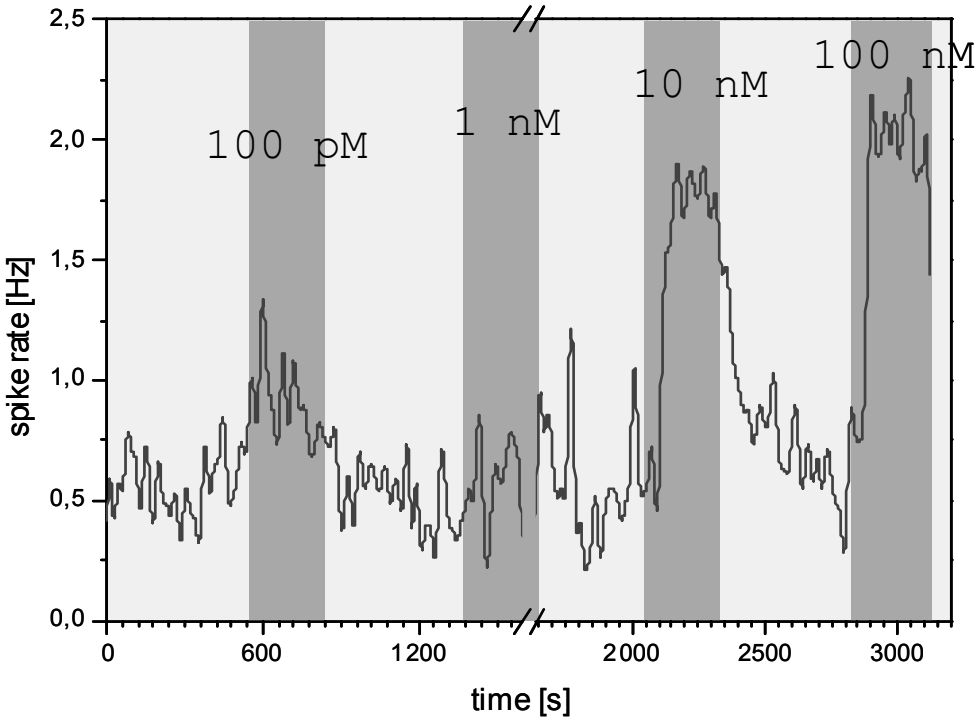

Figure 4-25: Rate measurements are shown over several concentration steps. Spike activity was given as the average rate calculated from intervals of 15 seconds. White areas indicated rinse cycles, whereas shaded areas refer to isoproterenol administration. Break down of electrical activity at 1 nM isoproterenol was due to air bubble transition. Base activity was in the range of 0.4 - 0.8 spikes per second [Pottek 2006]. The experiment was performed at 37°C.

After 24 minutes, during the second drug application phase (1 nM), air bubbles entered the fluidic system and caused transient activity reduction. Nevertheless, cardiomyocytes showed a strong effect to isoproterenol.

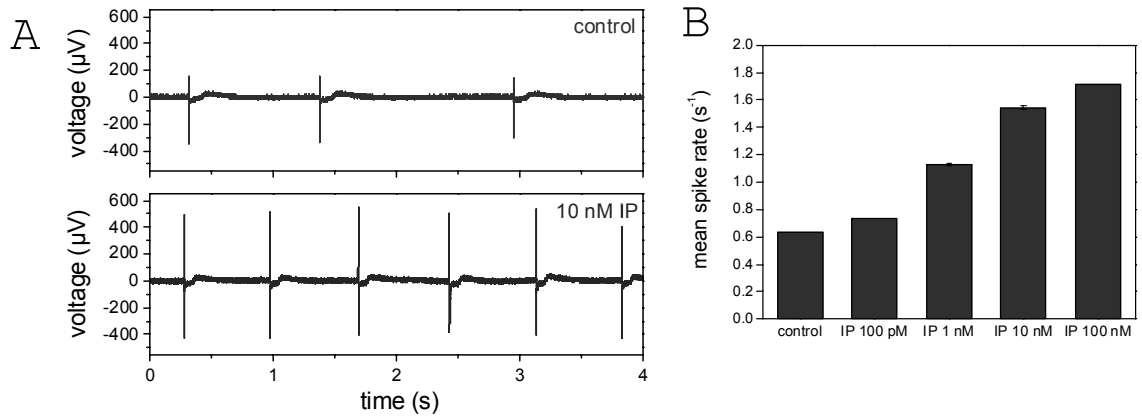

Figure 4-26: Isoproterenol administration to cardiomyocytes. (A) The spike rate was clearly improved upon 10 nM isoproterenol administration. (B) Increase of the mean spike rate due to isoproterenol administration at increasing concentrations [Pottek 2006].

Following drug application into the microfluidic system, the myocyte spike rate increased (Figure 4-26 A) and recovered during subsequent rinsing with pure culture medium. Signal acceleration was found to be dose-dependent. The system responded to an isoproterenol dose of about 100 pM and displayed saturation of the effect at 100 nM when spike rate was almost three times higher compared to the untreated condition (Figure 4-26 B).

In addition, the spike waveform was sensitive to isoproterenol treatment. The time interval between the initial Na^+ peak and the maximum of the repolarisation wave was decreased resulting in a shorter spike duration (Figure 4-27 B). This effect displayed dose-dependence with a threshold at 100 pM and a saturation at 100 nM isoproterenol. The interval was cut down to about 70 % of the original duration (Figure 4-27 A). Comparable values were also published by Jovanovic *et al.* [Jovanovic 2004].

In comparison to extracellular recordings on commercial MEA sensors, both effects were observed to a similar extent (not shown). The increase of signal frequency may also be due to a larger Ca^{2+} transient resulting in an artefact in the double layer caused by increased frequency of contraction. To analyse this it might have been interesting to apply butadione monoxamine to the cardiomyocyte culture. This substance is known to uncouple contractile proteins from electrical activity.

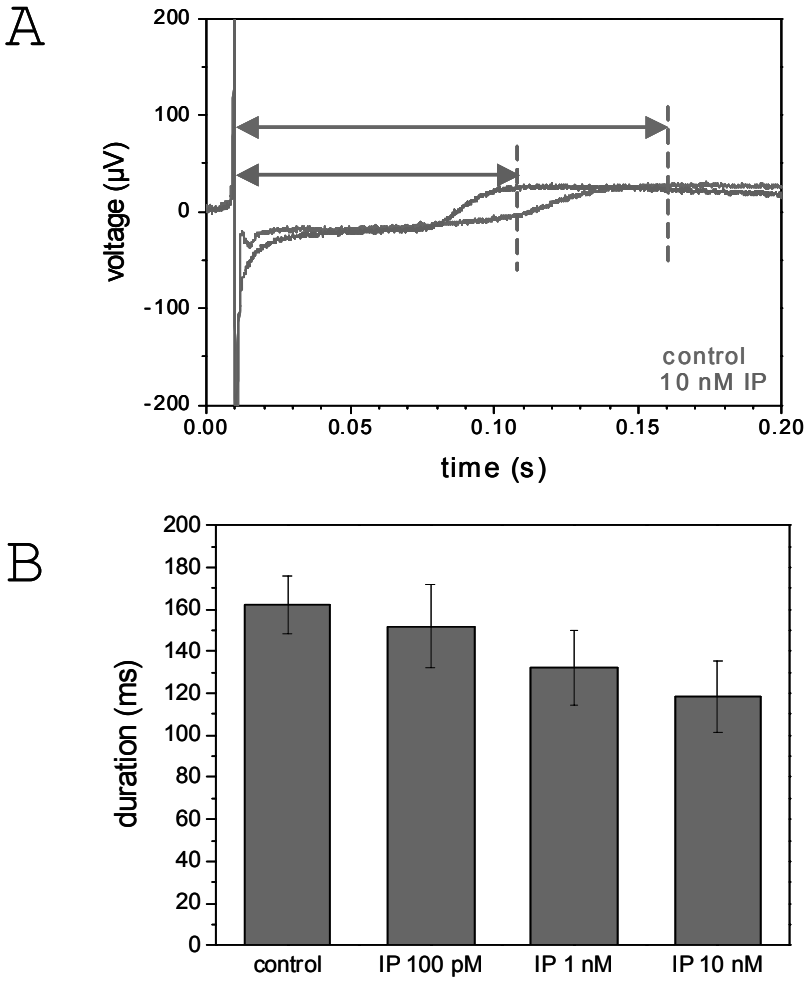

Figure 4-27: Spike duration was investigated on microfluidic MEA chips. (A) Administration of isoproterenol resulted in a decreased spike duration, which was defined as the time interval between the initial fast spike component and the maximum of the slow depolarisation wave (K^+ influx). (B) This effect was dose dependent [Pottek 2006].

The robustness of this system was not satisfying. Cells were strongly impaired after at least 30 minutes of operation which was too short to investigate substantial cell responses. The microfluidic chip was found to be part of this problem leading to a redesigned system using a step-like structure without direct streaming of medium across the cell culture. The existing device forced cell culture medium perpendicular to the cell culture surface (see Figure 3-6). Here, cells were directly confronted with streaming medium that although persistent adherence of cells requires shear stress free environment [Zantl 2004; personal communication].

Hence, the position of the microfluidic chip and the guidance of the channel were found to be central to impaired cell viability. Additionally, cells were located up-side-down on top of the

channel opening. This was part of the design concept, because the two openings, the injector port and the cell culture window, were etched into the silicon layer of the module and were therefore necessarily positioned in the same orientation. If air bubbles were transported inside the channel, they rushed across the cell culture with unfavourable effects for the cell culture. For instance, cells lost contact to the substrate and were rinsed off the sensor.

Several attempts were performed to improve the existing system. The flow rate was decreased which in turn caused an increased evaporation of injected fluids and a longer duration of rinsing cycles. General experiences with microlitre volumes applied to open, unsealed systems imply that evaporation is a problem as long no vapour-saturated atmosphere exists. But, after flow rate reduction from 10 µl/min to 0.4 µl/min, cells adhered to the chip for a longer period of time. About 65 % of the sensor arrays showed spikes with unimpaired waveform (Figure 4-23 B), within the first 15 minutes.

Spacers located on the MEA chip should prevent direct contact of streaming medium and cells. Therefore, PDMS spacers (thickness 0.2 to 0.9 mm) were placed between the MEA chip and the microfluidic chip. A hole, 1 mm in diameter, was mechanically punched into the spacer and aligned onto the cell culture. In practice, filling the spacers with culture medium was difficult, because air bubbles were trapped in the cavity of the spacer. Hence, cell viability was not improved by this method.

4.3 Microfluidic Cell-Based Sensor Platform

Based on the experiences with cells in a microfluidic environment (Chapter 4.2), a new concept was realised. In detail, a microfluidic platform was capable of screening living cells by impedance spectroscopy, single frequency impedance sensing and extracellular recording. Using this device, pharmacologically relevant responses of the cells can be monitored and evaluated.

Problems that arose using the previously described system were addressed with this new design. For instance, poor cell viability, evaporation of the injected fluid, and non-suitability for microscopy were identified as major disadvantages of the former system.

4.3.1 Set-up

In Figure 4-28 the sensor platform is shown with the peripheral instruments. Light source (Opto Sonderbedarf, Gräfelfing, Germany), temperature controller, and combined data acquisition and single frequency impedance sensing system were positioned on the left (top to bottom). The sensor holder was located in the central foreground. It was mounted on an X-Y table for moving the microscope focus across the cell sensor. Beneath the sample holder, multichannel amplifier and multiplexer board were mounted inside a aluminium box. The peristaltic pump for medium transport is shown in the centre background. The microscope objective and CCD camera were positioned above the measurement cell.

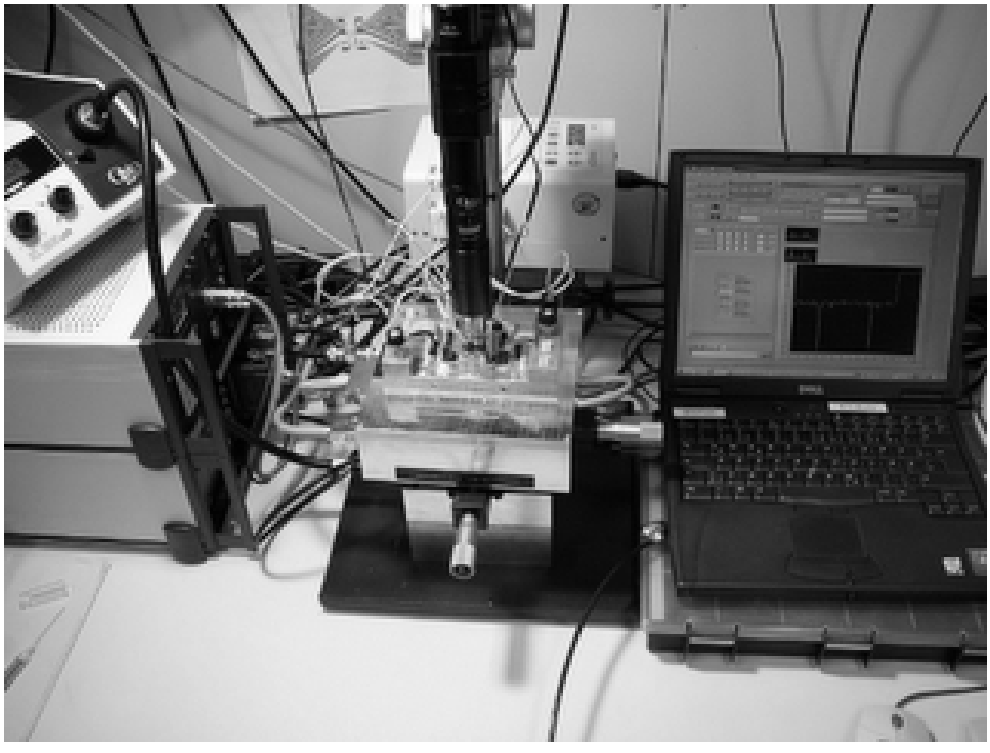

Figure 4-28: Biosensor platform with peripheral devices.

4.3.2 Evaluation of the Screening System

Cell Viability on Sensors

Cardiomyocytes and human tumour (OV-MZ-6) cells were cultured on MEA sensors at a density of 400,000 cells per ml and stored in an incubator (37 °C, 5 % CO_2 in O_2). Micrographs of cardiomyocytes were taken during cell culture using the microscope system described in Chapter 3.3.3.

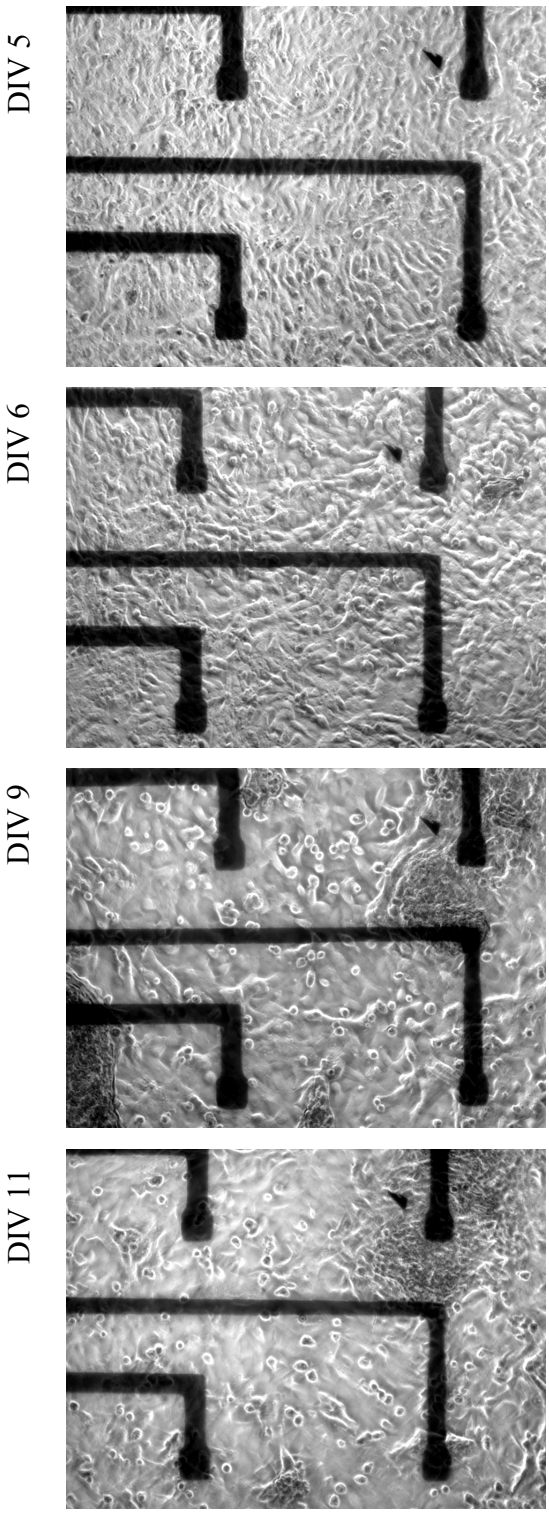

Figure 4-29: Long-term observation of cardiomyocytes. The age of the culture is indicated on the left as days *in vitro* (DIV). The experiment was performed at 37°C.

After 2 days of culturing the cardiomyocytes a monolayer will have remodelled and cells showed initial contractions after 3 days *in vitro* (DIV). Cells often gathered in groups that showed persistent contraction. In Figure 4-29 images of cardiomyocytes between 5 and 11 DIV are depicted. Cells showed a high grade of contractile activity.

The most critical procedure with respect to cell viability within the screening system was the sensor insertion at the beginning of each experiment. Because the sensor was immersed in a fluid during incubation, the peripheral contact pads on the MEA chip had to be dried before the sensor was inserted into the measurement system. During this step, culture chambers easily dried out or air bubbles were trapped inside the chamber (see next section). Nevertheless, most cell sensors showed electrical activity of a high quality for up to 8 hours.

Evaluation of the Fluidic Chamber

Throughout the experiments, sealing of the fluidic part against the MEA chip was identified as a difficult task. Air bubbles were easily trapped in the culture chambers between biosensor and lid and could not be removed even after fluid transport was started. The sealing was improved by a layer of Parafilm M (Brand, Wertheim, Germany) resulting in proper long-term water-tightness. Fluid injection was accomplished directly into the culture chambers because injection along the microchannel resulted in increased leakages.

Focusing on the visual performance of cells inside the system, they were not strongly influenced by flowing medium (at a flow rate of 81 µl/min and a duration of 45 min). Experiments revealed that 10 µl per minute is sufficient for proper exchange of nutrition. A compilation of time lapse images of tumour cells cultured inside a fluidic chamber is enclosed in the Appendix (Chapter 7).

4.3.3 Impedance Analysis

Impedance Spectroscopy of Tumour Cells on Various Electrode Types

Impedance spectra of confluent grown tumour cells (OV-MZ-6) were monitored on various electrodes. Therefore, the electrode impedance was monitored prior to and after enzymatic removal of a confluent cell layer using 0.025 % Trypsin/EDTA (Sigma). Culture medium or Trypsin solution were continuously pumped through the chambers at a rate of 10 µl/min. Different electrode types were investigated simultaneously: Interdigitated electrode couples, microelectrodes (30 µm), and large electrodes (300 µm) which were all described in detail in Chapter 3.2.4.

In Figure 4-30, impedance magnitude was analysed before and after cell detachment on the different electrode types. The values were normalised to the initial, cell-covered sensor and show that microelectrodes respond to cell coverage strongest - at least for frequencies around 80 kHz.

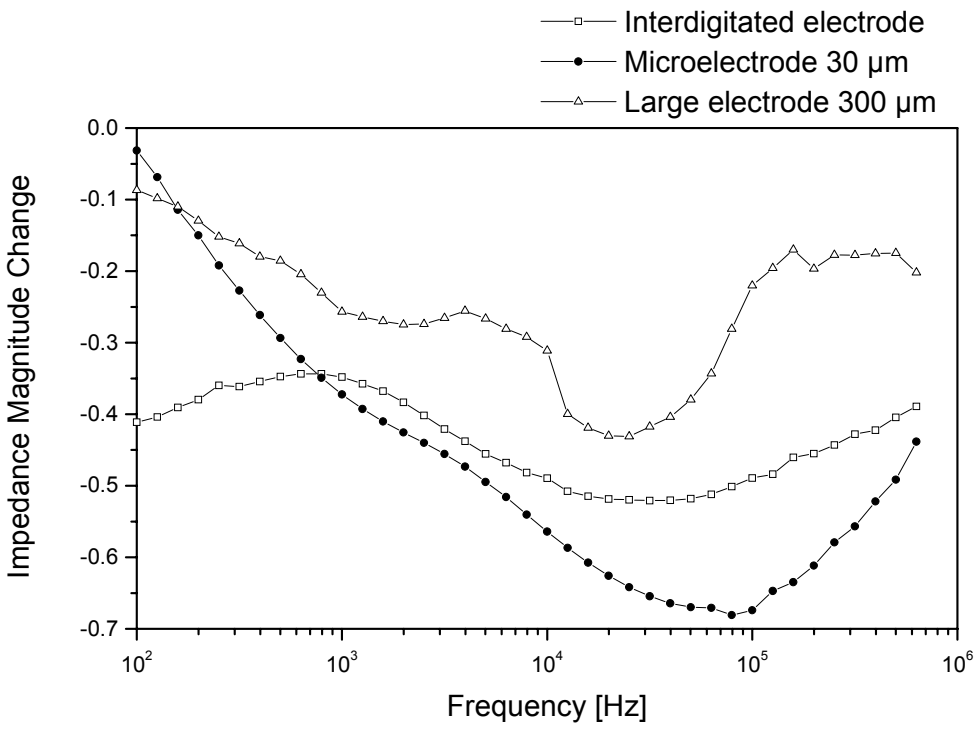

Figure 4-30: Cell detachment on three different electrode types monitored by EIS. Impedance values were normalised to the cell covered state of the sensor.

Impedance Sensing of Tumour Cells

The experiment described before was repeated with the single frequency impedance sensing system at a stimulation frequency of 95 kHz.

In Figure 4-31, the impedance magnitude change during detachment is shown again for the three types of electrodes. Upon Trypsin application, a dead time of about 15 minutes was observed until cells detached. During detachment, impedance values declined sharply for approximately 10 minutes and reached saturation after 20 to 30 minutes. The decline resulted in a decrease of 2.5 kΩ for the large electrode, of 4.4 kΩ for the interdigitated electrode, and of 7.8 kΩ for the microelectrode. Detachment was registered with the highest sensitivity by the microelectrode, which confirms previously presented results obtained by impedance spectroscopy.

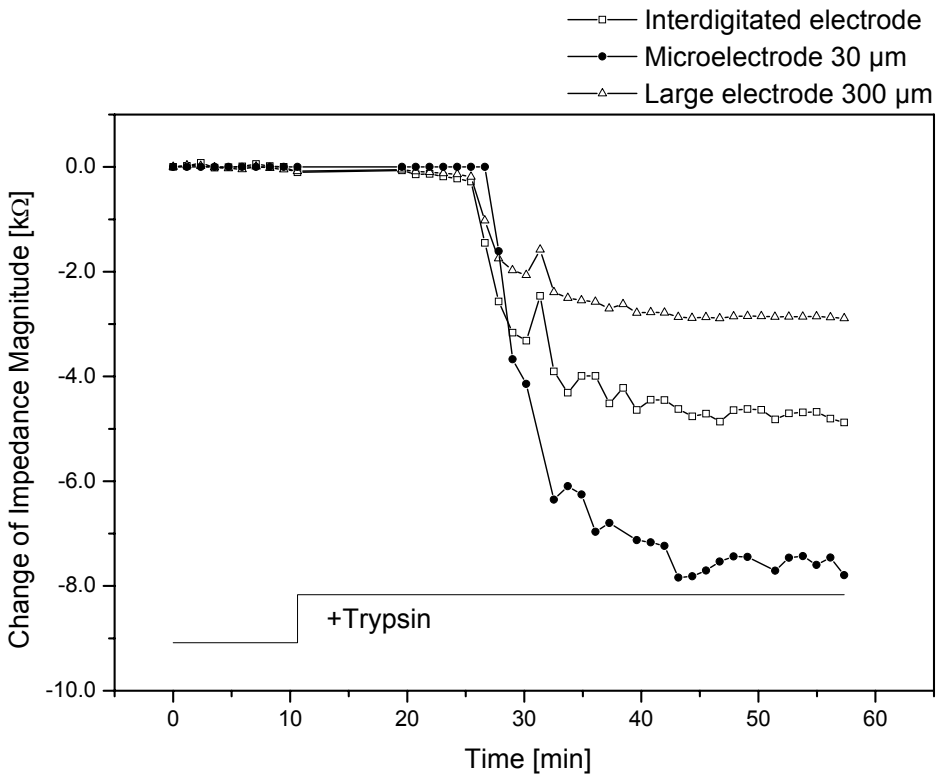

Figure 4-31: Impedance sensing results of a detachment assay. Three different electrode types were screened at 95 kHz during application of 0.025 % Trypsin. Data represent a single electrode each.

4.3.4 Extracellular Recordings

Spiking activity of Cardiomyocytes

Cardiomyocytes were seeded to culture chambers carrying microelectrodes. After an incubation period of 3 to 4 DIV sensors were placed into the sample holder and rinsed continuously with pre-warmed culture medium at a flow rate of 10 µl/min. Spiking activity was registered using the newly developed multi-channel filter amplifier and stored using the LabVIEW based application software.

When inserted into the sample holder and rinsed, cells showed an improved viability compared to the previous system. Signal distortion, as described before during long-term monitoring in the previous sensing system (Figure 4-23), was not apparent anymore even for incubation periods of up to 6 hours. This leads to the conclusion that the cell-substrate contact remained intact throughout the experiment due to reduced shear stress. Visual observation of the culture chamber underpins this finding.

The quality of extracellular recording (Figure 4-32) was found to be similar to the commercial system. In some cases, amplitudes exceeded values measured by the commercial system and the one presented in Chapter 4.2. The reason for this phenomenon is not clear – the gain factor of the multichannel amplifier was determined and implemented into the application software correctly. Crosstalk between the different (electrode) arrays was observed, which was diminished by setting the bandpass filter to appropriate values.

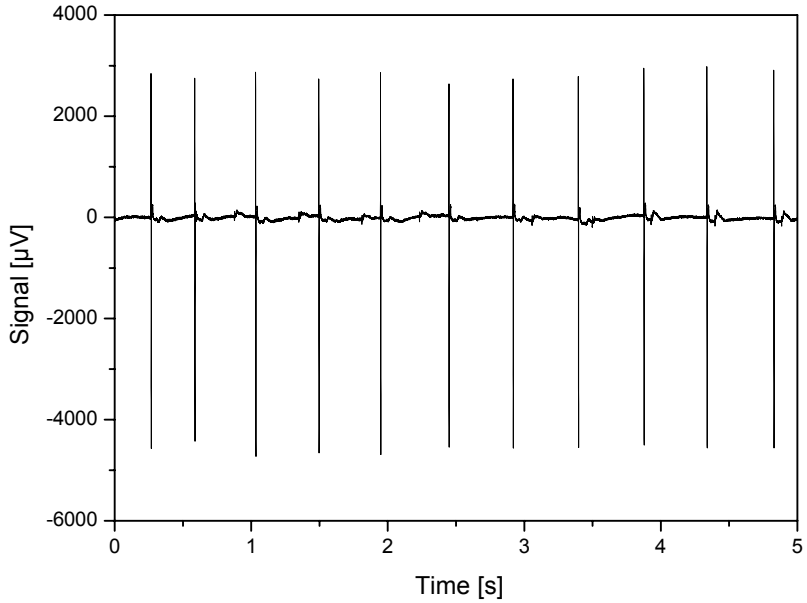

Figure 4-32: Spikes recorded using the sensor platform.

Response to isoproterenol

After a base activity was registered, isoproterenol was applied to cardiomyocytes at various concentrations from 10 pM to 1 µM. Chambers were rinsed with culture medium before the next drug concentration was applied. The spike rate of the cardiomyocytes during the first 15 minutes including application of 10 pM isoproterenol is given in Figure 4-33. The base activity was already strong and registered as 1.2 - 1.5 s^{-1}. The spike rate increased due to isoproterenol to a value of 2 spikes per second in average, partially reaching a spike rate of 3 s^{-1}. Subsequent rinsing did not result in a recovery of the original activity. Isoproterenol concentrations of 100 pM, 1 nM and 1 µM had similar effects on spike activity and are therefore not shown in detail. This result on the one side documents that the cell culture responded to the drug stimulus and, on the other hand, that the drug was not properly washed out after application.

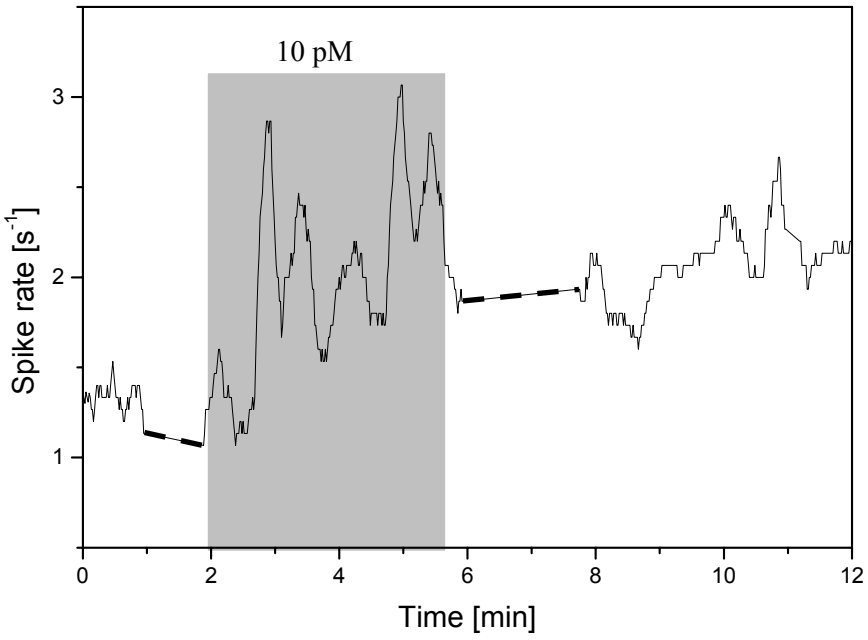

Figure 4-33: Effect of isoproterenol on spike rate of cardiomyocytes cultured in the sensor platform. Rate was averaged for a range of 15 seconds. Dashed lines represent intervals where no data points have been acquired. The experiment was performed at 37°C.

5 Conclusion and Outlook

5.1 Performance and Perspectives of the Sensor Platform

Experiments that have been performed using the sensor platform in its final configuration proved its capability of measuring cell-substrate interaction by single frequency impedance sensing and electrical activity by extracellular recording. The key feature, providing a stable cell culture inside the fluidic system, was clearly improved over the previous attempts and allows monitoring of cells for hours without cell impairment now. The optical microscope and the 16-channel multiplexer were important extensions of the existing systems, too. Interpreting cellular responses was much easier using simultaneous optical observation.

Although a considerable effort was put into the generation of a novel system, problems concerning the microfluidic cell chamber were still apparent. A leakage between the PDMS layer and the cell chip corrupted the electrical sensing and air bubbles were trapped in the cell chambers. The leakage was successfully sealed by an additional layer of Parafilm M (Brand, Wertheim, Germany), but this caused a cleft of approximately 200 µm between silicon (sensor) and PDMS (lid). This had two major impacts: Both fluid streams (*control* and *sample*) were short-cut and a dead volume was generated above the silicon chip. The latter caused difficulties in dose-response measurements as pharmaceutical compounds were supposably not completely removed by rinsing phases.

The employment of the two culture chambers was planned by co-culturing two different types of cells. Therefore, a cultivation protocol for harvesting hepatocytes from rat liver was being developed. Until the end of the project, establishing of the hepatocyte co-culture was not successfully achieved and the ‘final experiment’ was not accomplished. It was planned to apply the antidepressant amitriptyline (AT) to cardiomyocytes. AT is known to block sodium channels and therefore to decrease electrical activity [Ogata 1989]. AT is being transformed to inactive metabolised products by hepatic P450 enzymes [Cali 2005, Donato 2004]. When Cardiomyocytes are co-cultured with hepatocytes and are incubated with AT at micromolar concentrations, it is expected that initial electrical activity will be reduced. During the course of the experiment, hepatocytes mediate degradation of AT and therefore reduce the debilitating effect of the compound. This will, theoretically, result in increasing electrical activity.

The biosensor platform is also well-suited to perform detoxification experiments using nanocapsules [Jovanovic 2004, Duran 2005]. Here, a compound that reduces electrical activity (e.g. AT) is applied to the circulating medium flow. Then, nanocapsules are introduced into the stream and the concentration of the compound is decreased as it is bound inside the capsule core. The detoxification kinetic profile can, theoretically, be analysed using the microfluidic

platform by monitoring the electrical activity. Impedimetric monitoring of the Hepatocyte culture might provide information about cell viability.

As these examples show, the perspectives of the device are widespread. Analysis of cell-substrate interaction (impedance electrode array) and electrical activity may be performed under microfluidic conditions allowing less compound consumption and easy implementation of automated substance application. Besides the described co-culture approach, the platform is suited to perform biocompatibility and shear-force assays using optical observation of the microfluidic chamber. It is also conceivable to realise a toxicity sensing system for e.g. contaminated drinking water. Schalie *et al.* described a battery of biosensing systems as promising for this purpose [Schalie 2006]. Among the systems that detected the most relevant chemicals in contaminated drinking water was electric cell impedance sensing. The extension by a system component monitoring electrical activity of neuronal networks allowed the detection of another substance.

5.2 Electrode Area has a Profound Influence on Electrode Impedance

The investigation of the attachment of cells or bacteria on impedance based biosensors is an active field of research. It is well accepted that cell-spreading on electrodes leads to a reduced area on the electrode that is opposed to the electrolyte. Hence, electrode resistance is increased and electrode capacitance is decreased [Schwan 1963]. Analysis of the previously presented impedance results revealed that impedance magnitude increased by up to 170 % for a frequency that showed to be specific for the electrode size used. The frequency the sensor was most sensitive to cell-substrate interaction was found to be higher for small electrodes than for large ones (Figure 5-1).

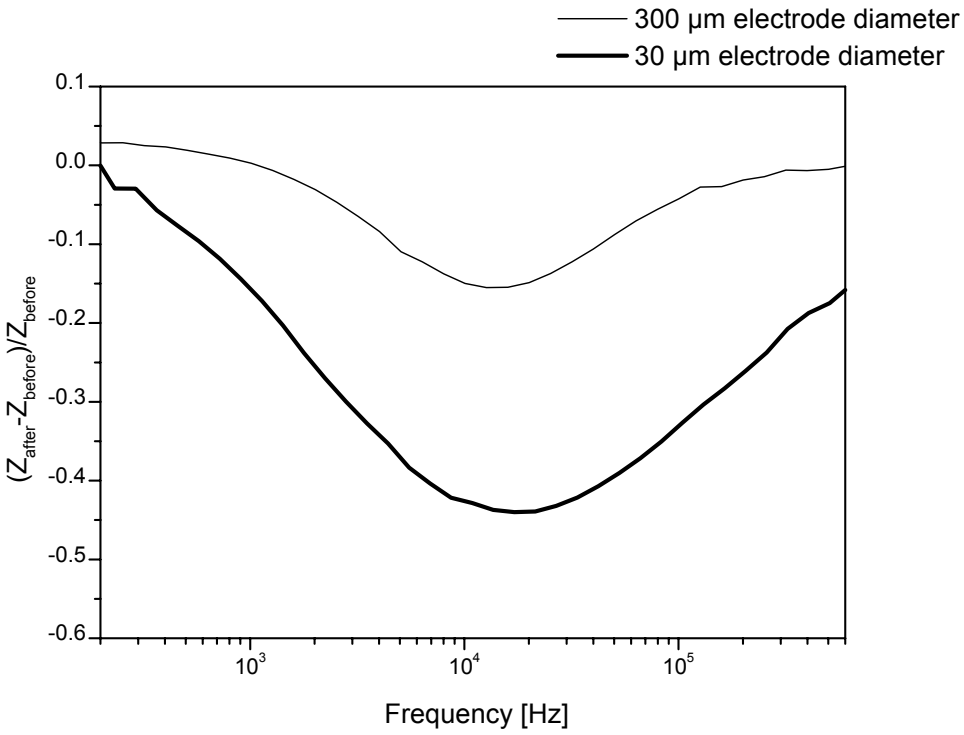

Figure 5-1: Sensitivity of different electrode sizes to cell detachment

This finding correlates to statements in publications that were compared for the sensitive frequency ranges (Table 5-1). Results were obtained for measuring MDCK-I epithelial cells on circular gold electrodes [Wegener 1996], suspensions of live and dead bacteria, *Listeria innocua*, on interdigitated electrodes [Gomez 2002], and 3T3 mouse fibroblasts and HCT116 human cancer cells on an array of gold microelectrodes [Huang 2004].

Table 5-1: Comparison of impedance results with other studies. f_{low} and f_{high} refer to frequency range that proved to be sensible to cell-substrate interaction. f_{max} refers to frequency of maximum impedance change.

	Wegener 1996	**Gomez 2002**	**Huang 2004**	**This work**	
Ex-periment	Covered/uncovered sensors	Live/dead cells in suspension	Dynamic adhesion (duration: 5 hrs)	Human ovarian cancer cells bare/cell covered	
Electrode area [cm²]	4.5×10^{-1}	4.6×10^{-3}	4×10^{-3}	9×10^{-4}	9×10^{-6}
Type of electrode	Circular gold electrodes	Interdigitated electrodes	Gold electrodes	Gold electrodes	
$\mathbf{f_{low}}$	0.04 kHz	0.6 kHz	2 kHz	1 kHz	5 kHz
$\mathbf{f_{max}}$	0.6 kHz	20 kHz	20 kHz	10 kHz	100 kHz
$\mathbf{f_{high}}$	8 kHz	600 kHz	---	100 kHz	800 kHz

Apparently, the electrode size determines the sensitive frequency range. The low frequency end (f_{low}) increases with rising electrode area, although Huang *et al.* report on results that do not fit into this statement. In principle, this is true also for the high frequency end (f_{high}) and for the frequency of highest sensitivity f_{max}.

Moreover, monitoring dynamic cell adhesion showed transition of the sensitivity maximum from high to low frequencies from 500 to 70 kHz for microelectrodes ($A = 9 \times 10^{-4}$ cm²). This was also confirmed for larger electrode sizes, e.g. 4×10^{-3} cm² [Huang 2004]. Hence, the result of single frequency impedance sensing of cell-substrate interaction is highly dependent on the frequency chosen for analysis. Cell attachment is first visible at high frequencies while disruption of cell monolayers can be first monitored at low frequencies.

The type of cells investigated also plays a role for selecting electrode size and geometry. Cells that are able of building tight junctions were measured using large electrodes while leaky cell layers were measured using small electrodes [Wegener 1996]. In contrary to this statement, smaller electrodes investigated in this thesis responded with larger absolute resistance changes and therefore in a more sensitive way than large electrodes, although human ovarian cancer cells used in this thesis are also building tight junctions to each other [Reuning, personal communication].

The present project aimed to investigate the possibility of gaining information at a higher lateral resolution for MEA chips compared to large electrodes. It turned out that detection was limited by cell coverage and sealing resistance in general. If too few cells covered the electrode and large areas of unoccupied space was available, impedance data showed only slight changes.

5.3 The Capacitance and Resistance of a Cell Membrane

Modelling EIS data of adherent human ovarian cancer cells by a constant phase element (CPE) in series with a resistor and capacitor in parallel proved to be a suiting model for the real-world situation. But, one has to bear in mind that the CPE is an empirically derived equation [Wegener 1996] and that it is difficult to interpret its physical meaning. Attempts were performed to model EIS data by a capacitor/resistor couple in parallel but the fitting did not meet the measured data and due to this poor accuracy the usage of the CPE was preferred.

Capacitances and resistances of cell membranes are often given as area-normalised values in literature. As an assumption of the capacitance serves the capacitance of a lipid bilayer that was found to be in the range of 0.5 µF cm^{-2} [Sackmann 1996] and therefore leads to an assumed capacitance of a cell membrane of 0.25 µFcm^{-2}. Several publications investigating cells on impedance-based sensors are presented and compared to results of this work in Tables 5-3 and 5-4.

Table 5-2: Area-normalised modelling of cell covered sensors using a capacitor as electrode impedance. Equivalent circuits used for modelling were $C_{electrode} - (R_{cell\ layer}//C_{cell\ layer}) - R_{bulk}$ [Wegener 1996, Hillebrandt 2001] and $R_{cell\ layer}//C_{cell\ layer}$ [Ehret 1997] with "–" counting for a series and "//" for a parallel connection.

	Wegener 1996	**Ehret 1997**	**Hillebrandt 2001**
Electrode area [cm²]	4.5 x 10^{-1}	2.5 x 10^{-1}	1.9 x 10^{-1}
Electrode type	Circular gold electrodes	Interdigitated electrodes	Indium-tin-oxide
Cell type	MDCK I	LS 174T (like fibroblasts)	HUVEC
$C_{electrode}$ [µF cm^{-2}]	9.4 ± 1	---	7.9
R_{bulk} [Ω]	248 ± 2	---	2500
$R_{cell\ layer}$ [Ωcm²]	112 ± 12	n/a	180
$C_{cell\ layer}$ [µFcm^{-2}]	1.3 ± 0.2	0.080	0.1
Measurements	8	1	1

Table 5-3: Area-normalised modelling of cell covered sensors using a CPE as electrode impedance. Unit for the CPE-T parameter was derived from $Fcm^{-2} = \Omega^{-1}cm^{-2}s$. Cells used were bovine aortic endothelial cells [Wegener 1999] and OV-MZ-6. Equivalent circuits used for modelling were $CPE - R_{bulk} - (R_{cell\ layer}//C_{cell\ layer})$ [Wegener 1999] and $CPE - (R_{cell\ layer}//C_{cell\ layer})$ with "–" counting for a series and "//" for a parallel connection.

	Wegener 1999	**This work (d=15µm)**	**This work (d=30µm)**	**This work (d=40µm)**
Electrode area [cm²]	2.5 x 10^{-1}	2.3 x 10^{-6}	9 x 10^{-6}	1.5 x 10^{-5}
CPE-T [$m\Omega^{-1}cm^{-2}s^{\alpha}$]	12400	0.6 ± 1.3	0.3 ± 1.3	0.036 ± 0.067
R_{bulk} [Ω]	283	---	---	---
$R_{cell\ layer}$ [Ωcm²]	5.1	0.07 ± 0.04	0.34 ± 0.25	0.33 ± 0.21
$C_{cell\ layer}$ [µFcm^{-2}]	0.6	9.9 ± 1.67	5.35 ± 4.2	0.88 ± 0.34
Measurements	1	3	7	3

Electrodes that were compared with the ones used in this work are evidently larger and therefore, suspicions may be due to this fact. First, the capacitance of the cell layer was reported in the range that was assumed before. The smaller the investigated electrodes became, the

higher the capacitance was. Hence, area-normalisation may not be an appropriate method to work on electrodes smaller than 1 x 10^{-5} cm^{-2} and therefore, values were always presented in the results section as absolute values.

Then, area normalised resistances showed to be smaller which might be due to the cell type that may not form very tight junctions as epithelial cells do.

6 References

Agostinis P., Buytaert E., Breyssens H. and Hendrickx N.: Regulatory pathways in photodynamic therapy inducted apoptosis. Photochem. Photobiol. Sci. 3, **2004**, 721-729

Andersson H., van den Berg A.: Microfluidic devices for cellomics: A review. Sensors and Actuators B 92, **2003**, 315-325

Applied Biophysics Inc.: Presentation available online at http://www.biophysics.com /pages/powerpoint/ecis2003.pdf (July **2004**)

Aravanis A.M., DeBusschere B.D., Chruscinski A.J., Gilchrist K.H., Kobilka B.K., Kovacs G.T.A.: A genetically engineered cell-based biosensor for functional classification of agents. Biosensors & Bioelectronics 16, **2001**, 571-577

Aumailley M., Gurrath M., Müller G., Calvete J., Timpl R., Kessler H.: Arg-Gly-Asp constrained within cyclic pentapeptides. Strong and selective inhibitors of cell adhesion to Vitronectin and Laminin fragment Pl. FEBS Lett. 291, **1991**, 50-54

Bard A.J.: Electrochemical Methods. John Wiley, New York, **1980**

Barsoukov E., Macdonald J.R. (editors): Impedance Spectroscopy. Second Edition. Wiley-Intersciences. Hoboken, USA, **2005**.

Bashir R.: BioMEMS: state-of-the-art in detection, opportunities and prospects. Advanced Drug Delivery Reviews 56 (11), **2004**, 1565-1586

Becciu A.: Analysis of neuronal data recorded with microelectrode arrays. Diploma thesis Universita di Cagliari, Italy, **2004**.

Beebe D.J., Mensing G.A., and Walker G.M.: Physics and Applications of Microfluidics in Biology. Annu. Rev. Biomed. Eng. 4, **2002**, 261-86

Berggren C., Bjarnason B., Johansson G.: Capacitive Biosensors. Electroanalysis 13 (3), **2001**, 173-180

Bio-Logic: Electrochemistry – Application note n°5. Precautions for good impedance measurements. Bio-Logic Science Instruments, Claix, France. Available online at http:/www.bio-logic.info/potentiostat/notes/Application%20note%205.pdf (Aug. 13th, **2007**)

Borkholder D.A.: Cell-based Biosensors using Microelectrodes, Dissertation submitted to the Department of Electrical Engineering, Stanford University, **1998**

Bousse L.: Whole cell biosensors, Sens. Actuators B 34 (1-3), **1996**, 270-275

Brash J.L.: Behavior of proteins at interfaces. Current Opinion in Colloid & Interface Science 1, **1996**, 682-688

Braun D., Fromherz P.: Fluorescence interference-contrast microscopy of cell adhesion on oxidized silicon. Appl Phys A 65, **1997**, 341-348.

Brischwein M., Baumann W., Ehret R., Schwinde A., Kraus M. & Wolf B.: Mikrosensorische Systeme in der zellbiologischen Grundlagenforschung und medizinischen Diagnostik. Naturwissenschaften 83, **1996**, 193-200

Bucher V., Brunner B., Leibrock C., Schubert M., Nisch W.: Electrical properties of a light-addressable microelectrode chip with high electrode density for extracellular stimulation and recording of excitable cells. Biosensors & Bioelectronics 16, **2001**, 205-210

Buitenweg J.R., Rutten W.L.C., Marani E., Polman S.K.L., Ursum J.: Extracellular detection of active membrane currents in the neuron-electrode interface. Journal of Neuroscience Methods 115, **2002**, 211-221

Buitenweg J.R., Rutten W.L.C., Willems W.P.A., van Nieuwkasteele J.W.: Measurement of sealing resistance of cell-electrode interfaces in neuronal cultures using impedance spectroscopy. Med. Biol. Eng. Comput. 36, **1998**, 630-637

Cali J., Sobol M., Donging M.A.: Screen for Cytochrome p450 Activity using a Luminescent Assay. Cell Notes 12, **2005**, 8-10

Carter S.B.: Principles of cell motility: the direction of cell movement and cancer invasion. Nature 208, **1965**, 1183-1187

Curtis A.S.G., Breckenridge L., and Connolly P.: Making real neural nets: design criteria, Medical Biol. Eng. Comput. 30, **1992**

DeBusschere B.D., Borkholder D.A. and Kovacs G.T.A.: Design of an integrated silicon-PDMS Cell Cartridge. Solid-State Sensor and Actuator Workshop Hilton Head Island. South Carolina, June 8-11, **1998**

DeBusschere B.D., Kovacs G.T.A.: Portable cell-based biosensor system using integrated CMOS cell-cartridges. Biosensors & Bioelectronics 16, **2001**, 543-556

DeSilva M., Zhang Y., Hesketh P.J., Maclay G.J., Gendel S.M. & Stetter J.R.: Impedance based sensing of the specific binding reaction between Staphylococcus enterotoxin B and its antibody on an ultra-thin platinum film. Biosensors & Bioelectronics 10, **1995**, 675-682

Dittrich P.S. and Manz A.: Lab-on-a-chip: microfluidics in drug discovery. Nature Reviews Drug Discovery 5, **2006**, 210-218

Dolmans D.E.J.G.J., Fukumura D. and Jain R.K.: Photodynamic therapy of cancer. Nature Reviews Cancer 3, **2003**, 380-386

Donato M.T., Jimenez N., Castell J.V., and Gomes-Lechon M.J.: Fluorescence-based assays for screening nine cytochrome P450 activities in intact cells expressing individual human p450 enzymes. Drug metabolism and disposition 32, **2004**, 699-706

Du H.-Y., Bay B.-H. and Olivio M.: Biodistribution and photodynamic therapy with hypericin in a human NPC murine tumor model. Int. J. of Oncology 22, **2003**, 1019-1024

Duran R.S. Jovanovic A.V., Chavez J.L., Joucheray T., Flint J.A., Varshney, Pottek M., Thielemann C., Morey T., Dennis D., Knoll W.: Modified silica core-shell nanocapsules – cellular characterisation and implications for drug detoxification. ACS Meeting San Diego, **2005**

ECVAM - European Centre for the Validation of Alternative Methods: Short-term in vitro assays for long-term toxicity. EU proposal PREDICTOMICS, LSHB-CT-2004-504761, **2004**

Ehret R., Baumann W., Brischwein M., Schwinde A., Stegbauer K. and Wolf B.: Monitoring of cellular behaviour by impedance measurements on interdigitated electrode structures. Biosensors & Bioelectronics 12, **1997**, 29-41

English, D.S.: Subcellular distributions and excited-state processes of hypericin in neurons. Photochem. Photobiol. 69, **1999**, 301-305

Ferrario A., Von Tiehl K., Wong S., Luna M. and Gomer C.J.: Cyclooxygenase-2 inhibitor treatment enhances photodynamic therapy-mediated tumor response. Cancer Res. 62, **2002**, 3956-3961

Fiehn H., Howitz S., Pham M.T., Vopel T., Buerger M., Wegener T.: Components and technology for a fluidic-ISFET-microsystem, in: A. van den Berg, P. Bergfeld (Eds.), Micro Total Analysis Systems. Proceedings of the μTAS '94 Workshop. Kluwer Academic Publishers, Dordrecht, **1994**, 289–292.

Freshney R.L.: Culture of Animal Cells: A Manual of Basic Technique, 3rd ed. Wiley, New York, **1994**

Gallant N.D., Frazier A.B., Collard D., and Garcia A.J.: Micropatterned Surfaces to Engineer Focal Adhesions for Analysis of Cell Adhesion Strengthening. Langmuir 18, **2002**, 5579-5584

Gawad G., Schild L. and Renaud Ph.: Micromachined impedance spectroscopy flow cytometer for cell analysis and particle sizing. Lab on a Chip 1, **2001**, 76-82

Geddes L.A.: Electrodes and the measurement of bioelectric events. J. Wiley, New York, **1972**

GeSiM: Microfluidics – Applications - Microelectrode Arrays. Available online at http:/www.gesim.de/front_content.php?idart=172 (May 25th, **2006**)

Giaever I. and Keese C.R.: A morphological biosensor for mammalian cells. Nature 366, **1993**, 591-592

Giaever I. and Keese C.R.: Micromotion of mammalian cells measured electrically. PNAS USA 88, **1991**, 7896-7900

Giaever I. and Keese C.R: Monitoring fibroblast behaviour in tissue culture with an applied electric field. PNAS 81, **1984**, 3761-3764

Goldsmith T.H.: Biology, evolution, and human nature. Wiley, New York, **2001**

Gomez R., Bashir R., Sarikaya A., Ladisch M.R., Sturgis J., Robinson J.R., Geng T., Bhunia A.K., Apple H.L., Werely S.: Microfluidic Biochip for Impedance Spectroscopy of Biological Species. Biomedical Microdevices 3 (3), **2001**, 201-209

Gomez, R.: Microscale electronic detection of bacterial metabolism. Sensors and Actuators B 86, **2002**, 198-208

Gross G.W., Rieske E., Kreutzberg G.W., Meyer A.: A new fixed-array multi-microelectrode system designed for long-term monitoring of extracellular single unit neuronal activity in vitro. Neurosci Lett 6, **1977**, 101-105

Gryte D.M., Ward M.D., Hu W.S.: Real-time measurement of anchorage dependent cell adhesion using a quartz crystal microbalance. Biotech. Prog. 9 (1), **1993**, 105-108

Guan J.G., Miao Y.Q., Zhang Q.J.: Impedimetric Biosensors. Journal of Bioscience and Bioengineering 97 (4), **2004**, 219-226

Halbach M.D., Egert U., Hescheler J., Banach K.: Estimation of action potential changes from field potential recordings in multicellular mouse cardiac myocyte cultures, Cellular Physiology and Biochemistry 13, **2003**, 271–284.

Hamann C.H., Vielstich W.: Elektrochemie. Wiley, Weinheim, **2005**

Hamill O.P., Marty A., Neher E., Sakmann B. and Sigworth F.: Improved Patch-Clamp Techniques for High-Resolution Current Recording from Cells and Cell-free Membrane Patches. Pflügers Archiv 391, **1981**, 85-100

Hapke S., Kessler H. and Reuning U., Arroyo de Prada N., Benge A., Schmitt M., Lengyel E.: Integrin $\alpha_v\beta_3$/Vitronectin Interaction Affects Expression of the Urokinase System in Human Ovarian Cancer Cells. Journal of Biol. Chem. 276 (28), **2001**, 26340-26348

Harris A.K.: Behavior of cultured cells on substrata of variable adhesiveness. Exp. Cell Res. 77, 285, **1973**

Harris C. M. & Kell D. B.: The estimation of microbial biomass. Biosensors 1, **1985**, 17-84

Hartmann C., Zozulya A., Wegener J., Galla H.-J.: The impact of glia-derived extracellular matrices on the barrier function of cerebral endothelial cells: An *in vitro* study. Experimental Cell Research **2007**, doi 10.1016/j.yexcr.2007.01.024

Hendrickx N., Volanti C., Moens U., Seternes O.M., de Witte P., Vandenheede J.R., Piette J., and Agostinis P.: Up-regulation of Cyclooxygenase-2 and Apoptosis Resistance by p38 MK in

Hypericin-mediated Photodynamic Therapy of Human Cancer Cells. J of Biol Chem 278 (52), **2003**, 52231-52239

Henning T., Kraus M., Brischwein M., Otto A.M. and Wolf B.: Relevance of tumour microenvironment for progression, therapy and drug development. Anti-Cancer Drugs 15 (7), **2004**, 7-14

Hillebrandt H., Abdelghani A., Abdelghani-Jacquin C., Aepfelbacher M., Sackmann E.: Electrical and optical characterization of thrombin-induced permeability of cultured endothelial cell monolayers on semiconductor electrode arrays. Appl. Phys. A 73, **2001**, 539-546

Hintsche R., Paeschke M., Wollenberger U., Schnakeberg U., Wagner B. & Lisec T.: Microelectrode arrays and application to biosensing devices. Biosensors & Bioelectronics 9, **1994**, 697-705

Hodgkin A.L., Huxley A.F.: A quantitative description of membrane current and its application to conduction and excitation in nerve. J. Physiol. 117, **1952**, 500-544

Howitz, S.: Components and systems for microliquid handling, BioMethods 10, **1999**, 31–73

Huang X., Nausieda I, Greve D.W., Domach, M.M., Nguyen D.: Development of active matrix biosensor array for cell screening. Proceedings of IEEE: Sensors, **2004**, 72-75

Hug T.S.: Biophysical Methods for Monitoring Cell-Substrate Interactions in Drug Discovery. Assay and Drug Development Technologies, Vol. 1 (3), **2003**, 1-10

IEH: Testing Requirements for Proposals under the EC White Paper ‚Strategy for a Future Chemical Policy' (Web Report W6), Leicester, UK, Institute for Environment and Health. http://www.li.ac.uk/ieh/webpup/webpup.html posted **2001** (Aug. 13th, 2007)

Ingebrandt S.: Charakterisierung der Zell-Transistor Kopplung. Dissertation am Fachbereich Chemie und Pharmazie. Mainz University, **2001**

Jovanovic A.V., Pottek M. Thielemann C., Knoll W. Duran R.S.: Toward detoxification of cardiomyocytes on microelectrode arrays using polymerized silica core-shell nanocapsules. ACS meeting Anaheim, **2004**

Jung D.R., Kapur R., Adams T., Giuliano K.A., Mrksich M., Craighead H.G., and Taylor D.L.: Topographical and Physicochemical Modification of Material Surface to Enable Patterning of Living Cells. Critical Reviews in Biotechnology 21 (2), **2001**, 111-154

Keselowsky B.G., Collard D.M., Garcia A.J.: Surface chemistry modulates Fibronectin conformation and directs integrin binding and specificity to control cell adhesion. Journal Biomed Mater Res 66 A, **2003**, 247-259

Kottra G. and Frömter E.: Rapid determination of intraepithelial resistance barriers by alternating current spectroscopy. Experimental procedures, Pflüger's Arch. 402, **1984**, 409-420

Kovacs G.T.A.: Micromachined Transducers Sourcebook. McGraw-Hill. New York, **1998**

Krause M.: Untersuchungen zur Zell-Transistor Kopplung mittels der Voltage-Clamp Technik. Dissertation. Dept. of Chemistry and Pharmacy, University of Mainz, **2000**

Lau J.H.: Flipchip Technologies. McGraw-Hill, New York, **1996**

Li J., Thielemann C., Reuning U., Johannsmann D.: Monitoring of integrin-mediated adhesion of human ovarian cancer cells to model protein surfaces by quartz crystal resonators: Evaluation in the impedance analysis mode. Biosensors and Bioelectronics 20, **2005**, 1333-1340

Liu C.D., Kwan D., Saxton R.E., and McFadden D.W.: Hypericin and Photodynamic Therapy Decreases Human Pancreatic Cancer in vitro and in vivo. Journal of Surgical Res. 93, **2000**, 137-143

Liu H.-N., Plopper G., Earley S., Chen Y., Ferguson B., Zhang X.-C.: Sensing minute changes in biological cell monolayers with THz differential time-domain spectroscopy. Biosensors and Bioelectronics 22, **2007**, 1075-1080

Lo C.M., Keese C.R. and Giaever I.: Impedance Analysis of MDCK Cells Measured by Electric Cell-Substrate Impedance Sensing. Biophysical Journal 69, **1995**, 2800-2807

Lodish H., Baltimore D., Berk A., Zipursky S.L., Matsudaira P., Darnell J.: Molekulare Zellbiologie. DeGruyter, Berlin, New York, 2nd edition, **1996**

Makowski M., Grzela T., Niderla J., Lazarczyk M., Mroz P., Kopee M., Legat M., Strusinska K., Koziak K., Nowis D., Mrowka P., Wasik M., Jakobisiak M. and Golab J.: Inhibition of Cyclooxygenase-2 Indirectly Potentiates Antitumor Effects of Photodynamic Therapy in Mice, Clin. Cancer Res. 9, **2003**, 5417-5422

Martinez-Poveda B., Quesada A.R., Medina M.A.: Hypericin in the dark inhibits key steps of angiogenesis in vitro. European Journal of Pharmacology 516, **2005**, 97-103

Matanguihan R.M., Konstantinov K.B. & Yoshida T.: Dielectric measurement to monitor the growth and the physiological states of biological cells. Bioprocess Eng. 11, **1994**, 213-222

McAdams E.T., Lackmeier A., McLaughlin J.A. and Macken D.: The linear and non-linear electrical properties of the electrode-electrolyte interface. Biosensors & Bioelectronics 10, **1995**, 67-74

Meiry G., Reisner Y., Feld Y., Goldberg S., Rosen M., Ziv N., Binah O.: Evolution of action potential propagation and repolarization in cultured neonatal rat ventricular myocytes, Journal of Cardiovascular Electrophysiology 12, **2001**, 1269–1277

Munevar S., Wang Y.I., Dembo M.: Traction Force Microscopy of Migrating Normal and H-ras Transformed 3T3 fibroblasts. Biophysical Journal 80, **2001**, 1744-1757

NMI: Annual Report 2002/2003. Natural and Medical Sciences Institute (NMI), Reutlingen, Germany, **2003**

Ogata N., Narahashi T.: Block of sodium channels by psychotropic drugs in single guinea-pig cardiomyocytes. Br J Pharmacol 91, **1989**, 905-913

Otto A.M., Brischwein M., Niendorf A., Henning T., Motrescu E., Wolf B.: Microphysiological testing for chemosensitivity of living tumor cells with multiparametric microsensor chips. Cancer Detection and Prevention 27, **2003**, 291-296

Paba V., Quarto M., Varriale L., Crescenzi E., Palumbo G.: Photo-activation of hypericin with low doses of light promotes apparent photo-resistance in human histiocytic lymphoma U937 cells. J. of Photochemistry and Photobiology B: Biology 60, **2001**, 87-96

Palmqvist E., Berggren Kriz C., Khayyami M., Danielsson B., Larsson P.O., Mosbach K. & Kriz D.: Development of a simple detector for microbial metabolism, based on a polypyrrole resistometric device. Biosensors & Bioelectronics 9, **1994**, 551-556

Park T.H. and Shuler M.L.: Integration of Cell Culture and Microfabrication Technology. Biotechnol. Prog. 19, **2003**, 243-253

Pottek M., Soerensen, P., Knoll W., Howitz S. and Thielemann C.: A Cell-based Microfluidic System for Drug Screening Applications. MSTnews 01, **2006**, 39-40

Powell D.W.: Barrier function of epithelia. Am. J. Physiol. 241, **1981**, G275-G288

Reinhard-King C.A., Dembo M., Hammer D.A.: Endothelial Cell Traction Forces on RGD-Derivatized Polyacrylamide Substrata. Langmuir 75, **2003**, 1573-1579

Reiss B., Janshoff A., Steinem C., Seebach J. and Wegener J.: Adhesion Kinetics of Functionalized Vesicles and Mammalian Cells: A Comparative Study. Langmuir 73, **2003**, 1816-1823

Richter K., Orfert M., Howitz S., Thierbach S.: Deep plasma silicon etch for microfluidic applications. Surface and COatings Technology 116-119, **1999**, 461-467

Ruoslahti E. and Pierschbacher M.D.: New perspectives in cell adhesion, Science 238, **1987**, 491- 497

Rutten W.L.C.: Selective electrical interfaces with the nervous system. Anna. Rev. Biomed. Eng. 4, **2002**, 407-452

Sackmann E.: Supported Membranes: Scientific and Practical Applications. Science 271, **1996**, 43-48

Schalie H. van der, James R.R., Gargan II T.P.: Selection of a battery of rapid toxicity sensors for drinking water evaluation. Biosensors and Bioelectronics 22, **2006**, 18-27

Schwan, H.P.: Determination of biological impedances. In Physical Techniques in Biological Research, ed. W.L. Nastuk, Vol. 6, Academic Press, New York, Electrophysiological Methods B, **1963**, 323-408

Small V.: http://cellix.imolbio.oeaw.ac.at (Apr 04th, **2005**)

Sorribas H., Braun D., Leder L., Sonderegger P., Tiefenauer L.: Adhesion proteins for a tight neuron-electrode contact. Journal of Neuroscience Methods 104, **2001**, 133-141

Spier R.E. and Griffith B.: An Examination of the Concepts Germane to the Oxygenation of Cultured Animal Cells. Developments in Biological Standards 55, **1982**, 81-92

Steininger J.: Signal processing for cell-based biosensors. Diploma Thesis. University of Applied Sciences Aschaffenburg, **2005**

Stelze M. & Sackmann E.: Sensitive detection of protein adsorption to supported bilayers by capacitance measurements. GBF Monogr. 13, **1989**, 339-346

Stett A., Egert U., Guenther E., Hofmann F., Meyer T., Nisch W., Haemmerle H.: Biological application of microelectrode arrays in drug discovery and basic research. Anal Bioanal Chem 377, **2003**, 486-495

Thielecke H., Mack A. , Robitzki A.: A multicellular spheroid-based sensor for anti-cancer therapeutics. Biosensors & Bioelectronics 16, **2001**, 261-269

Thumshirn G.: Multivalente zyklische RGD-Peptide und RGD-Mimetika für den Einsatz in Tumordiagnostik und Tumortherapie. Dissertation. Technical University, Munich, **2003**

Udin S.: Indium electrodes. Newsgroup posting. bionet.neuroscience (BIOSCI). Jun 28th, **1995**. Available online http://www.bio.net/mm/neur-sci/1995-June/018952 (Aug. 13th, 2007)

Vantieghem A., Assefa Z., Vandenabeele P., Declercq W., Courtois S., Vandenheede J.R., Merlevede W., de Witte P., and Agostinis P. FEBS Lett. 440, **1998**, 19-24

Viravaidya K., Sin A., and Shuler M.L.: Development of a Microscale Cell Culture Analog To Probe Naphthalene Toxicity. Biotechnol. Prog. 20, **2004**, 316-323

Walker M.J.A., Pugsley M.K.: Methods in cardiac Electrophysiology, CRC press, Boca Raton, **1998**

Wegener J., Keese C.R., Giaever I.: Electric Cell-Substrate Impedance Sensing (ECIS) as a Noninvasive Means to Monitor the Kinetics of Cell Spreading to Artificial Surfaces. Exp. Cell Res. 259, **2000**, 158-166

Wegener J., Sieber M., Galla H.J.: Impedance analysis of epithelial and endothelial cell monolayers cultured on gold surfaces. J. Biochem. Biophys. Methods 32, **1996**, 151-170

Wegener J., Zink S., Rösen P., Galla H.J.: Use of electrochemical impedance measurements to monitor beta-adrenergic stimulation of bovine aortic endothelial cells. Pflügers Arch – Eur J Physiol 437, **1999**, 925-934

Wegener: Online ressource: www.charite.de/gzg/Wegener-Referat.htm (**2006**)

Weis R. and Fromherz P.: Frequency dependent signal transfer in neuron transistors, Physical Review E 55, **1997**

White S.M., Constantin P.E., and Claycomb W.C.: Cardiac physiology at the cellular level: Use of cultured HL-1 cardiomyocytes for studies of cardiac muscle cell structure and function. J Am J Physiol Heart Circ Physiol 286, **2004**, H823-H829

Wiegand G., Arribas-Layton N., Hillebrandt H., Sackmann E. and Wagner P.: Electrical Properties pf Supported Lipid Bilayer Membranes. J. Phys. Chem. B, 106 (16), **2002**, 4245-4254

Wiegand G., Neumaier K.R., and Sackmann E.: Fast impedance spectroscopy: General aspects and performance study for single ion channel measurements. Rev. Scient. Instrum. 71 (6), **2003**

Young B.R., Pitt W.G., and Cooper S.L.: Protein Adsorption on Polymeric Biomaterials I. Adsorption Isotherms. Journal of Colloid and Interface Science 124 (1), **1988**

Yu N., Atienza J.M., Bernard J., Blanc S., Zhu J., Wang X., Xu X, Abassi Y.A.: Real-Time Monitoring of Morphological Canges in Living Cells by Electonic Cell Sensor Arrays: An Approach To Study G Protein-Coupled Receptors. Analytical Chemistry A 78(1), **2006**

Zeck G. and Fromherz P: Repulsion and Attraction by Extracellular Matrix Protein in Cell Adhesion Studied with Nerve Cells and Lipid Vesicles on Silicon Chips. Langmuir 75, **2003**, 1580-1585

Ziegler C: Cell-based biosensors. Fresenius J Anal Chem 366, **2000**, 552-559

7 Appendix

A - Cell Culture

7.1.1 Preparation of Media

Abstract	Media for the cultivation of cardiomyocytes and OV-MZ-6 are supplemented by various reagents
Preparation	Cardiomyocytes: (1) F-10 (2) ITS (3) Pen/Strep OV-MZ-6 medium: (4) DMEM (5) Gentimycin (6) HEPES buffer (7) Arginin (8) Asparagine for both : (9) Foetal calf serum
Instructions	OV-MZ-6 medium: Add to 500 ml of medium (4): 50 ml serum (9), 2 ml (5), 1 ml amino acid solution (see below), 5 ml buffer (6). Prepare amino acid solution from (7) and (8): Let 1.16 g Arginine (7) and 0.36 g Asparagine (8) dissolve in 20 ml MilliQ water. Pass solution through a 0.22 μm filter.
Remarks:	(4) 61965-026, Gibco (5) 15710-049, Gibco (6) 15630-056, Gibco (7) A-5131, Sigma (8) A-4159, Sigma (9) 10270-106, Gibco

7.1.2 Thawing Cells from Liquid Nitrogen

Abstract	Cryo-conserved OV-MZ-6 cells are transferred into culture medium for cultivation in incubator
Preparation	Cool down centrifuge to 4 °C Refrigerate at 4 °C: (1) OV-MZ-6 medium (see 7.1.1), 0 % FBS (2) OV-MZ-6 medium, 10 % FBS Place in water bath at 37 °C: (3) OV-MZ-6 medium, 0 % FBS (4) OV-MZ-6 medium, 10 % FBS Wear cryo-gloves and goggles.
Instructions	Take off cryo-tube from nitrogen tank and open it slightly (danger of explosion of a sealed tube). Clean outer surface with ethanol (70 %). Re-suspend cells with (1) and transfer all cells to test tube. Centrifuge (n = 1300 rpm, t = 5 min, T = 4 °C). Discard supernatant fraction and re-suspend pellet with (3). Wash cells gently. Centrifuge (n = 1300 rpm, t = 5 min, T = 22 °C), discard supernatant, wash in (4), and place appropriate cell number into tissue flask.
Remarks:	(1-4) 10270-106, Gibco

7.1.3 Freezing Cells

Abstract	Cell lines are stored for longer periods of time in liquid nitrogen
Preparation	Place in water bath at 37 °C: (1) Defreezing medium (10 % DMSO) and also PBS w/o Ca^{2+} and Mg^{2+} PBS with 0.025 % EDTA OV-MZ-6 medium with 10% FBS (according 7.1.4). Cryo-tubes, access to –70 °C freezer
Instructions	Follow preparation instruction 7.1.4 but re-suspend cells in the last step in (1). Prepare cell concentration of 5 million cells per ml avoiding air bubbles and place aliquots of 1ml into cryo-tubes. Place tubes in a rack and put them in the freezer (-20 °C) overnight. Next day place the rack into the –70 °C deep freezer. After 24 hrs the tubes can be placed in liquid nitrogen.
Remarks:	(1) 11101-011, Gibco

7.1.4 Passaging of OV-MZ-6 Cells

Abstract	Split cells and exchange used medium
Preparation	Place in water bath at 37 °C: (1) PBS w/o Ca^{2+} and Mg^{2+} (2) PBS with 0.05 % EDTA (3) OV-MZ-6 medium with 10 % FBS (see 7.1.1) (4) EDTA (1 % w/v) w/o Ca^{2+} and Mg^{2+} Prepare (2) of 19 ml (1) and 1 ml (4).
Instructions	Discard medium in tissue flasks and exchange against (1) to wash off loose cells and residual serum. Shake flask and replace (1) with (2). Place flask in the incubator for 5 min or until cells are suspended. Transfer contents of flask in a test tube and centrifuge it (n = 1300 rpm, t = 3 min). Discard supernatant and re-suspend cells in 1 ml (3). Count cells according to standard procedure. Place 10,000 cells into new flask and add (3). Place flask back into incubator.
Remarks	(1) 14190-094, Gibco (4) L 2113, Biochrom

7.1.5 Culturing Cardiomyocytes on Sensor Devices

Abstract	Cardiomyocytes already prepared as a cell suspension are incubated on sensor devices.
Preparation	(1) MilliQ water, sterile (2) Cardiomyocytes medium, 10 % serum, cooled 4 °C Place in water bath at 37 °C: (3) Cardiomyocytes medium, 10 % (4) Cardiomyocytes medium, 3 %
Instructions	Preparation of hearts results in a cell suspension. Count cells according to standard procedures. Add (2) to prepare a cell suspension of $8x10^6$ cells per ml. Store on ice. Sensor preparation: Remove surplus fibronectin solution and rinse with (1) at least 3 times. Shortly after drying with nitrogen place 50 µl (Flip-Chip MEA sensors) or 12.5 µl (microfluidic MEA sensors) on the sensitive area of the MEA chip. These volumes correspond to 400,000 and 100,000 cells, respectively. Leave sensors in the incubator for 2-3 hrs. Then apply (3) to the sensors carefully. 24 to 36 hrs later exchange medium against (4). Renew medium every 48 hrs using (4).

7.1.6 Hypericin Stock Solution

Abstract	Preparation of HY stock solution
Preparation	(1) DMSO (2) Hypericin, 1 mg (3) Syringe, 1 ml and needle (4) Eppendorf test tubes, 1.5 – 2 ml
Instructions	Hypericin is highly sensitive to illumination. Therefore, the equipment has to be wrapped in aluminium foil (2-4). Syringe (3) is filled with 1 ml of (1) and mixed with (2). Aliquots are placed in (4) and kept in the freezer at -20 °C.

7.2 B - MEA Sensors

7.2.1 Cleaning Protocol after Experiment

Abstract	Cleaning sensors after experiment
Preparation	Place in water bath at 37 °C: (1) Trypsin 0.25 % Leave at room temperature: (2) BM detergent, 3 % (3) Ultrasonol 7, 2%
Instructions	To remove all cellular residues sensors are incubated in (1) for 10 min in water bath at 37 °C. Rinse sensors thoroughly in MilliQ water and apply (2) for 30 min. Rinse sensors thoroughly and apply (3) for 30 min. Rinse and dry in nitrogen.
Remarks:	(1) T4049, Sigma-Aldrich Chemicals (2) BM-flüssig, Biomed, Oberschleißheim, Germany (3) Carl Roth, Karlsruhe, Germany

7.2.2 Sensor Preparation

Abstract	Preparation of sensors for EIS or extracellular recording experiments
Preparation	(1) BM detergent, 3 % (2) Ultrasonol 7, 2 % (3) PBS w/o Ca^{2+} and Mg^{2+} (4) aliquot of adhesion promoting protein (P)
Instructions	For surface activation with BM and subsequent neutralisation see Chapter 7.2.1. Desinfection with ethanol (70 %) for 10 min Rinsing and drying in nitrogen P (4) is applied on the sensor at concentration of 10 - 50 µg/ml in (3). AN amount of 50 – 100 µl is pipetted to the MEA hip, and the sensor is kept in the incubator for 2-6 hrs or in case of later cell addition is transferred to the fridge.
Remarks:	(1) BM-flüssig, Biomed, Oberschleißheim, Germany (2) Carl Roth, Karlsruhe, Germany

7.2.3 Platinising Solution

Abstract	Kohlrausch's solution for platinum black deposition on MEA chips (7.2.4)
Preparation	(1) Hexachloroplatinum acid hydrate (2) Lead(II)citrate trihydrate (3) Agarose (4) Microwave oven
Instructions	Prepare solution A and solution B: Solution A 1000 mg (1) and 50 mg (2). Add 100 ml MilliQ water. Keep (1) under Argon. Stir well when adding (2). Solution B: To 25 mg (3) add 100 ml MilliQ water. Let the polymer dissolve by heating up in a microwave oven. Place solutions A and B in a graduated flask and fill up to 250 ml with MilliQ water. Store solution in a dark glass bottle in the fridge.
Remarks:	Adapted from [Udin 1995] (1) Fluka 81080, Sigma-Aldrich Chemicals (2) Fluka 15326, Sigma-Aldrich Chemicals (3) Sigma A-4804, Sigma-Aldrich Chemicals

7.2.4 Platinising

Abstract	Deposition of platinum black on microelectrodes to reduce electrode impedance
Preparation	(1) Power box, (cables), multimeter (2) Ultrasonic bath (3) Platinum rod (coiled), diameter 1 mm (4) Platinising solution according to Chapter 7.2.3 (5) MEA chips with centralized galvanic contact
Instructions	Adjust (1) to appropriate values. For a whole wafer choose I = 2 A and E = 3 V. Connect galvanic contact (microelectrodes) to the negative output of power box (1). Connect the counter electrode (3) to the positive output. A beaker of (4) is placed into an ultrasonic bath (2). Put the MEA chips (5) and the counter electrode (3) into the platinising solution and start platinum deposition by switching on the power box under ultrasonic conditions. Control the deposition time with a stop watch.

7.3 C - Experiments

7.3.1 Isoproterenol on Cardiomyocytes

Abstract	Schedule for extracellular recording of cardiomyocytes. Spike rate can be enhanced by isoproterenol
Preparation	(1) Cardiomyocytes on sensors, at least 2 DIV (2) Isoproterenol (3) Phase contrast microscope (4) Setup with microfluidic chip, amplifier, and DAQ Place in water bath at 37 °C: (5) Cardiomyocytes medium F-10 supplemented with ITS, Pen/Strep w/o FBS
Instructions	Evaluate contractions under microscope Prepare solution of (2) freshly each time. (5) is used to dilute stock solution. Keep samples in the water bath. After insertion to extracellular recording system: First a basal activity has to be determined. Ideally, this is represented by 0.3 to 0.7 spikes per second. This activity shall be reached for each concentration step after rinsing. First medium without drug is first as a blind probe. As injection volume 10 µl are sufficient. Then isoproterenol concentrations beginning with 10 pM are applied followed by a rinsing cycle of at least 5 min.

7.3.2 Integrin Ligands on OV-MZ-6 Cells

Abstract	OV-MZ-6 cells are injected to the sensor at a certain stage of development (70-80 % confluence). Impedance spectroscopy is being performed on single microelectrodes monitoring the impact of integrin ligands on the cells.
Preparation	Place in water bath at 37 °C: (1) PBS w/o Ca^{2+} and Mg^{2+} (2) PBS with 0.025 % EDTA (3) OV-MZ-6 medium with 0 % FBS (4) Trypsin, 0.25 % (5) MilliQ water, sterile
Instructions	Cell preparation: Follow 7.1.4 until the last re-suspension step. For re-suspension use (3) and determine cell concentration by counting cells using a NEUGEBAUER counting chamber. Sensor preparation: Use sensors with fibronectin coated surface (7.2.2). Remove surplus fibronectin solution and rinse with (5) for at least 3 times. Dry in nitrogen and apply 1 ml of (3) onto culture dish. Record the impedance spectrum for an uncovered electrode, subsequently discard medium and inject 200 µl of the prepared cell suspension onto inner glass ring. Place the sensor in the incubator for at least 20 min before medium (3) is added to 1 ml and monolayer is formed. Record EIS spectrum for the cellular monolayer if no continuous measurement was chosen. Prepare c(-RGDfV-) and c(-RADfV-) solution at concentrations of 250 to 500 µg/ml in (3) and exchange medium against RGD/RAD containing solution. Incubate systems for 2 hrs followed by EIS scans. After the effect of RGD/RAD has reached an equilibrium, discard medium, and place (2) or (4) onto sensor. Record another spectrum of the electrode after cells are removed from the sensor.
Remarks:	See Chapter 7.1.4

7.3.3 Hypericin on OV-MZ-6 Cells

Abstract	OV-MZ-6 cells are supplied to the sensor at a certain stage of development (70-80 % confluence). Impedance spectroscopy is being performed on single microelectrodes monitoring the impact of hypericin on the cells in darkness and illumination, respectively.
Preparation	(1) Hypericin stock solution
Instructions	Follow procedure 7.3.2 until monolayer formation has been completed. Record the EIS spectrum for the electrodes covered with cells. (1) is diluted to the appropriate concentration and placed into the water bath at 37 °C until application onto the sensor.

To determine the effect on the cells in darkness, the sensor is wrapped in aluminium foil and placed into the incubator. For assessing the effect of illumination the foil is removed.

Time protocol:
Seed and incubate for 24 hrs
Add hypericin
Incubate in darkness for another 24 hrs
Wash twice, add new medium and photoactivate

7.3.4 Immunofluorescence with Anti-fibronectin

Abstract	Immunofluorescence detection of fibronectin bound to chip surface
Preparation	(1) Anti-fibronectin, FITC coupled, stock 2 mg/ml, 20 µl volume (light sensitive) (2) Paraformaldehyde, 2 % (3) PBS, pH 7.4 (4) Fluorescent Mounting Medium
Instructions	Fixation using (2) for 15 min at 4 °C. Three rinsing steps with (3) at room temperature. Apply (1) in 1:20 dilution with (3). Wrap in aluminium foil instantly and keep it in the fridge (4°C) over night. Three rinsing steps with (3) at room temperature. Mounting with (4). Store in darkness at 4 °C
Remarks:	Assess blind probes: Scratch a pattern in a fibronectin coated glass substrate. (1) DPC Biermann, Bad Nauheim, Germany (4) S3023: Dako Corporation

7.4 E - Calibration of the System for Single Frequency Impedance Analysis

Because the output of the lock-in amplifier (voltage) is not linearly correlated to the impedance the systems needs to be calibrated. Therefore, resistors of different values were measured with the ECIS system, and data were modelled by the Boltzmann function according to equation (7-1)

$$f(x) = \frac{1 - y_0}{1 + e^{(x - U_{1/2})/k}} + y_0 \tag{7-1}$$

where y_0 is a bias voltage, $U_{1/2}$ is the voltage after 50 % signal increase, and k is the slope.

In Figure 7-1 data of the calibration described above are shown. Settings B to E refer to the gain factors of the lock-in amplifier that were adapted according to the electrode type investigated.

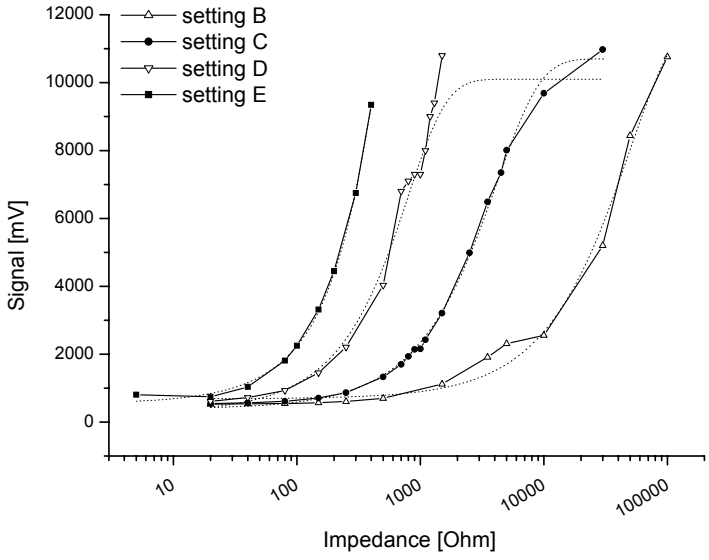

Figure 7-1: Calibration data for four different sensitivity settings and Boltzmann fittings. (Parameters: High dynamic mode, S1=off, τ=4, θ=0°)

7.5 F - Contents of the CD-ROM

Nanoplotter.mpg	Video clip showing the microfluidic biosensor system using extracellular recording during a measurement cycle.
CardiacMyocytes.exe	Beating cardiomyocytes on a microelectrode
Fluid.exe	Observation of cardiomyocytes in the microfluidic chamber